Petrogenesis of the Niğde Mafic Complex, Turkey: implications for the tectonic and geomorphic evolution of Central Anatolia

A Thesis
SUBMITTED TO THE FACULTY OF THE
UNIVERSITY OF MINNESOTA
BY

Molly Ray

IN PARTIAL FULFILLMENT OF THE REQUIREMENTS
FOR THE DEGREE OF
MASTER OF SCIENCE

Donna L. Whitney, Christian Teyssier

June 2016

Acknowledgements

I would like to thank and acknowledge my advisors, Donna Whitney and Christian Teyssier for providing me with the opportunity and support to do this research. I would also like to thank Bulent Tokay and Ekrem Tosun for their help with fieldwork in Turkey. Thank you to the members of the STAMP and CD-CAT groups, especially Côme Lefebvre, Maud Meijers, Gilles Brocard and Paul Umhoefer for your help with various aspects of the project.

Abstract

The Central Anatolian Crystalline Complex (CACC) is a high-grade metamorphic terrain that developed through a protracted history of collision, ophiolite obduction and arc magmatism during the closure of the Neotethys Ocean. The Central Anatolian Ophiolite (CAO) was emplaced onto the CACC during Cretaceous Neotethyan closure but is now highly dismembered. The Niğde Mafic Complex (NMC) is an association of metamorphosed and variably deformed gabbro, diabase, plagiogranite and ultramafic rocks in the southernmost metasedimentary massif of the CACC - the Niğde Massif. The Niğde Mafic Complex is described in detail for the first time, including its structural, petrologic and geochemical features. Mafic, ultramafic and felsic rocks from two adjacent regions, the Ecemiş Mafic Complex (EMC - east of the Niğde Massif - in the Ecemiş Fault corridor) and the Northern Region (isolated mafic-ultramafic outcrops north of the Niğde Massif) are also examined and compared. In addition, gabbro cobbles from basins adjacent to the Niğde Massif are investigated and their likely provenance is suggested.

Whole-rock XRF and ICP-MS data indicate a common, suprasubduction zone, ophiolite origin for rocks of the NMC, EMC and Northern Region, and confirm their correlation to the Central Anatolian Ophiolite. Despite variable mineral assemblages, isotropic gabbro from all three regions has similar geochemical features, including depleted LREE (La_N/Yb_N=0.40-0.89), high Mg numbers (61-87) and low TiO_2 (0.13-0.45 wt. %) that indicate a highly depleted mantle source, consistent with a forearc (or pre-arc) origin. Mineral compositions were determined through microprobe analysis. Gabbro mineral assemblages include magnesian orthopyroxene (En_{64-79}) and calcic plagioclase (An_{74-95}), which are typical of suprasubduction zone, water-saturated conditions for magma genesis. Post-kinematic muscovite, garnet and tourmaline-bearing granitoids intruded the NMC and are likely related to the crustally derived Üçkapılı Granite, limiting the age of ophiolite obduction and deformation to before ~85 Ma.

Results of hornblende-plagioclase geothermometry for the NMC indicate mid-upper amphibolite facies deformation and metamorphism at temperatures ranging from ~560 to 785°C, similar to conditions reported for the adjacent metasedimentary rocks of the Niğde Massif. Variations in mineral compositions and assemblages among the NMC, EMC and Northern Region reveal a metamorphic gradient whereby the NMC experienced mid-upper amphibolite-facies conditions associated with ductile deformation, and the EMC and Northern Region display evidence for low-grade metamorphism without significant ductile deformation. Overall these findings reveal that the Central Anatolian Ophiolite was locally deformed and metamorphosed in the mid-crust along with tectonically underlying metasedimentary units.

The Ulukışla and Ecemiş Basins, bordering the Niğde Massif locally contain abundant gabbro cobbles in Tertiary conglomerates. Gabbro cobbles from the Oligocene Çukurbağ Formation in the Ecemiş Basin have a mixture of island-arc tholeiite and boninitic geochemical affinities, whereas all cobbles from Messinian conglomerates of the $m_3$pl unit have boninitic geochemistry, exemplified by Ti/V ratios of less than 10. Based on the presence of metamorphic hornblende and the similarity of geochemical features, gabbro cobbles of the $m_3$pl unit may have been sourced in the Niğde Mafic Complex or in other parts of the CAO. This has implications for our understanding of the landscape evolution of the Niğde Massif region including the former extent of the Niğde Mafic Complex.

Table of Contents

List of Tables

List of Figures

Chapter 1

Structural and petrologic features of the Niğde Mafic Complex: implications for the Late Cretaceous development of the CACC

1.1 Introduction

Anatolia is made up of several continental fragments assembled during Late Cretaceous time when multiple subduction zones were contemporaneously operating in the Neotethys (Şengör and Yılmaz, 1981; Robertson *et al.,* 2013). At the center of the Anatolian microplate is the Central Anatolian Crystalline Complex (CACC) (Fig. 1.1a), which existed as a separate block of platform sedimentary rocks prior to Late Cretaceous collision and metamorphism (Görür *et al.,* 1984; Robertson *et al.,* 2013). Many aspects of CACC development, including the role of ophiolite obduction in its metamorphism, remain enigmatic, perhaps in part because of a dearth of information regarding the metamorphic and deformational features of the ophiolitic portion of the CACC.

Ophiolites of the CACC have been termed the Central Anatolian Ophiolite (CAO) (Yalınız *et al*., 1996) and are spatially associated with metasedimentary and plutonic massifs of the CACC (Fig. 1.1b). Geochronological data from metasedimentary and ophiolite units of the CACC reveal almost coincident ages for metamorphism, continental magmatism (Whitney *et al.,* 2003, 2007) and ophiolite genesis in Turonian time (Yalınız *et al*., 2000), a scenario that is difficult to resolve given that the ophiolites apparently overlie the metamorphic rocks and are intruded by syn-exhumational granitoids (Yalınız *et al.,* 1996). Ophiolite obduction has been proposed as the cause of high-grade metamorphism of the CACC (Akıman *et al.,* 1993), however the structural relationship between metasedimentary and ophiolite rocks has not been well documented, except locally with respect to extensional detachments (Lefebvre *et al*., 2011). Heating associated with crustal thickening in the CACC peaked at ~91 Ma (Whitney *et al*., 2003), before collision with the neighboring Tauride and Pontide microcontinents in the Maastrichtian-Paleocene (Görür *et al*., 1984; Clark and Robertson, 2002, 2005). As such, oceanic-continental collision and associated ophiolite obduction may have been a primary

cause of crustal thickening and high-grade metamorphism in Central Anatolia. The

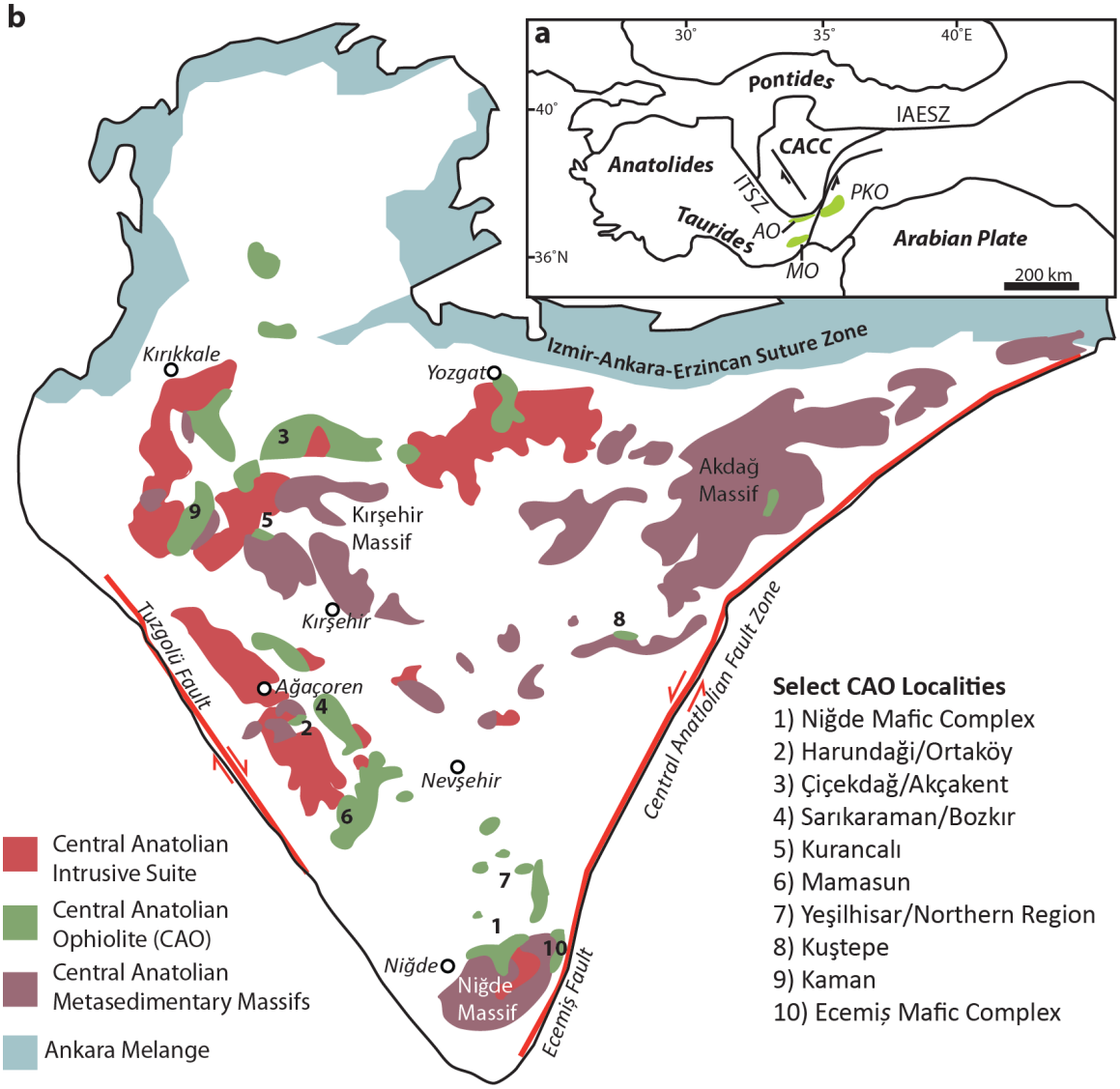

Figure 1.1 a) Regional map of the Anatolian Plate showing the location of the Central Anatolian Crystalline Complex (CACC). **b)** Major components of the CACC basement. Numbers are references for the Central Anatolian Ophiolite (CAO) mentioned in the text. AO: Alihoca Ophiolite, IAESZ: Izmir-Ankara-Erzincan suture zone, ITSZ: Inner Tauride suture zone, MO: Mersin Ophiolite, PKO: Pozanti-Karsanti Ophiolite. Modified from Lefebvre *et al.* (2013).

metamorphic and structural features of the CAO may ultimately provide insight into how crustal thickening occurred during this early stage of Anatolian assembly.

Within the Niğde Massif, the southernmost metamorphic massif of the CACC (Fig. 1.1b), a variably deformed, dominantly gabbroic unit occurs associated with felsic and mafic dikes and minor ultramafic rock. Previously named the Sineksizyayla

Metagabbro (Atabey, 1989; Atabey *et al*., 1990), these rocks are herein referred to as the Niğde Mafic Complex (NMC), which better reflects the lithologic heterogeneity within the unit as a whole. Floyd *et al.* (2000) correlated the mafic rocks of the NMC to the Central Anatolian Ophiolite. The presence of highly deformed ophiolitic rocks within the southernmost metamorphic massif of the CACC brings forth questions related to Anatolian assembly such as: 1) From which suture zone was the CAO derived? 2) When and under what conditions did ophiolite deformation occur with respect to the CACC metasedimentary rocks?

Examination of the magmatic, metamorphic and deformational features of the Niğde Mafic Complex reveals the interrelationship between subduction, obduction and high-temperature metamorphism and deformation that affected the southern CACC in Late Cretaceous time. Understanding the evolution of the CACC during this period of Anatolian tectonism may provide insight into how continental crust assembles and grows in modern complex collision zones such as the Caribbean and Polynesia, the relationship between ophiolite obduction and metamorphism, and the complexity of interpreting metamorphic features in orogenic ophiolite complexes where there has been overprinting of magmatic, hydrothermal and metamorphic events.

1.2 Geologic Setting

1.2.1 Central Anatolian Crystalline Complex

The Central Anatolian Crystalline Complex (CACC) is a wedge-shaped terrane separated from the Pontides to the north by the Izmir-Ankara-Erzincan suture zone and from the Taurides to the south by the Inner Tauride Suture (Fig. 1.1a). The Central Anatolian and Tuz Gölü strike-slip faults delineate the eastern and western boundaries of the CACC, respectively, and may also coincide with the Inner Tauride Suture (Fig. 1.1b).

The CACC is characterized by the presence of three major high-grade metamorphic massifs, the Akdağ, Kırşehir and Niğde Massifs (Akıman *et al*., 1993), which are largely comprised of metasedimentary rocks. The metasedimentary basement is dominated by metacarbonates that are considered to be the metamorphosed equivalent of the Gondwanan continental margin sequences exposed in the Tauride Belt, based on

correlative stratigraphy and faunal assemblages (Kocak and Leake, 1994). The Central Anatolian Ophiolite (CAO) is in tectonic contact with these metasedimentary units and is comprised of mafic, ultramafic and plagiogranitic intrusions as well as pelagic sediments and volcanic rocks (Yalınız *et al.,* 1996). Late Cretaceous mafic and felsic plutons crosscut both the ophiolite and metasedimentary rocks (Yalınız *et al.,* 1996). Dominantly Neogene volcanic and sedimentary rocks unconformably rest above this metasedimentary, ophiolitic and plutonic basement.

Paleomagnetic data from the intrusive suites of the CACC suggest that there may have been significant, internal rotation within the CACC since Late Cretaceous time (Görür *et al*., 1984; Lefebvre *et al*., 2013). These data allow reconstruction of the CACC as an elongate north-south oriented ribbon, rather than the presently observed wedge (Lefebvre *et al*., 2013). In this reconstruction, the magmatic suite is interpreted as a continental arc. Rotation occurred owing to Paleocene-Eocene continental collision between the CACC, Pontide and Tauride blocks and was partly accommodated by internal strike slip faults (Lefebvre *et al.*, 2013).

The pressure-temperature-time (P-T-t) history of the CACC includes an extended period of high-grade metamorphism and deformation (~92-84 Ma) followed by exhumation of the metasedimentary massifs and intrusion of granitic and bimodal plutons through ~70 Ma (Whitney *et al*., 2003; İlbeyli, 2005). Deformational features and thermobarometry from the Niğde Massif indicate that high-grade metamorphism occurred as a result of crustal thickening in a transpressional orogen (Whitney *et al*., 2001, 2003, 2007). Lefebvre *et al.* (2013) suggested that an eastward dipping subduction zone below the Late Cretaceous CACC contributed to metamorphism and intrusion of the magmatic suite. Field relations, such as crosscutting Late Cretaceous granitoids indicate that ophiolites were obducted prior to burial of the sedimentary protoliths (Floyd *et al*., 1998). The combination of ophiolite obduction, arc magmatism and crustal thickening related to collision may have contributed to metamorphism and deformation of the CACC.

1.2.2 Central Anatolian Ophiolite (CAO)

The term CAO is used here to describe a number of isolated fragments of suprasubduction zone (SSZ)-type ophiolite distributed throughout the CACC (Yalınız *et al*., 1996; Fig. 1.1b). In some previous uses, CAO has referred to both the SSZ ophiolite fragments thrust above metasedimentary units as well as mafic amphibolite interlayered with marble in the metamorphic massifs (Yalınız *et al*., 1996). These two units are, however, unrelated and readily distinguished on structural, geochemical or stratigraphic bases (Floyd *et al*., 2000). In this paper only the overthrust ophiolite fragments will be referred to as the CAO, consistent with use of the term in more recent publications (i.e. Kocak *et al*., 2005; Toksoy-Köksal *et al.,* 2009; van Hinsbergen *et al*., 2016).

The most complete exposures of the CAO come from the Sarıkaraman and Çiçekdağ localities (Fig. 1.1b), where gabbro is associated with pillow lavas and pelagic sediments, indicating an oceanic origin (Yalınız *et al*., 1996; Yılmaz and Boztuğ, 1998). Isolated klippen and monadnocks of gabbro in the CACC are also attributed to the CAO (Floyd *et al*., 2000; Kocak *et al*., 2005; Fig. 1.1b). Gabbro from relatively complete ophiolites, such as Sarıkaraman, has similar lithologic associations, geochemistry and mineral assemblages to the isolated gabbro occurrences, indicating that they were part of the same ophiolite nappe, which has since been fragmented through faulting and erosion (Floyd *et al.*, 2000). Gabbro also occurs locally as part of the Late Cretaceous magmatic suite that intruded the metasedimentary massifs and is distinct from ophiolitic gabbro in that it consists of igneous magnesiohornblende with rare pyroxene, has transitional geochemistry (from gabbro-diabase-granite) and has sinuous contacts with granite (Kadıoğlu *et al*., 2005; Kocak *et al.,* 2005).

In the Sarıkaraman ophiolite, isotropic gabbro and crosscutting plagiogranite (trondhjemite) are in tectonic contact with a sheeted dike complex that merges into pillow basalt and rhyolite. All units are cut by diabase dikes, and the structurally highest unit consists of pelagic sediments and olistostromes (Yalınız *et al*., 1996). Importantly, all units of the Sarıkaraman ophiolite are cut by continentally derived monzogranite that has a K-Ar hornblende age of 81.5 Ma, indicating that the obduction event occurred before intrusion of the late magmatic suite (Yalınız *et al*., 1999).

Ultramafic rocks are not well exposed in the CAO compared to other Eastern Mediterranean ophiolites (Dilek *et al.,* 1999). They are most voluminous in the eastern and southeastern parts of the CACC, especially to the east of the Niğde Massif, in the Yeşilhisar region, and at Kuştepe (Yalınız and Göncüöğlu, 1998; Ilbeyli, 2008; Fig. 1.1b). Elsewhere, such as in the northern Niğde Massif, small amounts of metaultramafic rocks occur as boudins within gabbro-dominated shear zones (this study).

Metamorphic minerals and textures are observed in all localities of the CAO, yet the metamorphic and deformational features have not been the focus of any previous studies. Volcanic rocks in the ophiolites typically contain greenschist-facies assemblages that have in some cases been attributed to ocean-floor hydrothermal metasomatism (İlbeyli, 2008) or to contact metamorphism (Yılmaz and Boztuğ, 1998). On the other hand, higher-grade conditions in the gabbro, indicated by ubiquitous hornblende replacing pyroxene (amphibolitization) have been attributed to late magmatic processes (Kocak *et al.,* 2005). Although late magmatic and ocean-floor recrystallization likely resulted in some mineralogic changes, the effects of post-obduction regional metamorphism cannot be discounted, especially in the case of high-temperature amphibolitization. As will be demonstrated in this paper, textures in gabbro and associated lithologies in the Niğde Mafic Complex clearly show the effect of post- (or syn-) obduction metamorphism. Table 1.1 lists primary and secondary assemblages in gabbro as reported from various studies of the CAO.

Field relations require that the CAO must have been emplaced prior to Late Cretaceous peak metamorphism of the metasedimentary units (Yalınız *et al*., 1999). For example, the Terlemez Granitoid intrudes the Sarıkaraman ophiolite and has an age of 81.5 ± 1.9 Ma (K-Ar in hornblende; Yalınız *et al*., 1999). Thus the ophiolite must have been emplaced onto the metasedimentary protoliths prior to burial in order to be intruded by Campanian granitoids during subsequent exhumation. These field relations are at odds with the present geochronologic framework, as the peak metamorphism of upper amphibolite facies, sillimanite gneiss in the Niğde Massif was ~91 Ma (Whitney *et al*., 2003), which overlaps with faunal ages for epi-ophiolitic pelagic sediments (Turonian-Campanian; Yalınız *et al*., 2000). In addition, a ~91 Ma U/Pb zircon age for plagiogranite

from the Sarıkaraman Ophiolite implies synchronous oceanic and continental magmatism in the CACC and CAO (van Hinsbergen *et al*., 2016). Nonetheless, as discussed in later sections, structural and thermobarometric data from this study of the Niğde Mafic Complex require that ophiolite obduction preceded high-grade metamorphism. Clarification of the precise age relations may ultimately be resolved by additional geochronologic studies from the sparsely dated ophiolite.

Gabbro mineral assemblage	**Reference**
Cpx + Pl (An$_{75-93}$) ± Bt + *Hbl*	Kocak and Leake (1994) (2)
Cpx + Pl ± *Act* ± *Tlc* ± *Ep*	Yılmaz and Boztuğ (1998) (3)
Cpx + Pl ± Zrn ± Ttn + *Hbl* ± *Act* ± *Pl (An$_{45-67}$)*	Yalınız and Göncüoğlu (1999) (4)
Cpx + Pl + Hbl (Ts, Prg) ± *Act* ± *Hbl* ± *Ab* ± *Ep*	Toksoy-Köksal *et al.* (2001, 2009) (5)
Cpx + Pl (An$_{75-93}$) ± Hbl (Ts) +*Hbl (Mhb)* ± *Act* ± *Bt*	Kocak *et al.,* (2005) (2, 6, 7)
Cpx + Pl (An$_{68-89}$) + Hbl ± Opx ± Ol + *Act* ± *Chl* ± *Ab* ± *Ep* ± *Cal* ± *Srp*	İlbeyli (2008) (3, 8)
Cpx+ Pl (An$_{74-95}$) ± Hbl (Ts) ± Opx ± Ol ± *Hbl (Mhb)* ± *Act* ± *Pl (An$_{36-68}$)* ± *Qz* ± *Ttn*	This study (1)

Table 1.1: Representative mineral assemblages for gabbro of the CAO from select publications. Secondary mineral assemblage is italicized. Magmatic minerals are bolded. Where quantitative analyses were obtained for plagioclase and hornblende, compositional information is included. Numbers after references refer to map localities on Figure 1.1b. Mineral abbreviations are from Whitney and Evans (2010).

As a whole, the Central Anatolian Ophiolite bears the hallmark qualities of "Tethyan-style" ophiolites, which have suprasubduction zone affinities and are obducted when passive continental margins are dragged into a subduction zone (Moores, 1982; Wakabayashi and Dilek, 2003). In contrast to other Tethyan-style ophiolites of southern Anatolia, the CAO is amphibolitized and associated with high-grade continental platform metasedimentary rocks (Kocak and Leake, 1994). Ophiolites of the Tauride Belt, south of the Inner Tauride suture zone, are associated with unmetamorphosed platform sedimentary rocks and, aside from mélanges, metamorphic soles and basal tectonites, the ophiolites lack deformation features (Dilek *et al*., 1999; Sarıfakioğlu *et al.,* 2013). The

Niğde Mafic Complex is within 50 km of the Pozantı-Karsantı (Aladağ) and Alihoca ophiolites of the Tauride Belt, however it is petrologically and structurally more similar to the CAO (Floyd *et al*., 2000) and is separated from the Taurides by the Inner Tauride suture zone and the Ecemiş Fault (Fig. 1.1b). Hornblende $^{40}Ar/^{39}Ar$ ages from metamorphic soles of the Tauride Ophiolites indicate subduction initiation within the Inner Tauride seaway at 92-89 Ma and obduction on to the Tauride Platform by the end of the Cretaceous period (Dilek and Whitney, 1997; Dilek *et al.,* 1999; Parlak *et al.,* 2013).

1.2.3 Niğde Massif

The Niğde Massif is a high-relief metamorphic core complex at the southern tip of the Central Anatolian Crystalline Complex (Whitney and Dilek, 1997) (Fig. 1.1b). A south-dipping detachment fault separates the Niğde Massif from the Ulukışla Basin along its southern edge. The left lateral Ecemiş Fault forms the eastern boundary of the massif. To the north and west, unconformable Neogene sediments and volcanic rocks obscure the underlying bedrock (Fig. 1.2a).

The oldest rocks of the Niğde Massif are metasedimentary continental margin sequences and include the Gümüşler, Kaleboynu and Aşıgediği Formations (Atabey, 1989). In the core of the dome, the Gümüşler Formation contains migmatite, indicating that high-grade conditions were accompanied by crustal anatexis (Whitney *et al.,* 2003). Amphibolite (metabasite) is interlayered with metasediments in the Aşıgediği, Kaleboynu and Gümüşler formations and is geochemically distinct from amphibolite of the Niğde Mafic Complex (Floyd *et al*., 2000; this study). The Niğde Mafic Complex, exposed within the northern part of the massif, is part of the Central Anatolian Ophiolite and consists of metamorphosed and deformed gabbro, diabase and plagiogranite with minor ultramafic rocks (Fig. 1.2a). The gabbro has been named the Sineksizyayla Gabbro (Atabey, 1989) and described as locally highly deformed and metamorphosed (Whitney and Dilek, 1998). The peraluminous, crustally-derived Üçkapılı Granite intruded during exhumation and doming and is relatively undeformed (Whitney *et al*., 2003).

The Niğde Massif is a migmatite-cored dome in which foliations are overall concentric about an apex in the northwestern region of the massif (Fig. 1.2a). The high-

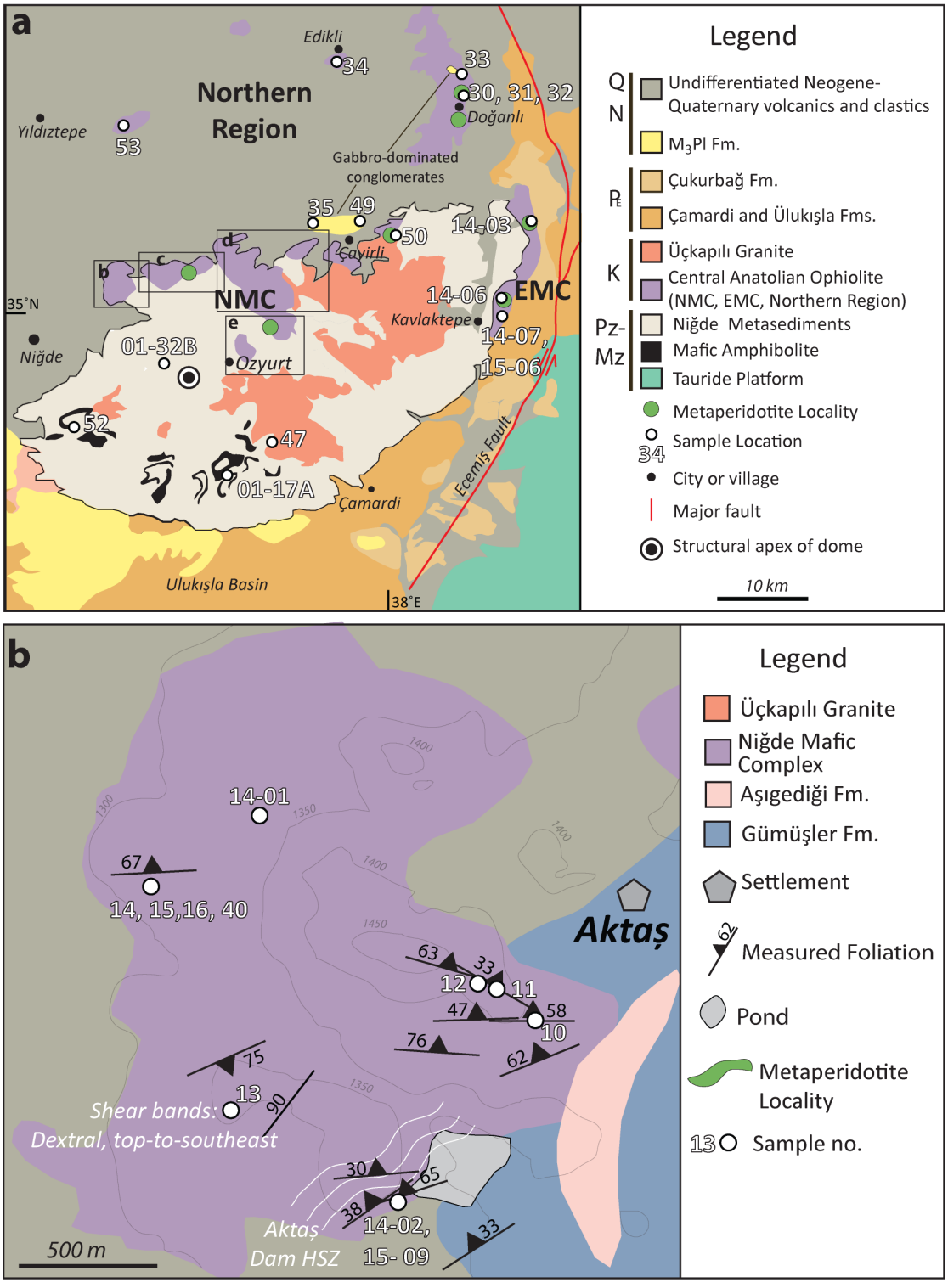
a
Northern Region
Edikli
34
33
30, 31, 32
Doğanlı
Yıldıztepe
53
Gabbro-dominated conglomerates
35
49
50
14-03
Çayirli
d
c
b
NMC
EMC
14-06
Kavlaktepe
14-07,
15-06
35°N
Niğde
01-32B
e
Ozyurt
52
47
01-17A
Çamardi
Ecemiş Fault
Ulukışla Basin
38°E
Legend
Q
N
Undifferentiated Neogene-Quaternary volcanics and clastics
M3Pl Fm.
P
E
Çukurbağ Fm.
Çamardi and Ülukışla Fms.
K
Üçkapılı Granite
Central Anatolian Ophiolite (NMC, EMC, Northern Region)
Pz-Mz
Niğde Metasediments
Mafic Amphibolite
Tauride Platform
Metaperidotite Locality
34
Sample Location
City or village
Major fault
Structural apex of dome
10 km
b
14-01
67
14, 15,16, 40
Aktaş
63
33
12
11
47
58
10
76
62
75
13
90
Shear bands:
Dextral, top-to-southeast
30
65
38
14-02,
15- 09
33
Aktaş
Dam HSZ
500 m
Legend
Üçkapılı Granite
Niğde Mafic Complex
Aşıgediği Fm.
Gümüşler Fm.
Settlement
62
Measured Foliation
Pond
Metaperidotite Locality
13
Sample no.

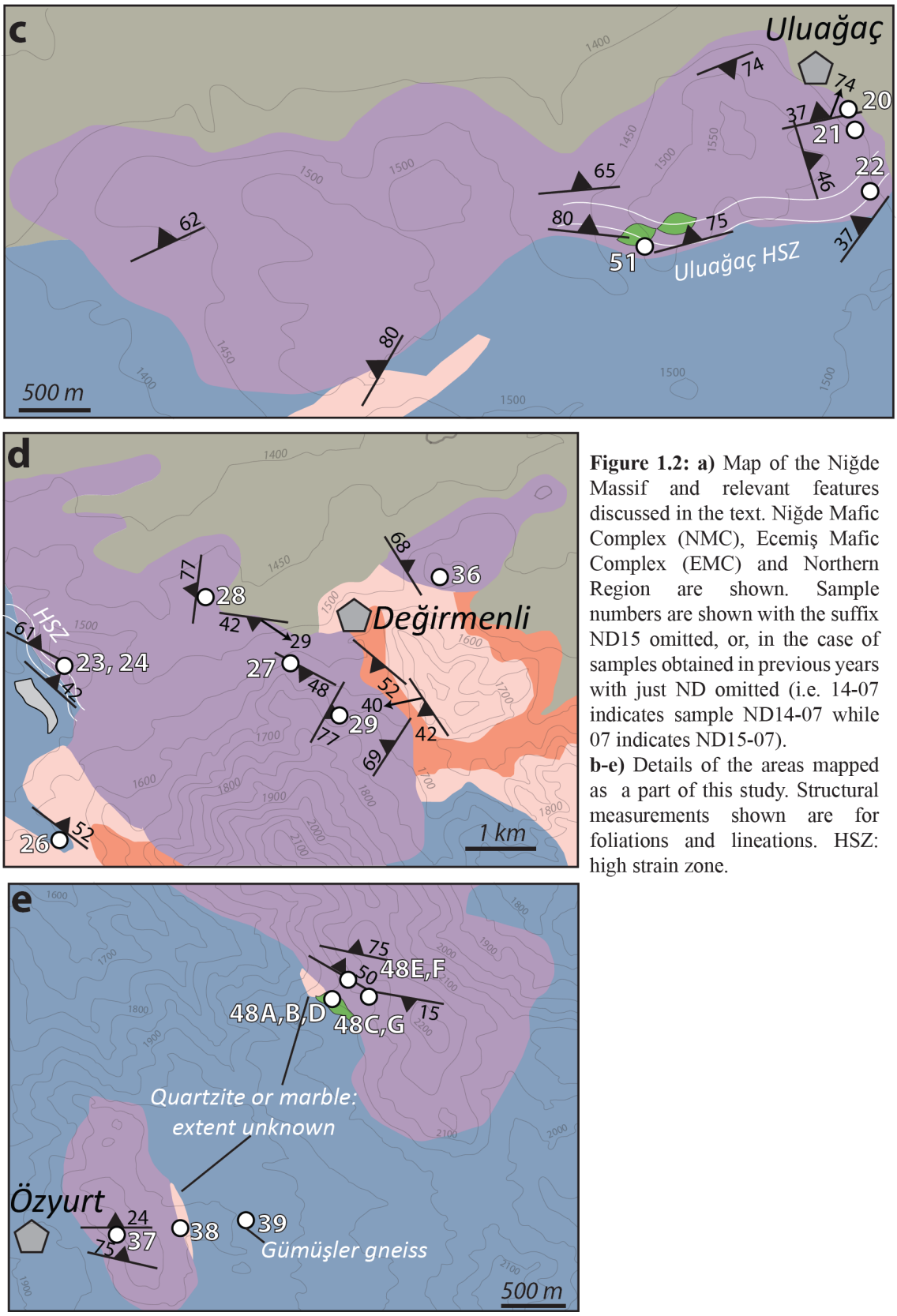

Figure 1.2: a) Map of the Niğde Massif and relevant features discussed in the text. Niğde Mafic Complex (NMC), Ecemiş Mafic Complex (EMC) and Northern Region are shown. Sample numbers are shown with the suffix ND15 omitted, or, in the case of samples obtained in previous years with just ND omitted (i.e. 14-07 indicates sample ND14-07 while 07 indicates ND15-07).
b-e) Details of the areas mapped as a part of this study. Structural measurements shown are for foliations and lineations. HSZ: high strain zone.

grade fabric, including migmatitic layering and mineral lineations, indicates top-to-north shearing and ductile flow approximately parallel to the strike of the Ecemiş Fault, which is the southern segment of the Central Anatolian Fault Zone (Whitney *et al*., 2007). This fabric is overprinted in top-to-south ductile shear zones associated with exhumation under a transtensional stress regime (Whitney *et al*., 2007).

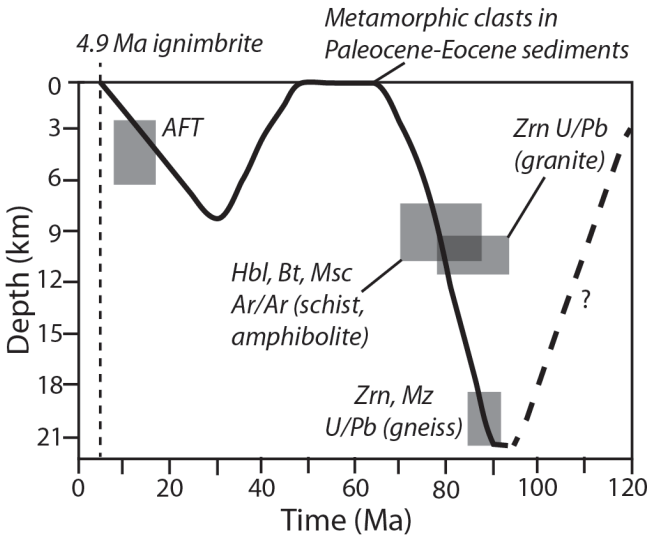

Figure 1.3: Depth-time path modified from Whitney *et al*. (2008) with data from Whitney and Dilek (1998), Fayon *et al.* (2001), Whitney *et al.* (2001, 2003), Gautier *et al.* (2002). Black dashed line shows two cycles of burial and exhumation for metasedimentary rocks of the Niğde Massif. Dating methods and minerals are indicated. AFT: Apatite Fission Track, Bt: biotite, Hbl: hornblende, Msc: muscovite, Mz: monazite, Zrn: zircon.

The Niğde Massif contains a record of two cycles of burial and exhumation (Umhoefer *et al*., 2007; Whitney *et al*., 2008; Idleman *et al.,* 2014) (Fig. 1.3). The age of peak metamorphic conditions is indicated by ~91 Ma zircon rims in high-grade sillimanite-K-feldspar schist from the core of the dome (U/Pb; Whitney *et al*., 2003). The Üçkapılı Granite was emplaced at shallow crustal levels (3-4 kbar) at ~90 Ma. The depth-time histories of the granite and host gneiss as well as the extensional shear zones indicate that transtension was a driver of exhumation and pluton emplacement (Whitney *et al*., 2003; 2007). Exhumation and cooling continued through latest Cretaceous time (Whitney *et al.,* 2003, 2007), and culminated in unroofing by Paleocene time when metamorphic and granitic clasts appear in the Ulukışla Basin sedimentary rocks (Gautier *et al*., 2002; Umhoefer *et al*., 2007). A second period of burial is inferred by the resetting of apatite fission track ages in the basin and underlying metamorphic and plutonic rocks and perturbation of $^{40}Ar/^{39}Ar$ spectra in metamorphic rocks (Whitney *et al*., 2003; Fayon and Whitney, 2007; Umhoefer *et al*., 2007). This second cycle of burial and exhumation may have been caused by a period of transpression along the Ecemiş Fault related to Eocene

Arabia-Eurasia collision (Idleman *et al.,* 2014). Final exhumation was completed by mid-late Miocene time (AFT; Fayon *et al*., 2001). The multiple exhumation cycles and orogen-parallel crustal flow are a result of the Niğde Massif's location in a long-lived wrench zone, possibly corresponding to mid-crustal levels of an ancestral Ecemiş Fault at the CACC southeastern margin during oblique collision (Umhoefer *et al*., 2007, Whitney *et al*., 2007).

1.3 Description of the Field Area

1.3.1 Field lithologic relations

The Niğde Mafic Complex contains components typical of the lower part of a suprasubduction zone (SSZ) ophiolite. In order of decreasing abundance, the major rock types are gabbro, plagiogranite, diabase and ultramafic rocks, all of which have been variably metamorphosed and deformed. Also present in the field area are pegmatitic gabbro, amphibole veins, and leucocratic segregations within the metagabbro.

Within the northern part of the Niğde Massif, gabbro (and associated mafic and felsic intrusions) is typically found at the local elevation highs, resulting in a series of gabbro hills above valleys and lowlands underlain by metasedimentary rocks (Fig. 1.2b-e). Field relations within the Niğde Mafic Complex are comparable to other exposures of the CAO, such as the lower section of the Sarıkaraman Ophiolite (Yalınız *et al.,* 1996).

The main rock type is amphibolitized gabbro, which is intruded by plagiogranite and diabase. Metaperidotites are locally found near the contact with metasedimentary units, as blocks or lenses in gabbro, or with unclear contacts. Isoclinal folds and mylonite zones deform all of the mafic complex lithologies in high strain zones, which were found near inferred contacts with the Gümüşler Formation (Aktaş Dam high strain zone [HSZ]-Fig. 1.2b, Uluağaç HSZ Fig. 1.2c). The mafic complex is crosscut by dikes of undeformed muscovite-tourmaline pegmatite (samples 22D, 40C) and garnet-bearing aplite dikes (sample 48F). All of the aforementioned units have been affected by brittle to semi-brittle faulting (Fig. 1.4).

Figure 1.4: Field photo from Aktaş (sample locality 40) displaying field relations observed in the Niğde Mafic Complex. Light dike is plagiogranite, dark cross-cutting dike is diabase. Brittle faults have affected the entire sequence.

1.3.2 Map-scale lithologic variations

Three gabbro dominated units are distinguished within the study area based on metamorphic and lithological variations: the Niğde Mafic Complex (NMC) – within the northern Niğde Massif, the Ecemiş Mafic Complex (EMC) – a gabbro and serpentinite unit within the Ecemiş Fault corridor – and the Northern Region – the area north of the Niğde Massif/Mafic Complex margin where a series of isolated outcrops of mafic-ultramafic rock are exposed (Fig. 1.2a). The contact between the Ecemiş Mafic Complex and the metasedimentary units of the Niğde Massif was inferred to be a thrust fault by Keskin *et al*. (2010) although the contact is not exposed. It is unclear how the Northern Region is related to the Niğde Massif because Tertiary volcanic and sedimentary units overly most of the basement. Samples from the Ecemiş Mafic Complex and Northern Region prove extremely useful as comparisons to the Niğde Mafic Complex and allow an interpretation of ophiolite extent and structure.

Ecemiş Mafic Complex

Whitney *et al*. (2007) established that metasedimentary rocks in the eastern part of the Niğde Massif had distinct structural and thermochronological characteristics compared to the western part of the massif and therefore that a tectonic zone occurs

separating the eastern and western belts of the Niğde Massif. As part of this study, gabbro and ultramafic rock samples were obtained from the Ecemiş Mafic Complex just east of the Niğde Massif in order to make petrologic comparisons with rocks from the Niğde Mafic Complex, which is primarily in the western belt of the Niğde Massif. The most distinctive feature of the EMC is the presence of massive ultramafic rocks, which are mostly serpentinized. The main rock types in the EMC are olivine gabbro and clinopyroxene gabbro, which have been variably altered to actinolite, iddingsite and serpentine minerals. In contrast, olivine-bearing gabbro was not found in the Niğde Mafic Complex. Hornblende is absent in the EMC gabbros, whereas it is ubiquitous in the rest of the study region. The EMC also apparently lacks plagiogranite and diabase dikes.

Planar fabrics were noted in outcrop in the EMC, although in thin section the rocks can be seen to lack deformation microstructures, suggesting that the layering is compositional. The EMC lithologies seem to correspond to the layered gabbro-ultramafic unit in a typical ophiolite sequence, and therefore may have formed in the lower part of the oceanic crust and uppermost mantle.

Niğde Mafic Complex

The Niğde Mafic Complex refers to the mafic, ultramafic and plagiogranite outcropping mostly in the northern half of the Niğde Massif and was the primary area mapped for this research. Beyond the northern boundary of the Niğde Mafic Complex, relief is subdued and Neogene volcanic rocks derived from the Cappadocia volcanic center are the most widely exposed lithology. The contact between metagabbro and Neogene volcanic rocks is a nonconformity that is well exposed along the northern edge of the Niğde Massif, near Uluağaç (Fig. 1.2c) and in a roadcut southeast of Çayırlı (Fig. 1.2a). Thick beds of conglomerates derived almost entirely from the mafic complex are also found north of the Niğde Massif, and these commonly form small topographic highs (Figs. 1.2a, 1.5).

The main rock type in the Niğde Mafic Complex is a deformed and amphibolitized gabbro or gabbronorite. Small amounts of ultramafic rock are found as blocks within metagabbro, and the metagabbro is cut by mafic and felsic dikes.

Metadiabase dikes here have a grain size of 0.5-1 mm and there is a lack of basalt or other upper crustal units in the NMC. Plagiogranite is abundant in this part of the mafic complex, and in some places is more voluminous in outcrop than gabbro, although most commonly plagiogranite occurs as dikes 1-2 meters in width. Altogether these features indicate a higher crustal level of the ophiolite than the Ecemiş Mafic Complex. The variable grain size and abundance of plagiogranite dikes and pegmatitic gabbro in the NMC are consistent with an origin as the varitextured and isotropic gabbro layer of the oceanic crust.

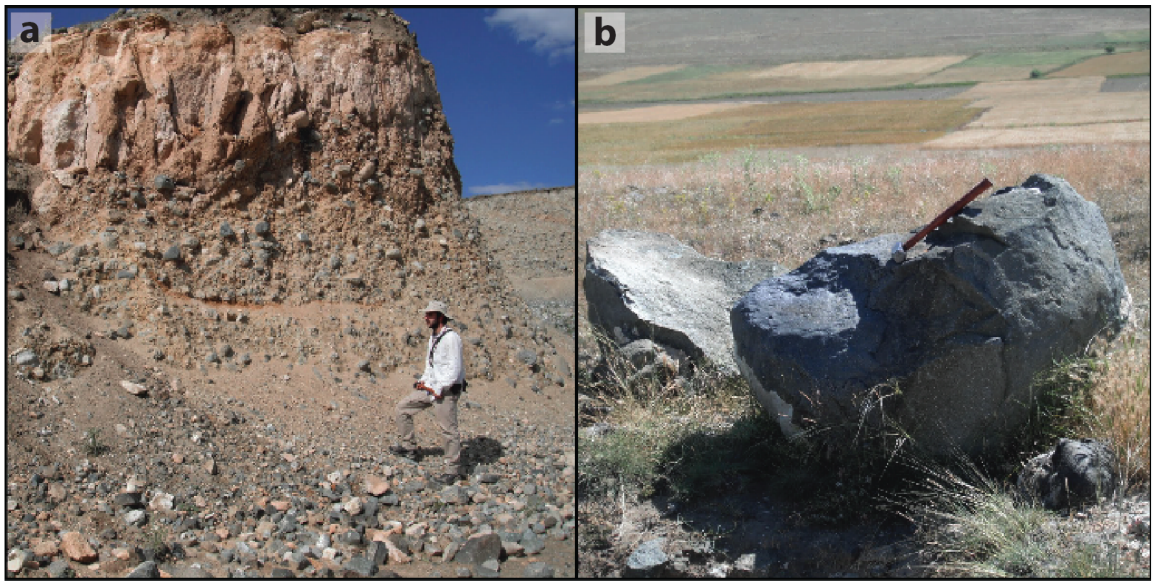

Figure 1.5: a) Gabbro-dominated conglomerate that forms a small hill north of Çayirli, near sample location 35 (Fig. 1.2a). Red, overlying material is Cappadocian ignimbrite of probable Miocene age. **b)** Diabase boulder (sample 49b) observed in (on) conglomerate outside of Çayirli. The boulder preserves an igneous texture.

Northern Region (Edikli, Yıldıztepe, Doğanli)

Neogene volcanic rocks cover most of the basement in the Northern Region, although gabbro monadnocks dot the landscape for some 40 km beyond the northern boundary of the Niğde Massif (Fig. 1.1b). The Doğanlı Valley northeast of the Niğde Massif (Fig. 1.2a) has poor outcrop but is mapped as ophiolite on the MTA geologic map (Keskin *et al*., 2010). Where bedrock is exposed in the Doğanlı Valley, it is serpentinite, plagiogranite, diabase and gabbro. At Edikli (Fig. 1.2a), a monadnock is composed of olivine and hornblende metagabbro, some of which shows brittle deformation features

such as cataclasite. A monadnock near Yıldıztepe, farther west, exposes large quantities of basalt in contact with pegmatitic gabbro and isotropic hornblende gabbro. The presence of basalt at Yıldıztepe is interesting because it is geochemically identical to diabase dikes of the Niğde Mafic Complex (see section 1.5), and thus this region may expose an upper crustal level of the ophiolite compared to what is observed in the Niğde Massif. The gabbro monadnocks farther north (see locality 7 on Fig. 1.1b) have been investigated by Kocak *et al*. (2005) and correlated to the CAO, indicating that ophiolite underlies much of the region between the Niğde Massif and Cappadocia but is now covered by Tertiary volcanic rocks.

1.4 Petrographic Features and Mineral Chemistry

1.4.1 Methods

Thin sections from samples collected in the field area (65 from the NMC, 11 from the EMC, and 8 from the Northern Region) were analyzed petrographically for mineral assemblages and textural features. Descriptions of each sample are provided in Appendix 1. Unless specified, individual samples are referred to in the text with the suffix ND15- omitted. Mineral compositions were analyzed in 19 select thin sections using a JEOL JXA-8900R electron microprobe at the University of Minnesota. The analytical accelerating voltage was 15 kV with a beam current of 20 nA and a spot size of 5 μm hydrous minerals and 1 μm for anhydrous phases. Representative mineral compositions are reported in Appendix 2.

1.4.2 Gabbro

Gabbro in the study area varies from undeformed to protomylonitic in high strain zones. In non-mylonitized samples, the average grain size is between 0.5 and 3 mm, or up to several centimeters in pegmatitic veins. Mineral assemblages and textures vary significantly between the eastern (EMC), western (NMC) and northern parts of the study area and are described separately below. A more detailed discussion of deformation microstructures is presented in section 1.6.

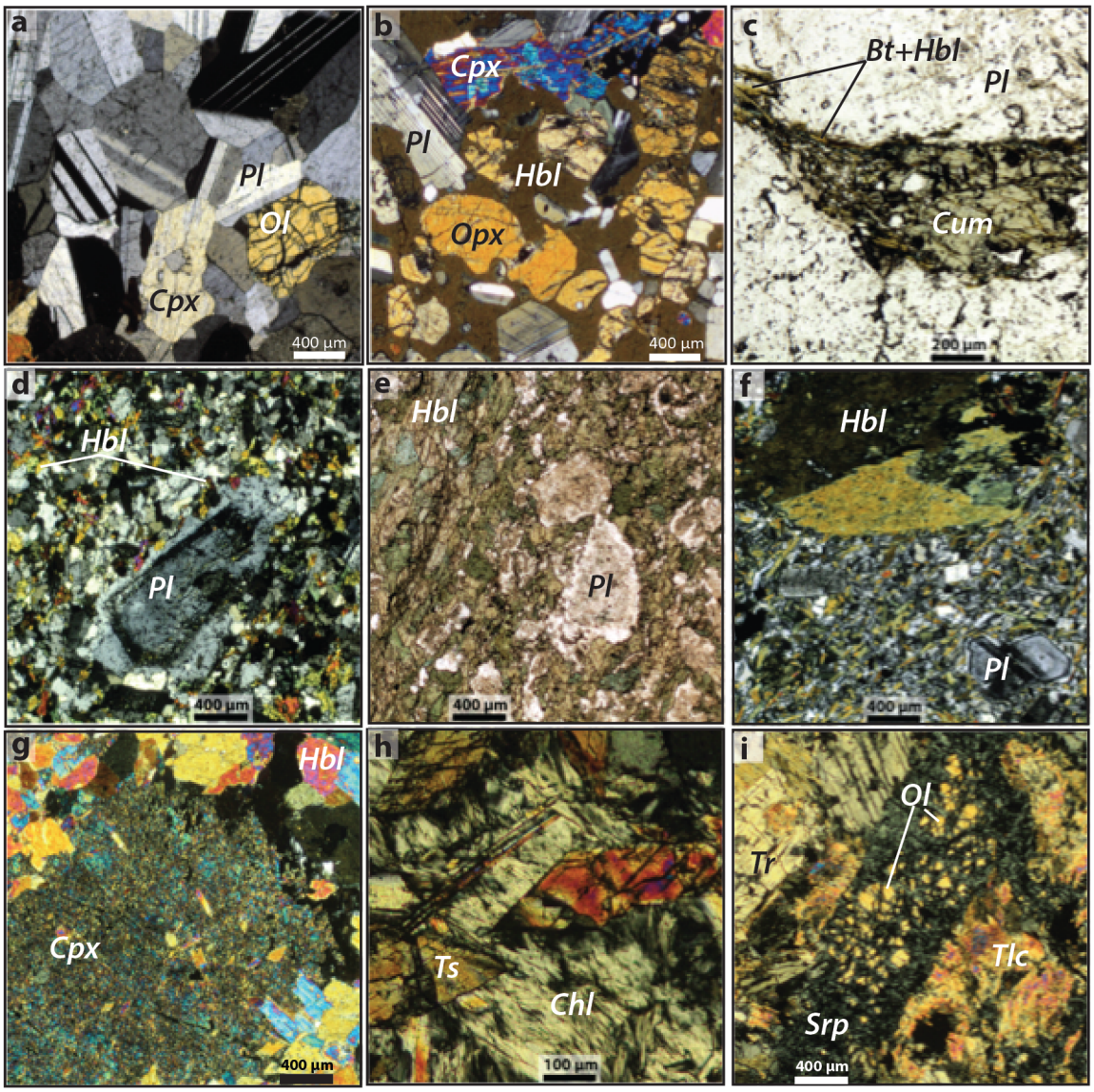

Figure 1.6: Photomicrographs of various lithologies from the field area. **a)** Sample ND15-06, olivine gabbro from the EMC. **b)** Sample ND15-36B, gabbronorite from the NMC with poikilitic hornblende. **c)** Sample ND15-40A, cummingtonite plagiogranite from the NMC. **d)** Sample ND15-29, metadiabase from the NMC. **e)** Sample ND15-48C, metadiabase from the NMC, note foliation in uppef left corner and phenocrysts in center. **f)** Sample ND15-49B, igneous textured diabase cobble from the Çayirli conglomerate (Fig. 1.2a). **g)** Sample ND15-23, clinopyroxenite from the NMC, partially replaced by polygonal-textured hornblende. **h)** Sample ND15-51E, chlorite schist from the NMC. **i)** Sample ND15-48D, forsterite-tremolite-talc metaperidotite from the NMC, note the elongate olivine crystal which is mostly replaced by mesh textured serpentine. Bt: biotite, Chl: chlorite, Cpx: clinopyroxene, Cum: cummingtonite, Hbl: hornblende, Ol: olivine, Pl: plagioclase, Srp: serpentine, Tr: tremolite, Ts: tschermakite,

Gabbro from the Ecemiş Mafic Complex is olivine-clinopyroxene gabbro (samples ND14-06B, C, D; ND14-07A; ND15-06) or clinopyroxene gabbro. (ND14-

06A). Mineral compositions from one EMC olivine gabbro (ND14-07A) are Fo_{83} (olivine), En_{48} (clinopyroxene) and An_{85} (unzoned plagioclase). EMC gabbros typically have anhedral, rounded olivine and pyroxene and subhedral, unzoned plagioclase (Fig. 1.6a). Alteration to greenschist-facies minerals is variable, with some samples displaying purely igneous textures and others being almost completely replaced by secondary minerals. Where alteration occurs, olivine is replaced by green, mesh-textured serpentine, clinopyroxene is locally mantled by needle-like actinolitic aggregates (uralite) and some plagioclase is saussuritized. Plagioclase in the EMC gabbros has well developed albite and pericline twins. Many of the gabbros from the EMC are altered to secondary minerals such as serpentine and actinolite however they do not show any deformational fabrics, suggesting relatively static conditions for metamorphism.

Within the Niğde Mafic Complex, gabbroic rocks show a diversity of textures reflecting variable degrees of amphibolitization and deformation. Relict clinopyroxene ± orthopyroxene indicate that the protolith of most of the NMC metagabbro was clinopyroxene gabbro or two-pyroxene gabbro (gabbronorite) (Fig. 1.7b). Mineral compositions vary between samples from En_{64} – En_{79} for orthopyroxene, En_{37} – En_{45} for clinopyroxene, $An_{74\text{-}90}$ for plagioclase cores and $An_{49\text{-}71}$ for plagioclase rims. Orthopyroxene is pleochroic from pale pink to green and occurs as small equant grains or as larger, poikilitic crystals. Cumulate layering is preserved in sample 48E from the Özyurt region (Fig. 1.2e) as alternating pyroxene-rich and plagioclase-rich bands. Plagioclase in unamphibolitized and undeformed gabbronorites has distinct, straight albite twinning. Amphibole occurs in all NMC gabbros and is either bluish-green or brown, and shows a wide variety of textures (Fig. 1.7).

The vast majority of gabbro samples from the NMC are amphibolitized. In these samples, hornblende is the predominant mafic mineral and occurs as polygonal textured mats (Fig. 1.7a), pseudomorphs of pyroxene (Fig. 1.7b), coronae around clinopyroxene, and less commonly as poikiloblasts (Fig. 1.6b) or fine-grained aggregates along grain boundaries. The hornblende in metagabbro of the NMC is typically magnesiohornblende and is pleochroic in shades of green or less commonly, brown. Relict clino- and/or orthopyroxene can commonly be observed at the center of a few hornblende grains even

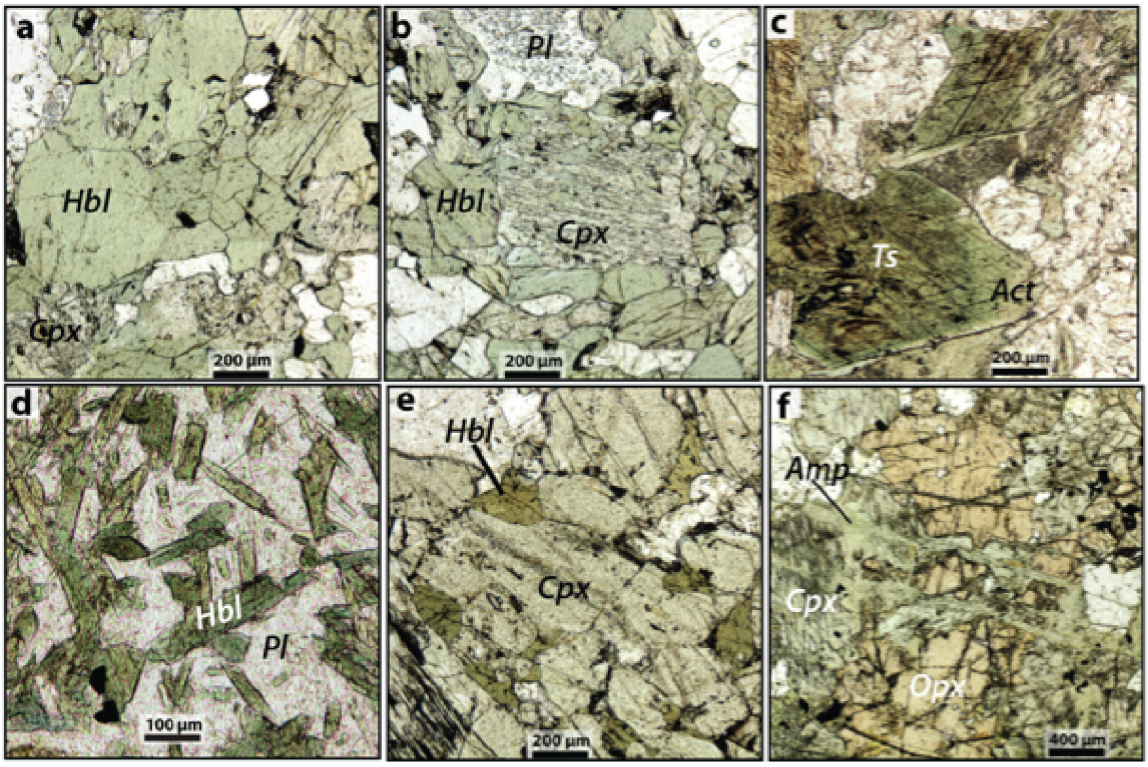

Figure 1.7: Some of the diverse amphibole textures observed in the field area. **a)** Sample ND15-48G, metagabbro from the NMC displaying polygonal texture of hornblende. **b)** Sample ND15-48G metagabbro from the NMC in which hornblende is partially replacing clinopyroxene. **c)** Sample ND15-53A, tschermakite gabbro from the Northern Region in which igneous textured tschermakite is rimmed by actinolite aggregates. **d)** Sample ND15-49B, diabase from the Çayrli conglomerate (Fig. 2a) displaying acicular, euhedral texture of hornblende. **e)** Sample ND15-48E, gabbronorite from the NMC with interstitial brown hornblende. **f)** Sample ND15-36A, gabbronorite from the NMC in which a vein of fine-grained amphibole crosses pyroxene. Act: Actinolite, Amp: amphibole, Cpx: clinopyroxene, Hbl: hornblende, Opx: orthopyroxene, Pl: plagioclase, Ts: tschermakite.

in the most severely amphibolitized samples. Plagioclase commonly has fuzzy and serrated phase boundaries with hornblende and has less defined twin planes in amphibolitized samples. In mylonitized gabbro, hornblende defines the foliation and is flattened or fish-shaped. Plagioclase in amphibolitized gabbros typically shows evidence for deformation, such as deformation twins, bent twins, undulose extinction or dynamic recrystallization features such as porphyroclast wings, amoeboid grain boundaries or grain size reduction. In one mylonitic gabbro (ND14-02B), feldspar porphyroclasts (An_{78-87}) are mantled by less anorthitic wings (An_{49-68}) (Appendix 2).

In the Northern Region, a diverse range of gabbro types was observed, including tschermakite gabbro (53A) in which euhedral, diamond shaped, poikilitic tschermakite and plagioclase (An_{85-91}) are overprinted by aggregates of needle-like actinolite (Fig.

1.7c). At the same location, pegmatitic hornblende gabbro (53C) intrudes uralitized gabbro. At Edikli, an olivine-clinopyroxene gabbro (34B, C) occurs in which an igneous texture is mostly preserved but the clinopyroxene contains blebs of hornblende with extremely variable compositions ranging from tremolitic hornblende (7.4 Si pfu) to tschermakite (6.4 Si pfu). In samples 34A and D from Edikli, a network of veins along which fibrous hornblende is concentrated displace plagioclase and amphibole grains.

Where preserved, igneous minerals such as calcic plagioclase and magnesian pyroxene are typical of magmatic rocks generated above intraoceanic subduction zones (Fig 8a; Burns, 1985). Igneous pyroxenes record the compositions of host magmas during crystallization and their compositions can be used as an indicator of tectonic affinity (Leterrier *et al.,* 1982; Beccaluva *et al*., 1989). The high Si and low Ti and Al content of analyzed clinopyroxenes indicates that they crystallized from a low or very low Ti magma typical of island-arc tholeiites and boninites (Figs. 1.8b-e). In addition, clinopyroxene from all three subregions of the study area are compositionally similar (Figs. 1.8b-e), suggesting a similar magmatic source despite differences in overall mineral assemblages and textures described above.

1.4.3 Plagiogranite

Plagiogranite dikes occur throughout the field area, in association with gabbro. In many cases, blocks of gabbro are present as inclusions in the granitic dikes. Mylonitic zones are commonly parallel to and concentrated along plagiogranite dike boundaries. In thin section, plagiogranite from the Niğde Mafic Complex has a bimodal grain size distribution with anhedral, interlobate grain boundaries indicative of dynamic recrystallization and recovery (see section 1.6 for detailed description of microstructures). Plagiogranites contain subequal amounts of quartz and plagioclase, with lesser amounts (5-30%) of amphibole. Perthite is observed in some protomylonitic plagiogranites. Hornblende (partially replaced by biotite) is the most common accessory phase in the plagiogranites, however in two samples cummingtonite occurs instead of hornblende. Cummingtonite is partially replaced by biotite and hornblende in sample 40A (Fig. 1.6c)

and by chlorite in sample 31. Zircon is also observed as an accessory phase in two protomylonitic samples (ND14-02E; ND15-09I).

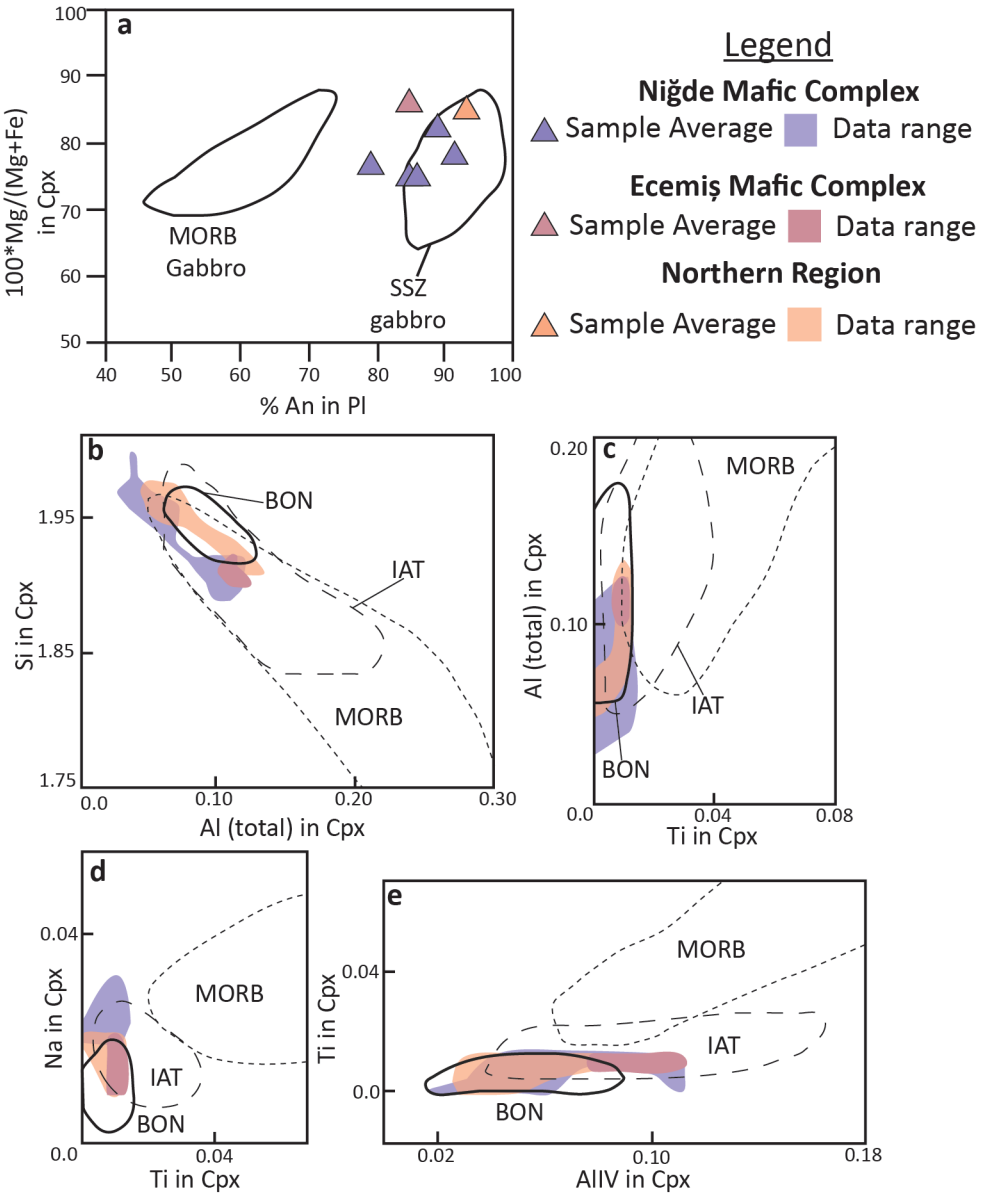

Figure 1.8: Tectonic discrimination diagrams based on mineral chemistry. **a)** % An vs. Mg# for coexisting plagioclase and clinopyroxene cores in gabbro from the various parts of the study area. Each triangle indicates the average of multiple grains within a single thin section, calculated using atomic proportions. Fields are based on Burns (1985) and Parlak *et al.* (1996). **b-e)** Covariations of various elements (in atomic proportions) with tectonic affinity fields from Beccaluva *et al.* (1989). Colored fields indicate the range for all analyses from multiple samples within each region. BON: boninite, Cpx: clinopyroxene, IAT: island-arc tholeiite, MORB: mid-ocean ridge basalt, Pl: Plagioclase, SSZ: suprasubduction zone.

Plagioclase in the granitoids has normal zoning and cores are variably saussuritized. In sample 40A, plagioclase compositions are An_{43-55} in cores and An_{27-35} in rims. Plagioclase twinning is typically faint (albite, pericline, Carlsbad) or absent, and twins are commonly bent or tapered as a result of deformation. Alkali feldspar shows perthitic lamellae and myrmeckite. Quartz shows undulose extinction and is dynamically recrystallized. Biotite is oriented in the plane of foliation along grain boundaries and replacing relict amphibole.

1.4.4 Diabase and Basalt

Metadiabase from the Niğde Mafic Complex occurs as aphanitic to porphyritic dikes or sills intruding the metagabbro. In thin section, diabase appears similar to the amphibolitized metagabbro but has a smaller overall grain size (~500 μm) and strongly zoned plagioclase phenocrysts and glomerocrysts, which have been transformed into porphyroclasts in deformed samples. The mineral assemblage for one metadiabase (sample 40B) is magnesiohornblende, normally zoned plagioclase (rims: An_{45-67}, cores: An_{74-91}), alkali feldspar, biotite and quartz. One sample (20) also preserves relict clinopyroxene. In the metamorphosed dikes, a bimodal grain size distribution and zoned plagioclase phenocrysts reveal the diabase protolith, however many also show a foliation defined by hornblende, a polygonal texture within hornblende mats, and interlobate phase boundaries between plagioclase and hornblende indicative of subsolidus recrystallization (Figs. 1.6d, e).

Comparison can be made between metadiabase of the Niğde Mafic Complex (samples 14, 20, 28, 29, 40B, 48C) and two unmetamorphosed samples inferred to be representative of its protolith - the Yıldıztepe basalt from the Northern Region (sample 53B; Fig. 1.2a) and a diabase boulder from a conglomerate near Çayırlı (sample 49B; Figs. 1.2a, 1.5b). The Yıldıztepe basalt is geochemically identical to diabase from the NMC (see section 5) and the Çayırlı diabase boulder has a similar texture and mineral assemblage to the metadiabase but lacks recrystallization or deformation features (Figs. 1.6f, 1.7d).

The Yıldıztepe basalt (sample 53B) is aphanitic (grain size ~100-200 μm) with an intergranular groundmass of roughly 50% amphibole, 40% plagioclase, 10% quartz and accessory Fe-Ti oxides. Amphibole in the Yıldıztepe Basalt contains cores of tschermakite and magnesiohornblende, but is mostly pseudomorphed by actinolite.

The Çayirli boulder (sample 49B) contains euhedral, zoned plagioclase phenocrysts and partially resorbed, twinned hornblende phenocrysts within a groundmass of plagioclase and hornblende (Fig. 1.6f). Groundmass hornblende in both of the unmetamorphosed samples is randomly oriented with acicular and diamond shaped cross sections (Fig. 1.7d). The lack of relict pyroxene in most (meta)diabase and basalt suggests that the primary mafic phase was amphibole in most of the dikes, perhaps tschermakite as observed in the Yıldıztepe basalt (sample 53B).

1.4.5 Ultramafic Rocks

Ultramafic rocks in the field area include hornblendite, clinopyroxenite and peridotite. Hornblendite (samples 38A, B), found near Özyurt in the Niğde Massif (Fig. 1.2e), contains coarse (1-5 mm), euhedral brown hornblende (tschermakite-magnesiohornblende) and minor clinopyroxene. Clinopyroxenite (samples 23, 27) from near Değirmenli (Fig. 1.2d) consists of coarse (>1 cm) clinopyroxene crystals that have been partially or fully replaced by mats of polygonal textured hornblende (Fig. 1.6g). In the Uluağaç high strain zone (Fig. 1.2c), hornblende-chlorite schist (Fig. 1.6h) occurs in the shear zone along with mylonitized gabbros and serpentinite boudins.

Peridotites in the region (Fig. 1.2) are typically serpentinized and appear to be either harzburgites or wehrlites based on the presence of both mesh and bastite textures, rarely with relict olivine and orthopyroxene. Accessory phases are spinel (magnetite, chromite and hercynite) and alteration products. Serpentinite tends not to outcrop and is typically observed only in excavations, roadcuts or gullies. Based on the higher number of observed serpentinite localities in the Ecemiş Mafic Complex and the Doğanlı Valley (Northern Region) (Fig. 1.2a), ultramafic rock appears to underlie much of the eastern part of the field area. In the NMC, metaperidotites occur only as small (meter scale) blocks typically near the contact with metasedimentary rocks.

Near Özyurt (Fig. 1.2e), undeformed, serpentinized talc-forsterite-tremolite rock occurs (samples 48A, D) containing elongate "jackstraw" or spinifex-textured olivine (cf. Evans and Trommsdorff, 1974). In these rocks, olivine (or mesh-textured serpentine pseudomorphs of olivine), occurs in a groundmass of talc and tremolite, in which tremolite has partially replaced talc (Fig. 1.6i).

1.5 Geochemical Features

Whole rock geochemistry was obtained for the mafic and felsic rocks of the study area as well as structurally lower, metabasic amphibolites interlayered with the Niğde Massif metasediments in order to ascertain their geochemical features and tectonic affinities. In addition, the NMC analyses were compared to literature data from other ophiolite bodies of the CAO and the Taurides in order to correlate them to a larger, regional ophiolite.

1.5.1 Methods

Samples analyzed for whole rock geochemistry include 6 diabase (Northern Region: 2; NMC: 4), 4 plagiogranite (Northern Region: 1; NMC: 3), 14 gabbro (EMC: 3; Northern Region: 1; NMC: 10) and 4 amphibolites (Aşıgediği Formation: 3; Gümüşler Formation: 1). The least altered and deformed samples from each lithologic group were analyzed for whole-rock geochemistry at Macalester College using a Philips PW-2400 X-ray fluorescence (XRF) spectrometer and Super-Q analytical software. Samples were crushed to gravel size in a Chipmunk jaw-crusher and further ground to a powder using a shatterbox. Tungsten carbide and steel containers were used to grind samples for major and trace element analysis, respectively. A detailed description of the preparation procedure and analytical methods is given in Vervoort *et al*. (2007).

Major element concentrations were determined from glass beads, fused from a mixture of rock powder, lithium metaborate/tetraborate, ammonium nitrate and hydrobromic acid solution. Loss on ignition (LOI) was calculated from the weight loss between drying (two hours at 105°C) and ignition (one hour at 1000°C). Trace-element concentrations were determined from pressed powder pellets. Pellets were constructed

from a mixture of rock powder and polyvinyl alcohol pressed in a stainless steel apparatus.

A subset of 7 gabbro (EMC: 2; Northern Region: 1; NMC: 4), 2 diabase (NMC), 1 basalt (Northern Region) and 2 amphibolite (Aşıgediği: 1; Gümüşler: 1) samples was further analyzed for rare earth and certain trace elements using inductively coupled plasma mass spectrometry (ICP-MS) after decomposition of 100 mg of rock powder in a mixture of hydrofluoric and nitric acids at the University of Wisconsin-Eau Claire. The tungsten-carbide container used for grinding samples used for ICP-MS resulted in contamination of Nb, thus interpretation of this element is made with caution. Incomplete zircon dissolution is reflected by anomalously low Zr and Hf values for the two amphibolite samples (ND01-32B and ND15-47B), as such the Zr and Hf values obtained using XRF are used instead for these two samples.

1.5.2 Whole-rock geochemical features of mafic rocks

Because many of the gabbros from the study area are strongly amphibolitized, it is necessary to use a geochemical indicator to identify cumulate gabbros prior to deriving tectonic or petrogenetic interpretations. Pearce (1996) suggests that samples with Ni > 200 ppm, Sc > 50 ppm and Al_2O_3> 20 wt. % may have significant accumulated olivine, pyroxene or plagioclase, respectively. For this study the Ni parameter was raised to 250 ppm in order to accommodate two of the three EMC gabbros that have Ni contents of ~225 ppm, but that do not have a cumulate texture.

Despite the range of textures and mineral assemblages, noncumulate gabbro of the Niğde Mafic Complex, Ecemiş Mafic Complex and Northern Region shows relatively limited major element compositional variation with SiO_2 contents between 46-50 wt. %, very low TiO_2 contents (.13-.45 wt. %) and Mg numbers between 61-87 (calculated as 100*Mg/(Mg+Fe) where total Fe_2O_3 was converted to Fe^{2+}). Basaltic diabase has SiO_2 from 49-55 wt. %, TiO_2 from .23-.49 and Mg # from 63-71. An andesitic diabase (sample 29) has SiO_2 of 61 wt. %, TiO_2 of .65 wt. % and Mg # of 46. Samples of mafic amphibolite from the Aşıgediği and Gümüşler formations of the Niğde Massif differ from the mafic complex rocks in having lower Mg # (48-60) and higher TiO_2 (.50-2.91 wt. %).

All of the gabbro and diabase from the mafic complexes are subalkaline and display a tholeiitic fractionation trend (Fig. 1.9). The gabbro and diabase are also characterized by Zr values of less than 30 ppm and low Ti/V ratios of 6-11, whereas Gümüşler and Aşıgediği amphibolites within the Niğde Massif have Zr contents from 58-295 ppm and Ti/V ratios of 27-72.

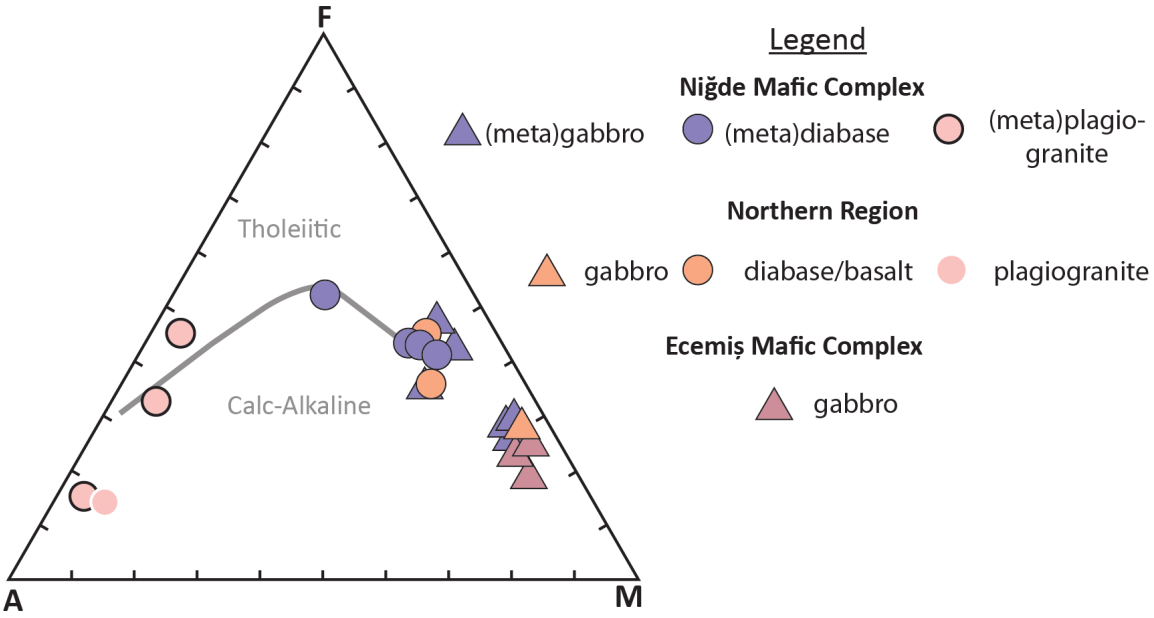

Figure 1.9: AFM diagram for various rock types found in the mafic complexes. Fields for calc-alkaline and tholeiitic rocks are from Irvine and Barager (1971). A=Na_2O+K_2O, F=FeO total (all Fe_2O_3 converted to FeO), M=MgO.

The low Ti/V ratios of the gabbro and diabase are typical of a suprasubduction zone environment (Shervais, 1982) (Fig. 1.10b). The mafic complex rocks have compositions that plot in the field of boninites (Figs. 1.10a, b), which are commonly associated with forearc or pre-arc settings (Pearce *et al.,* 1984). The strong depletion in high field strength elements (Hf, Zr, Ti) relative to MORB and variable enrichment in large ion lithophile elements (Sr, Rb, Ba) displayed by the gabbro (Fig. 1.11a) and diabase/basalt (Fig. 1.11b) is typical of suprasubduction zone magmas (Pearce *et al.*, 1984). The humped, enriched patterns displayed by the Gümüşler and Aşıgediği amphibolites (Fig. 1.11b) are more typical of incompatible-element enriched magma such as ocean island basalt (Pearce *et al*., 1984).

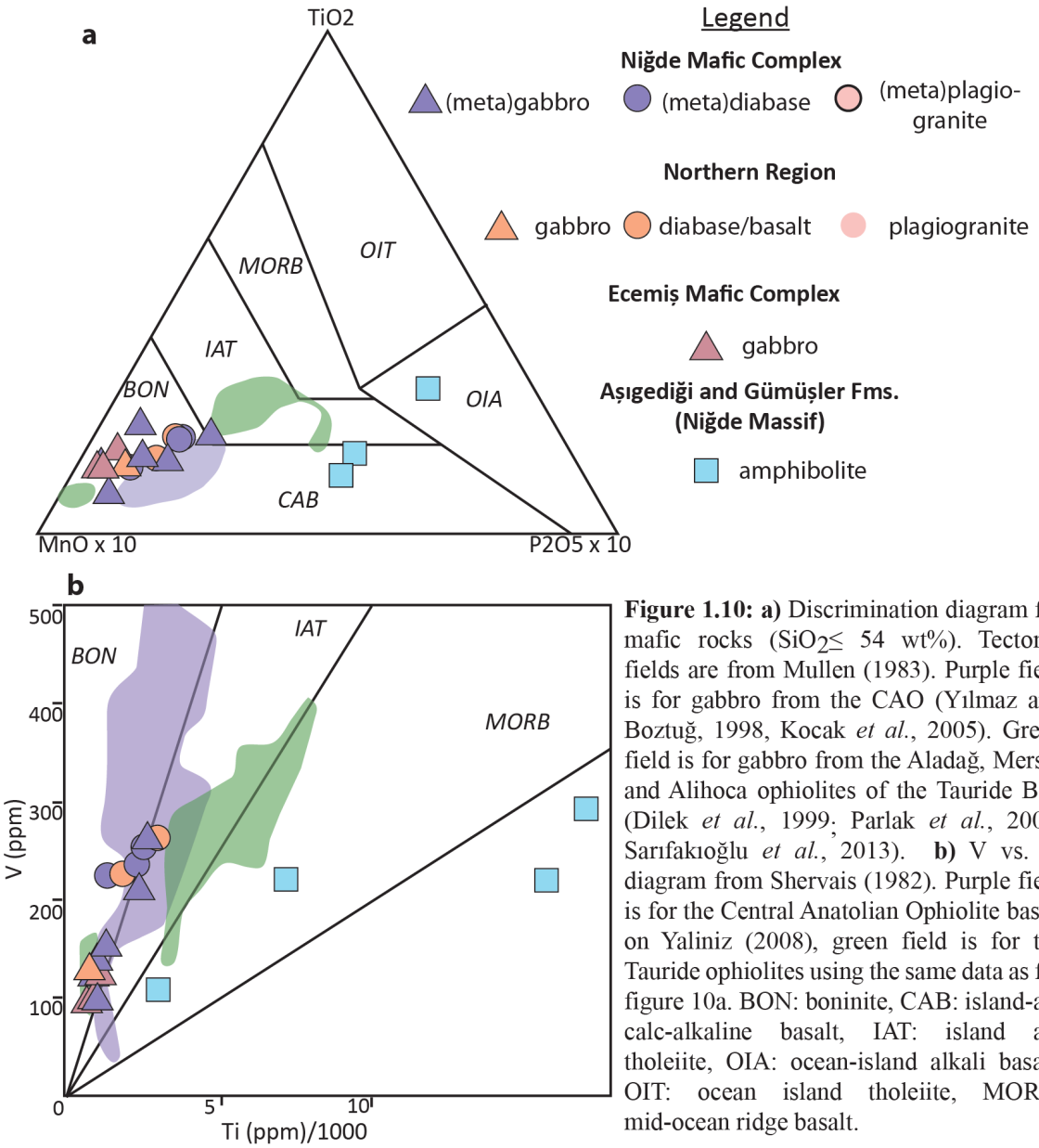

Figure 1.10: a) Discrimination diagram for mafic rocks ($SiO_2 \leq$ 54 wt%). Tectonic fields are from Mullen (1983). Purple field is for gabbro from the CAO (Yılmaz and Boztuğ, 1998, Kocak *et al.*, 2005). Green field is for gabbro from the Aladağ, Mersin and Alihoca ophiolites of the Tauride Belt (Dilek *et al.*, 1999; Parlak *et al.*, 2000; Sarıfakıoğlu *et al.*, 2013). **b)** V vs. Ti diagram from Shervais (1982). Purple field is for the Central Anatolian Ophiolite based on Yaliniz (2008), green field is for the Tauride ophiolites using the same data as for figure 10a. BON: boninite, CAB: island-arc calc-alkaline basalt, IAT: island arc tholeiite, OIA: ocean-island alkali basalt, OIT: ocean island tholeiite, MORB: mid-ocean ridge basalt.

The chondrite-normalized rare earth element diagram reveals strikingly similar patterns for gabbro from the NMC, EMC and Northern Region (Fig. 1.12a) with depleted LREE (La_N/Yb_N=0.40-0.89), a positive Eu anomaly, flat MREE, and flat or slightly negative HREE. Of the three diabase/basalt samples analyzed for REE (Fig. 1.12b), two (40A and 53B—Yildiztepe Basalt) show distinct patterns, with nearly flat or gently sloping patterns (La_N/Yb_N=0.96-2.19) and no significant Eu anomaly. A third diabase sample (28) has a pattern identical to the gabbro and was likely comagmatic with the main suite of gabbroic rocks. The amphibolites from the Aşıgediği and Gümüşler

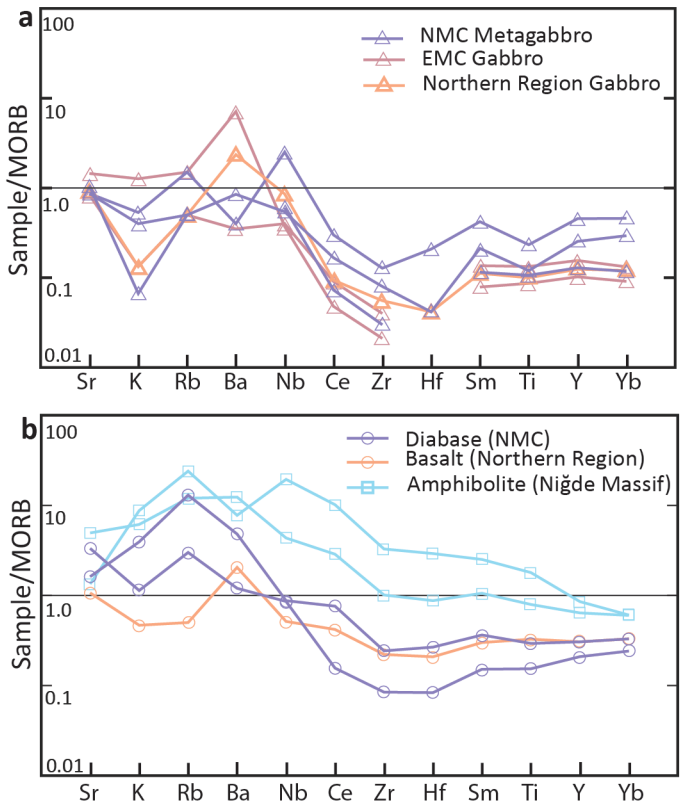

Figure 1.11: MORB-normalized incompatible element spider diagrams for mafic rocks of the study area. Normalizing values are from Pearce (1982). **a)** Comparison of gabbro from the three subregions within the study area. **b)** Diabase from the NMC, basalt from the Northern Region and amphibolite from the Aşıgediği and Gümüşler Formations of the Niğde Massif. EMC: Ecemiş Mafic Complex, NMC: Niğde Mafic Complex.

formations show a pattern distinct from both those previously described, with a negatively sloping pattern enriched in LREE (La_N/Yb_N=4.37-15.80; Fig. 1.12b). The negative slope of the Aşıgediği amphibolites indicates a fertile (undepleted) source, while the positive-humped slopes of the gabbro indicates a depleted N-MORB source for the NMC, EMC and Northern Region gabbros (Winter, 2010). The late dikes (40B, 53B) have a slightly more negative pattern that may reflect melting of a less depleted source or a lesser degree of partial melting with time. The distinct Eu anomaly in the gabbros may reflect the presence of high-Ca plagioclase, in which Eu is a compatible element.

Despite their widely varying mineral assemblages, rocks from the Niğde Mafic Complex, Ecemiş Mafic Complex and Northern Region are geochemically very similar. The main pattern that can be observed is the more magnesian nature of EMC gabbros (Fig. 1.9), consistent with their inferred position near the lowest part of the ophiolite. The Yıldıztepe basalt of the Northern Region (sample 53B) is nearly identical geochemically to a metadiabase dike from Aktaş, in the NMC (sample 40B; Fig. 1.2b) (Appendix 3). Samples from all three regions show a suprasubduction zone, depleted and subalkaline character.

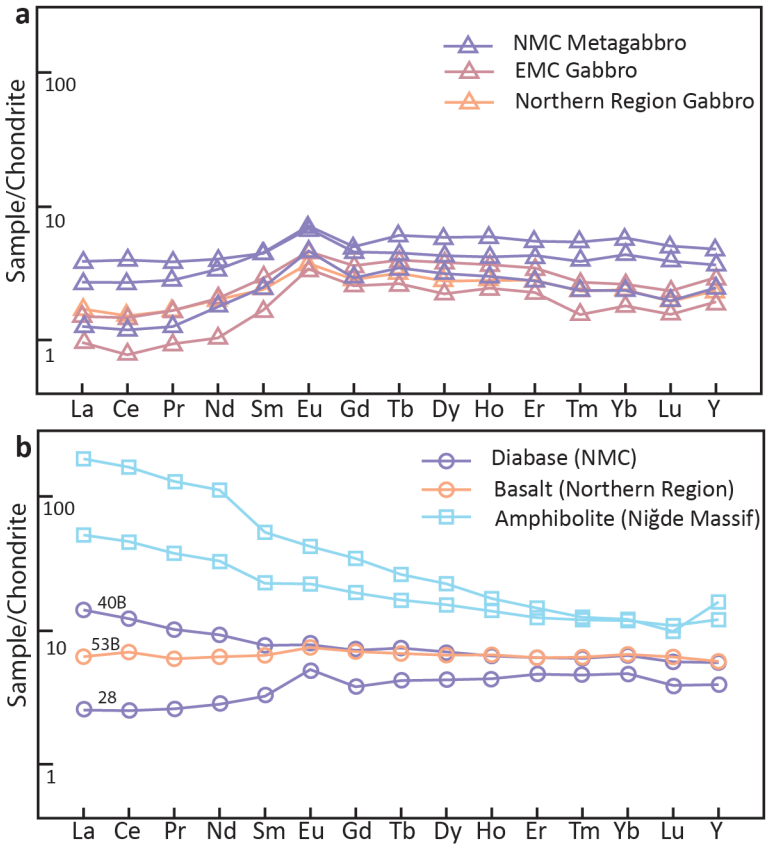

Figure 1.12: Chondrite-normalized rare earth element plots for mafic rocks of the study area. Normalizing values are from Sun and Mcdonough (1989). **a)** Gabbro from the NMC, EMC and Northern Region. **b)** Diabase from the NMC, basalt from the Northern Region and amphibolite from the Aşıgediği and Gümüşler Formations of the Niğde Massif. EMC: Ecemiş Mafic Complex, NMC: Niğde Mafic Complex.

Noncumulate gabbro (screened using the parameters Ni < 200 ppm, Sc < 50 ppm and Al_2O_3< 20 wt. %) from other parts of the Central Anatolian Ophiolite is also commonly boninitic (Figs. 1.10a, b). Nearby ophiolites of the Tauride Belt (Fig. 1.1a) typically have gabbro and diabase that plot in the field of island arc tholeiite, although lesser amounts of boninitic rocks also occur (Sarıfakioğlu *et al.,* 2013; Figs. 1.10a, b). Overall the geochemical features of the mafic complex gabbro and diabase are similar to their counterparts elsewhere in the CAO.

1.5.3 Geochemical features of plagiogranites

Plagiogranites from the study area (NMC and Northern Region) have SiO_2 contents from 73-79 wt. %, K_2O contents of 0.09-0.25 wt. % and Na_2O between 3.7-4.5 wt. %. The plagiogranites are calcic (Fig. 1.13a) and borderline metaluminous-peraluminous (A/CNK of .94-1.01).

Oceanic plagiogranites are characterized geochemically by having less than 1 wt. % K_2O, low Rb (less than 20 ppm) and calcic character (Pearce *et al*., 1984b; Maniar and Piccoli, 1989). The plagiogranites from the Niğde Mafic Complex and Northern Region

have the aforementioned characteristics, and trace element concentrations also reflect their origin in a subduction-influenced environment. Plagiogranites originating at suprasubduction zone ridges are influenced by slab-derived fluids and tend to show a combination of volcanic arc and ocean ridge geochemical characteristics (Pearce *et al*., 1984b). As shown in Fig. 1.13c, granitic samples from the mafic complex plot mostly in the field of volcanic arc granites or near the border with ocean ridge granites. Plagiogranites from the SSZ Troodos Ophiolite and the Sarıkaraman locality of the CAO have similar geochemical characteristics to the plagiogranites from the study area (Figs. 1.13b, c).

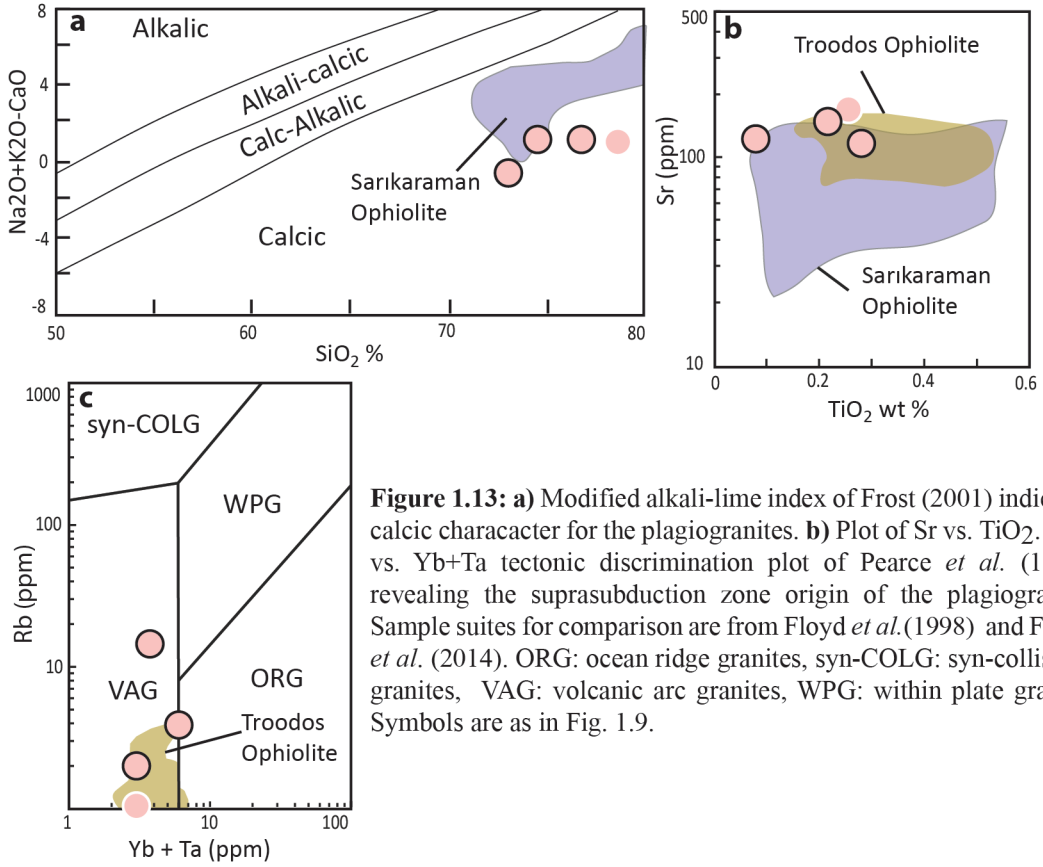

Figure 1.13: a) Modified alkali-lime index of Frost (2001) indicating calcic characacter for the plagiogranites. **b)** Plot of Sr vs. TiO_2. **c)** Rb vs. Yb+Ta tectonic discrimination plot of Pearce *et al.* (1984b) revealing the suprasubduction zone origin of the plagiogranites. Sample suites for comparison are from Floyd *et al.*(1998) and Freund *et al*. (2014). ORG: ocean ridge granites, syn-COLG: syn-collisional granites, VAG: volcanic arc granites, WPG: within plate granites. Symbols are as in Fig. 1.9.

1.6 Deformation Features

A notable feature of the Niğde Mafic Complex is the prevalence of foliation, layering and folding reflecting ductile deformation. Of interest is whether the deformation occurred prior to, during, or after ophiolite obduction. Comparison of the deformational and metamorphic features of the NMC to the adjacent Niğde Massif

metasedimentary rocks will reveal the timing of ophiolite emplacement with respect to tectonism and metamorphism and has implications for our understanding of the role of ophiolite obduction to development of the CACC.

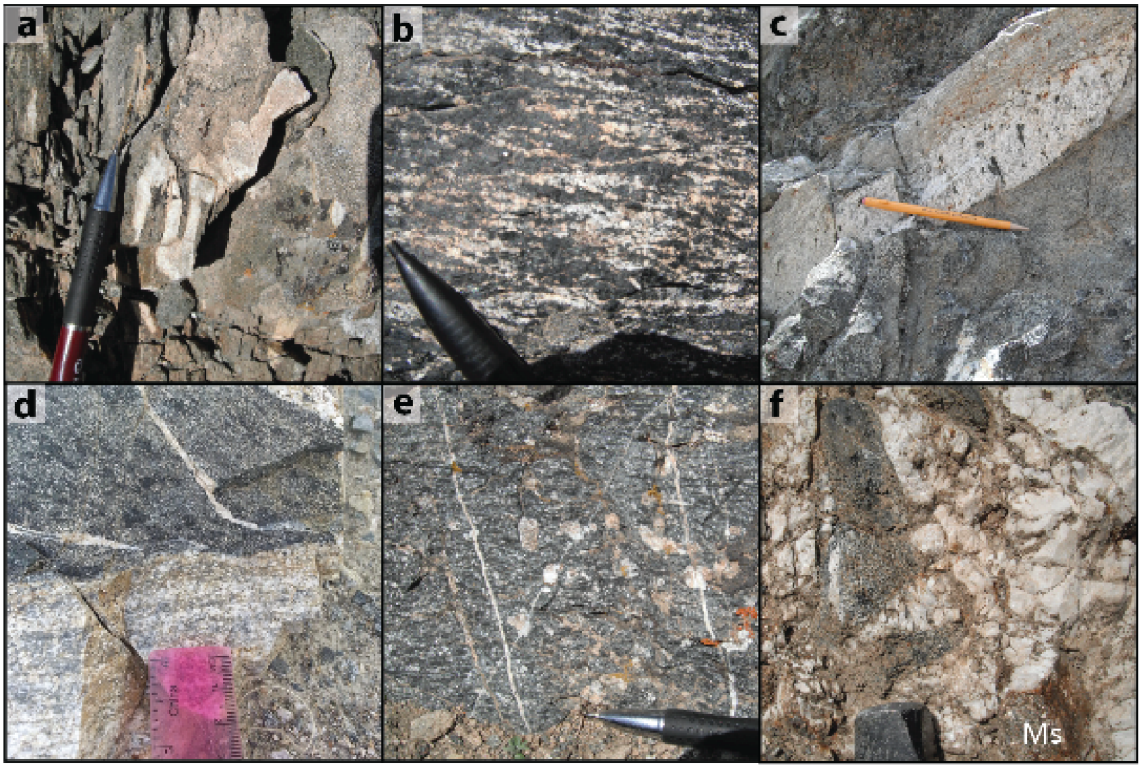

Figure 1.14: a) Isoclinally folded leucovein in metagabbro from the Uluağaç High Strain Zone (sample locality 51; Fig. 1.2c). **b)** Shear bands in metagabbro from near sample locality 11 (Fig. 1.2b). **c)** Folded plagiogranite dike, mylonitized along one margin (Aktaş High Strain Zone; Fig. 1.2b). **d)** Change in foliation plane at lithologic boundary (Aktaş High Strain Zone - sample locality 09; Fig. 1.2b). **e)** Foliated metadiabase partially retaining porphyritic texture (foliation is paralell to pencil). From sample locality 48c (Fig. 1.2e). **f)** Foliated block of gabbro in a granitic pegmatite dike, note the coarse muscovite book (Ms) in the right hand corner with sledge hammer head for scale. From sample locality 40 (Fig. 1.2b).

1.6.1 Structural Features

Foliations were observed at nearly all map stops in the Niğde Mafic Complex (Fig. 1.2b-e), while measurable foliations were not observed at the comparatively few stops in the Northern Region and EMC. Foliation in the NMC is typically defined by a layering of amphibole and plagioclase rich bands (Fig. 1.14b). Where more than 80% of the outcrop was mylonitized (recrystallized and foliated) a high strain zone is indicated on Figure 1.2. Away from high strain zones, deformation is highly variable with outcrop ranging from undeformed to foliated within a few meters, mylonitization is commonly

concentrated in narrow zones along lithologic contacts (Fig. 1.14c). Ductile deformation features observed in the NMC were folded dikes and veins, compositional layering, boudinage, foliation defined by amphibole and biotite and mylonitization (Figs. 1.14, 1.15). In some locations the foliation is deflected at dike contacts, giving the appearance that the dike crosscuts foliation (Fig. 1.14d). In the high strain zones, mafic and felsic dikes are transposed into the plane of foliation (Fig. 1.15). Mylonitization was observed to affect all NMC units (plagiogranite, diabase, ultramafic and gabbro) at the scale of the field area thus the main deformation phase post-dated intrusion of plagiogranite and diabase but pre-dated intrusion of undeformed, cross-cutting pegmatite and aplite dikes related to the Üçkapılı Granite, in which foliated gabbro xenoliths occur (Fig. 1.14f).

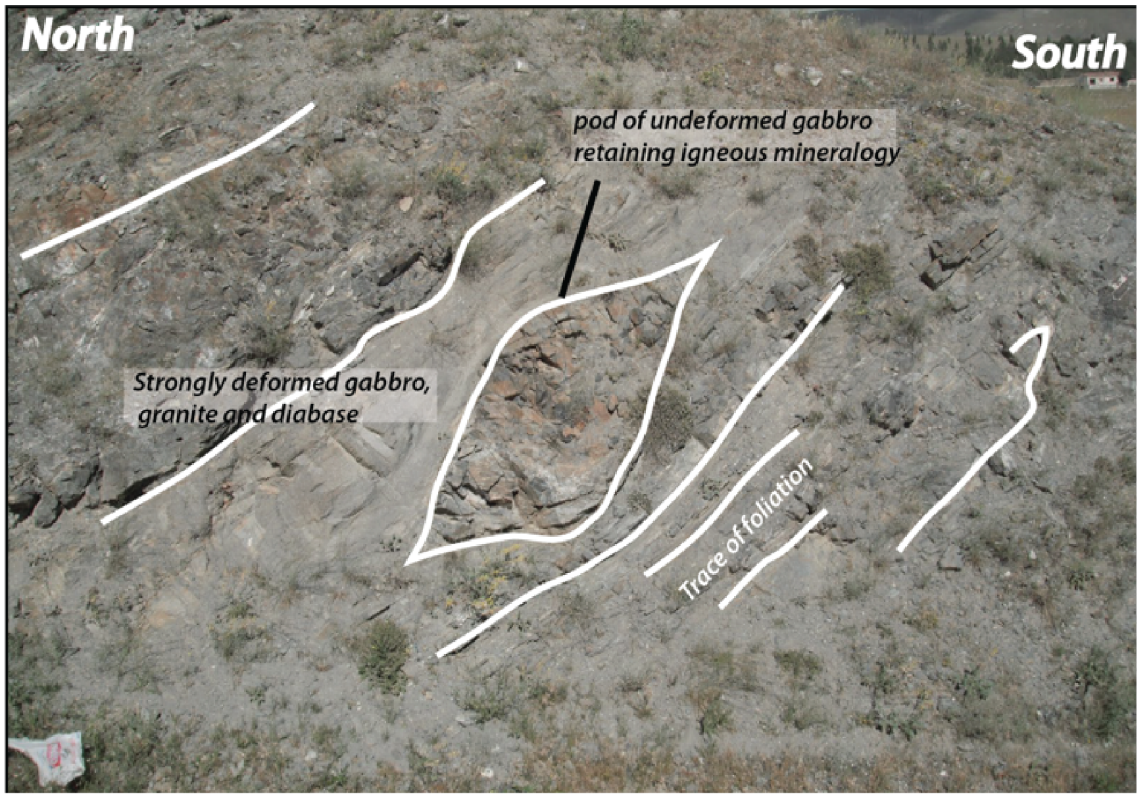

Figure 1.15: Mylonitized gabbro, diabase and plagiogranite at the Aktaş Dam high strain zone (Fig. 1.2b). Dike layers are transposed into the plane of foliation. A boudin of gabbro remains relatively undeformed.

In high strain zones, grain size is typically reduced (Fig. 1.14c) and planar mylonitic fabrics are developed within the various lithologies. Boudins of ultramafic or coarse-grained gabbro occur surrounded by banded mafic and felsic mylonite (Fig. 1.15). Foliations in the high strain zones are variable as a result of folding at different scales.

Isoclinally folded veins are common in high strain zones (Fig. 1.14a). High strain zones were only observed near the inferred contact between the mafic complex and the Gümüşler Formation and outcrops uphill from contacts typically showed less intense deformation with mylonitic rocks occurring in narrow zones.

Foliations in the mafic complex are typically north dipping (Figs. 1.2, 1.16), and concentric about the structural apex of the Niğde Massif (Fig. 1.2a) consistent with the orientation of foliation in the underlying metasedimentary rocks. Top-to-south dextral shear bands were observed in the field. Cross sections, constructed using foliation measurements from this study and from Gautier *et al.* (2008), indicate similar structural orientations within the metasedimentary Gümüşler and Aşıgediği units and within the mafic complex (Fig. 1.16). The resulting structure is one in which the mafic complex forms the uppermost layer of the core complex, folded in with the other units and dipping away from the structural apex of the dome. The mafic complex is in some locations mapped in contact with Gümüşler Formation (dominantly gneiss and schist) and in other locations in contact with Aşıgediği Formation (dominantly marble) (Figs. 1.2b-e). No direct contact was observed between the mafic complex and underlying units, however in those locations where metasedimentary and mafic complex rocks were exposed in close proximity (e.g., Özyurt, Fig. 1.2e) quartzite or marble was the closest non-igneous lithology and was in every case topographically lower than the mafic complex.

The MTA geologic map (Atabey, 1989) indicates that most of the metasedimentary bedrock in the northwestern Niğde Massif is the gneiss-dominated Gümüşler Formation. Gneiss was observed near contacts, but typically at structurally lower levels than marble or quartzite. In at least one location (sample locality 22; Fig. 1.2c), bedrock previously mapped as Gümüşler Formation turned out to be deformed mafic complex. In general, contacts where the adjacent unit is mapped as Gümüşler Formation were strongly tectonized both within the gabbro and in adjacent gneiss. At contacts where the adjacent lithology was observed to be marble/quartzite (Aşıgediği Formation), broad high strain zones were not observed, although mafic complex rocks are foliated and metamorphosed with narrow protomylonite zones throughout the NMC. The

top-to-south shear indicators, north-directed dips, isoclinal folds and broad distribution of strain are consistent with thrusting in a ductile deformation zone.

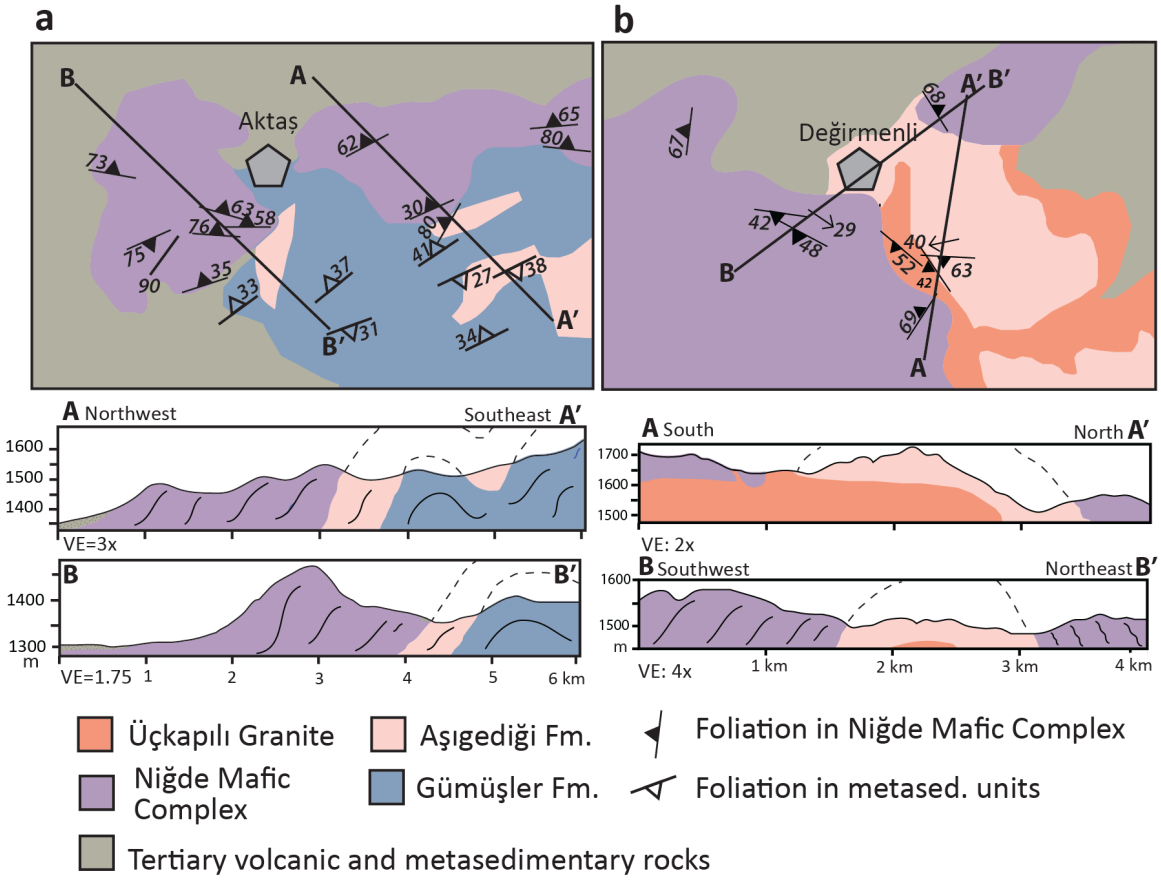

Figure 1.16: a) Cross sections through the Aktaş region (Fig. 1.2b) showing a folded, northward dipping structure. **b)** Cross sections through the Değirmenli region (Fig. 1.2c) showing the mafic complex and marble folded above a granitic intrusion. Foliations with empty triangles are from Gautier *et al.* (2008).

1.6.2 Deformation Microstructures: Niğde Mafic Complex

Microstructures in protomylonite from high strain zones indicate ductile deformation and synkinematic mineral growth. Plagiogranite mylonite from the Aktaş Dam high-strain zone (Fig. 1.2b) shows a core and mantle structure with feldspar porphyroclasts >1 mm in diameter that display deformation twins, undulose extinction and truncated concentric zoning (Fig. 1.17a). In the plagiogranite mylonites, disseminated, fine-grained biotite and hornblende define a foliation wrapping around porphyroclasts with polygonal, recrystallized feldspar and quartz (Fig. 1.17a, c). Coarser hornblende forms fish shaped and in some cases skeletal grains that have been partially

retrograded to biotite. Quartz is elongate and occurs as recrystallized grains, veins and in strain shadows. Quartz and feldspar in the mylonitized plagiogranites appears to be recrystallized by subgrain rotation (regime 2) as indicated by the presence of flattened porphyroclasts with subgrains and seriate grain size distribution. Myrmeckite is abundant in some of the plagiogranites and occurs along the plane of foliation within alkali feldspar porphyroclasts (Fig. 1.17b).

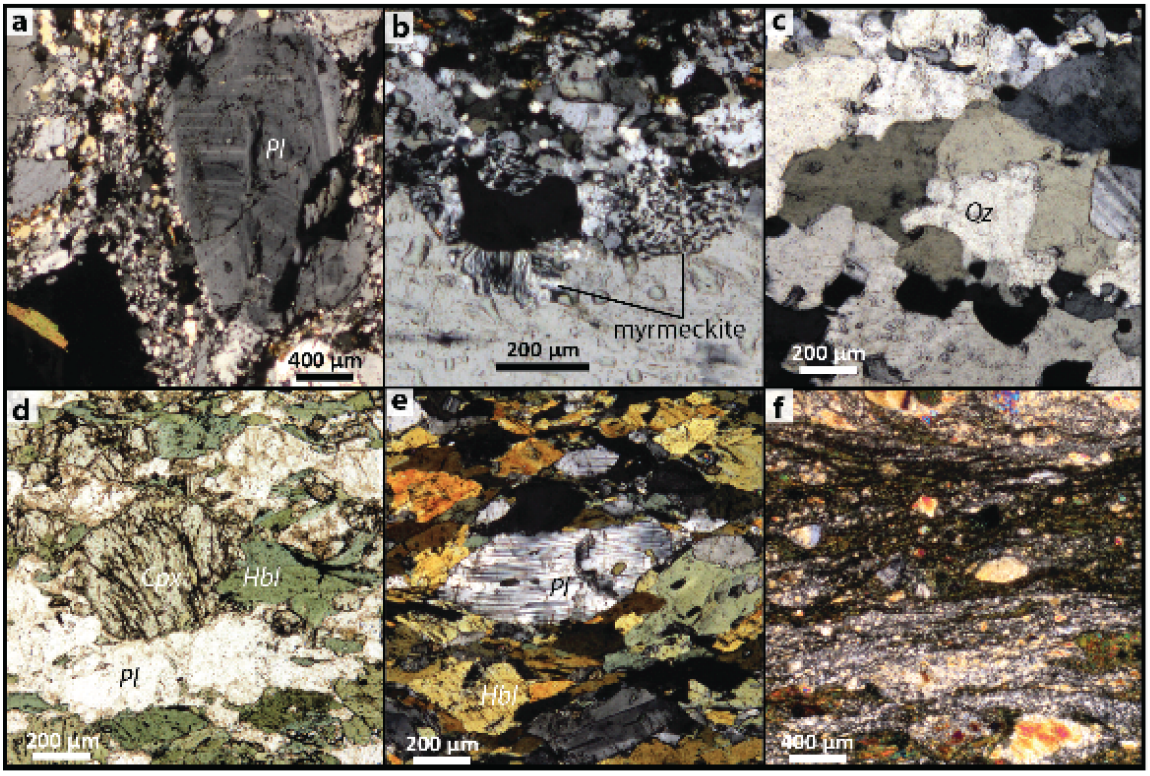

Figure 1.17: Deformation microstructures in the Niğde Mafic Complex and Northern Region. **a)** Plagiogranite mylonite showing core and mantle structure. Igneous zoning is truncated in the plagioclase porphyroclast (ND15-09I; Aktaş high strain zone (HSZ)). **b)** Myrmeckite colonies on an feldspar porphyroclast developed within the plane of foliation (ND15-09I; Aktaş HSZ). **c)** Subgrains in quartz indicative of dynamic recrystallization (ND14-02D; Aktaş HSZ). **d)** Mantled porphyroclast of clinopyroxene in which hornblende forms the rim (ND14-02B; Aktaş HSZ). **e)** Fabric in a gabbroic mylonite showing fish-shaped hornblende and a plagioclase porphyroclast with bent deformation twins (ND14-02A; Aktaş HSZ). **f)** Cataclasite developed in a metagabbro from the Northern Region (ND15-34D). Cpx: clinopyroxene, Hbl: hornblende, Pl: plagioclase, Qz: quartz.

Mylonitized metagabbro and diabase of the high strain zones are more equigranular and comprised of fish shaped hornblende and zoned porphyroclastic plagioclase (Fig. 1.17e) with An_{78-87} cores and An_{49-68} wings. Clinopyroxene grains are observed as mantled porphyroclasts with hornblende wings in some samples (Fig. 1.17d).

Highly deformed metadiabase samples can be distinguished in the field where dike contacts are identifiable, and have finer grain size than mylonitized gabbros and in some cases contain relict phenocrysts of plagioclase (Fig. 1.14e).

1.6.3 Deformation microstructures: Northern Region

In plagiogranite sample 31 from the Northern Region (Doğanli) (Fig. 1.2a), feldspar is not dramatically zoned and retains a coarse grain size (up to 5 mm). Quartz is dynamically recrystallized, whereas feldspar is not. Deformation features in plagioclase from this sample include deformation twins and undulose extinction. Quartz has a seriate grain size distribution and amoeboid grain boundaries. This sample also contains cummingtonite that is partially replaced by chlorite. Sample 34D is amphibolitized gabbro cut by a cataclasite zone containing angular feldspar in a microcrystalline groundmass and with amphibole stringers in the plane of foliation (Fig. 1.17f).

1.7 Thermobarometry

The thermal history of the Niğde Mafic Complex has been partially reconstructed using electron microprobe data (Appendix 4) and a number of geothermometers that provide information about conditions of igneous crystallization, metamorphism and deformation (Table 1.2).

Application of the two pyroxene geothermometer of Wells (1977) to four gabbronorites from the Niğde Mafic Complex and the Northern Region yields temperatures ranging from 842-954°C with an average of 883°C. These are interpreted as the temperatures of crystallization for the metagabbro protoliths.

Because of the diversity and textural ambiguity of some amphibole in the mafic complex, a Ti-in-hornblende geothermometer (Otten, 1984) was applied to amphiboles with less than 7.5 Si pfu (magnesiohornblende-tschermakite), in order to obtain a general estimate of formation temperature and especially to evaluate whether certain amphiboles may be magmatic or metamorphic. Because titanium is not in excess for all the samples for which this thermometer was applied, the temperatures reported represent a *minimum* formation temperature (Otten, 1984). Averages from each hornblende-bearing sample are

listed in Table 1.2; two averages are shown where a bimodal distribution of Ti content reflects two phases of amphibole crystallization. Average temperatures range from 579°C to 797°C.

	T (Primary)	T (Primary) Average	T (Secondary) Average	T (Secondary) at 5 kbar
Method	**Two-px**[1]	**Ti-in-Hbl**[2]	**Ti-in-Hbl**[2]	**Pl-Hbl**[3]
Sample no./unit				
ND14-02B/NMC	-	-	620	**681-741**
ND15-15/NMC	**867-895**	-	650	**736-786**
ND15-22C/NMC	-	-	693	**728-743**
ND15-34B/NR	**837-890**	-	599	-
ND15-36A/NMC	-	797	600	-
ND15-36B/NMC	**884-954**	-	599	-
ND15-40B/NMC	-	-	624	**680-762**
ND15-48E/NMC	**895-922**	-	-	-
ND15-51F/NMC	-	-	-	**559-620**
ND15-53A/NR	-	768	579	-
ND15-53B/NR	-	724	599	-
ND15-53C/NR	-	760	606	-

Table 1.2: Summary of thermobarometric results for mafic rocks (gabbro, diabase and basalt) of the study area All temperatures are in °C. Superscript in row two identifies the reference for each method: 1: Wells (1977), 2: Otten (1984), 3: Holland and Blundy (1994). Letters in column one indicate the region for each sample, NMC: Niğde Mafic Complex, NR: Northern Region. Preferred values are bolded (two-px and Pl-Hbl). Values from the Ti-in-Hbl method are for qualitative assessment only. '-' indicates that no calculation was made for that particular thermometer because of an inappropriate assemblage or mineral composition. See text for discussion.

The Holland and Blundy (1994) edenite-tremolite geothermometer was applied to analyzed assemblages containing paragenetic hornblende and plagioclase from the Niğde Mafic Complex. Calculated temperatures at 5 kbar are 736-786 °C for an amphibolitized gabbronorite from near Aktaş (sample 15; Figs. 1.2b, 1.18c) and 680-762 °C for a metadiabase from the same outcrop (sample 40B; Fig. 1.18d). A protomylonite from the Aktaş Dam high strain zone (sample 14-02B; Figs. 1.2b, 1.18a) yields temperatures from 681-741°C. Protomylonites from the western and eastern parts of the Uluağaç high strain zone (Fig. 1.2c) yield temperatures of 559-620°C (sample 51F) and 728-743°C (sample 22C; Fig. 1.18b) respectively.

In summary, the most reliable thermometers for the NMC mafic rocks (Wells, 1977 and Holland and Blundy, 1994) indicate igneous crystallization temperatures of 837-954°C and metamorphism/deformation temperatures from 559-786°C. Application of the single crystal Ti-in-hornblende thermometer of Otten (1984) provides minimum

temperatures that are in agreement with these findings as igneous-textured hornblendes yield temperatures of 724-797°C and metamorphic-textured hornblendes yield temperatures of 579-693°C.

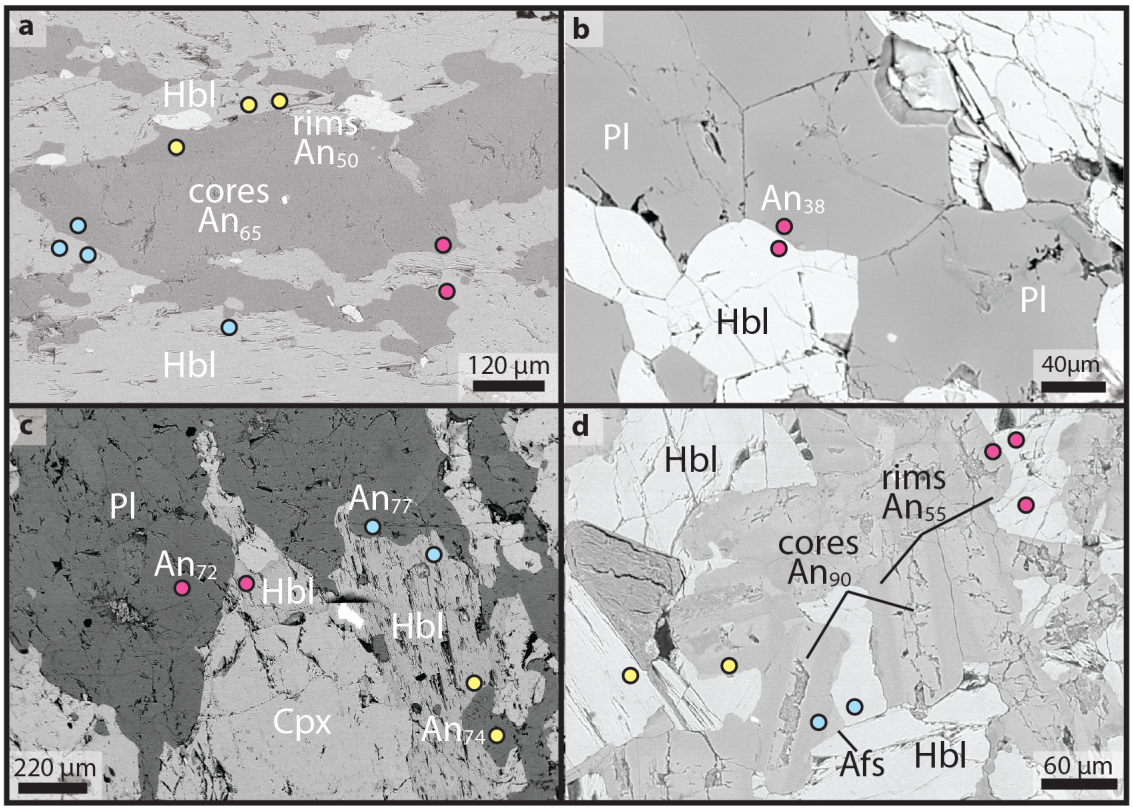

Figure 1.18: BSE image showing some of the points used for the Holland and Blundy (1994) plagioclase-hornblende geothermometer. All samples are from the Niğde Mafic Complex. **a)** ND14-02B, mylonite from the Aktaş high strain zone. **b)** ND15-22C: Amphibolite from the Uluağaç high strain zone. **c)** ND15-15: Metagabbronorite. **d)** ND15-40B: Metadiabase. Colored points identify plagioclase and hornblende pairs used for the calculations (Appendix 4). Afs: alkali feldspar, An: anorthite, Hbl: hornblende, Pl: plagioclase.

1.8. Discussion

The petrologic and structural features of the Niğde Mafic Complex have important implications for the origin of the Central Anatolian Ophiolite and for our understanding of the tectonic evolution of the Central Anatolian Crystalline Complex. In order to apply these findings to the regional tectonic evolution, a correlation of the NMC to the Central Anatolian Ophiolite must first be proven, thus I present the structural/field evidence for an ophiolitic origin of the NMC (Section 1.8.1) and an assessment of the tectonic setting of magmatic petrogenesis (Section 1.8.2). Once correlation to the CAO has been established, I discuss the metamorphic features of the NMC including an

evaluation of the various parageneses of amphibole in the mafic rocks of the NMC (Section 1.8.3) followed by a synthesis of the petrographic observations and thermobarometric data to determine the metamorphic grade of the NMC and the possible causes of metamorphism (Section 1.8.4). Finally these findings are incorporated into the regional tectonic context, and a model for Cretaceous development of the NMC is proposed (Section 1.8.5).

1.8.1 Origin of the mafic complex

Because of the fragmented nature of the Niğde Mafic Complex and because continental intrusive gabbro also occurs in the CACC metamorphic massifs (Kadıoğlu *et al*., 2003), the question of whether the NMC consists of ensialic intrusive gabbro (i.e., that intruded during the metamorphic and plutonic history of the Niğde Massif) or represents part of an ophiolite sequence that was tectonically emplaced onto the Niğde Massif needs to be evaluated. In the field, direct contact between the metasedimentary and gabbroic units was not observed. However, in some locations, metasedimentary and gabbroic rocks were found within tens of meters of one another; in this case, gabbro was uphill from marble, gneiss or quartzite (Figs. 1.2b-e). Cross sections, incorporating foliations from the various Niğde Massif units, reveal that the mafic complex is structurally higher than metasedimentary rocks and dipping away from the core of the dome (Fig. 1.16). High strain zones are common near the inferred contact, and unknown from higher portions of the mafic complex, suggesting that the contacts are tectonic.

The lack of intrusive field relations between the NMC and metasedimentary rocks suggests that these units were not in contact during the magmatic development of the NMC. No metasedimentary xenoliths were observed in the mafic complex and no diabase dikes were observed within the metasedimentary units, although diabase dikes are numerous in the mafic complex and crosscut gabbro. In the Niğde Massif, amphibolite interlayered with the metasedimentary units may have originally been intrusive or volcanic (Kocak *et al*., 2007) but does not represent intrusive offshoots of the NMC as it has very different chemical composition (Figs. 1.10-1.12; Appendix 3), mineral assemblage, and structural occurrence than the metagabbro and diabase of the NMC

(Floyd *et al*., 2000; this study). Autochthonous, intrusive rocks in the CACC metamorphic massifs are syn- to post-tectonic and mostly preserve relatively undeformed igneous mineral assemblages and textures (Kadıoğlu *et al*., 2003), whereas, as shown in this thesis, the plutonic rocks of the Niğde Mafic Complex have experienced substantial post-magmatic deformation and recrystallization.

The lithologic association of metaperidotite, plagiogranite, gabbro and diabase is characteristic of ophiolites and unlikely to occur in any continental intrusive mafic complex. Plagiogranite, gabbro and diabase from the NMC have a suprasubduction zone tectonic affinity, similar to other exposures of the CAO (Floyd *et al*., 2000). The pseudostratigraphy of the NMC is very similar to other exposures of the CAO, which are also thrust above metasedimentary units and intruded by granitoids of the late magmatic suite (Kocak and Leake, 1994; Yalılnız *et al*., 1996; Yılmaz *et al*., 1998). Mineralogic similarities between the Niğde Mafic Complex and other exposures of gabbro in the CAO include very calcic plagioclase ($An_{>68}$), magmatic tschermakite, secondary magnesiohornblende and two pyroxenes (Table 1.1). Overall the Niğde Mafic Complex correlates well with other exposures of the Central Anatolian Ophiolite, suggesting that they once formed a coherent ophiolite sheet that has since been fragmented and eroded.

Most previous studies of the CAO have suggested that the ophiolite was derived from an intra-oceanic subduction zone within the Izmir-Ankara-Erzincan Ocean to the north of the CACC (Yalılnız *et al*., 1996; Yılmaz and Boztuğ, 1998; Floyd *et al*., 2000; Yalılnız *et al*.; 2000; Yalılnız, 2008). However, the presence of Central Anatolian Ophiolite rocks at Niğde, in the southernmost part of the CACC, calls this into question. The distribution of lithologies within the CAO is contrary to what would be expected from south-directed emplacement, as ultramafic rocks representing the deepest part of the ophiolite are exposed primarily in the southeastern part of the CACC (Niğde Mafic Complex, Ecemiş Mafic Complex, Kuştepe, and Yeşilhisar/Doğanli; Fig. 1.1b) (Yalınız and Göncüoğlu, 1998; Ilbeyli, 2008; this study) and upper-level volcanic portions are best exposed in the north and west (Çiçekdağ, Sarıkaraman and Kaman; Fig. 1.1b).

Reconstructions based on paleomagnetic data (Görür *et al*., 1984; Lefebvre *et al*., 2013) indicate that large-scale block rotations within the CACC since latest Cretaceous

time have reorganized the terrane from an originally elongate north-south continent to its present wedge-shape (Fig. 1.19). Within this framework it is conceivable that obduction, at least of the southern portions of the CAO, occurred by underthrusting of the CACC microcontinent beneath an eastward (rather than northward) dipping subduction zone as has been suggested in some other paleotectonic studies (Görür *et al*., 1984; Van Hinsbergen *et al*., 2016).

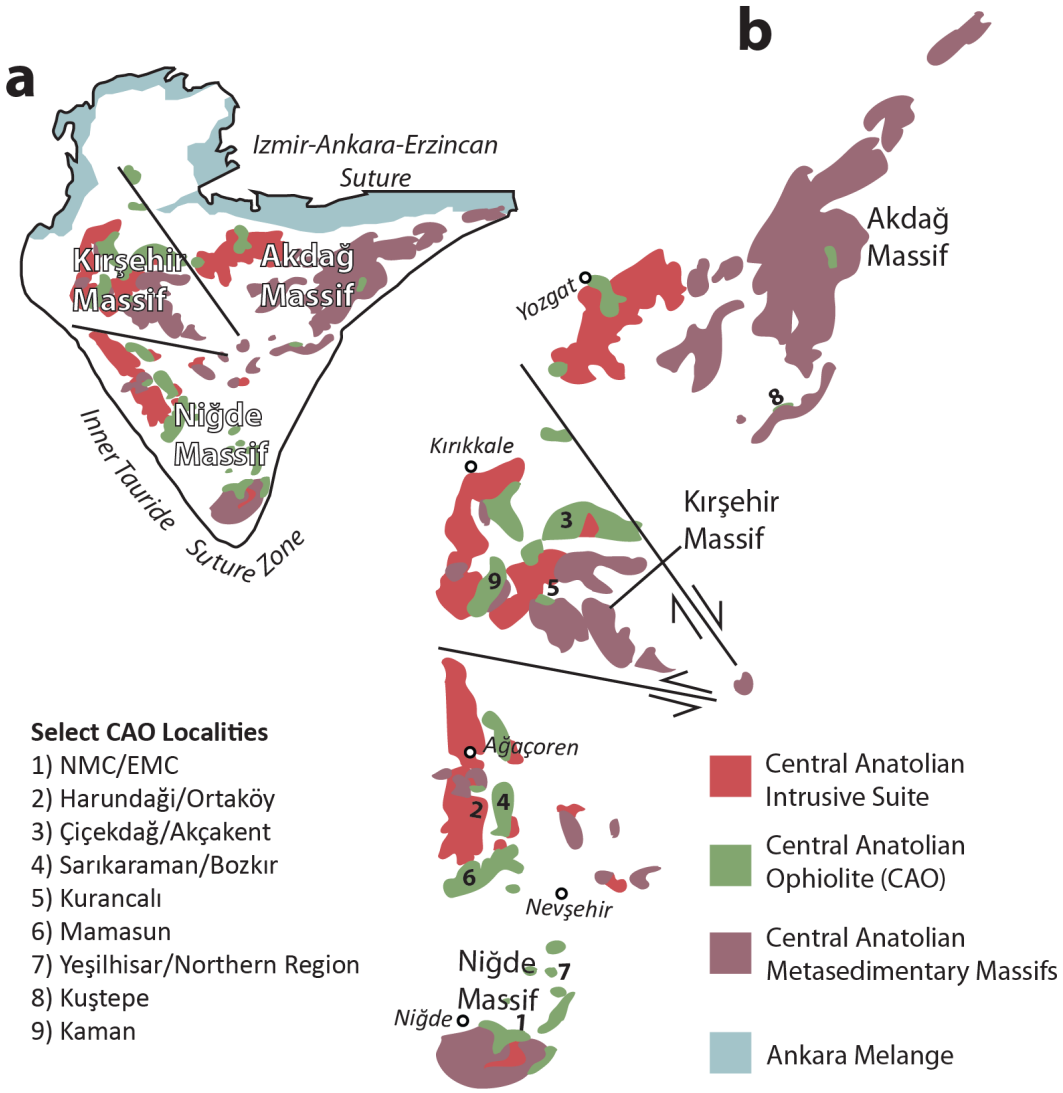

Figure 1.19: a) Reference map of the CACC in its present-day orientation with major metamorphic terranes labelled in white. **b)** Preferred Late Cretaceous reconstruction of Lefebvre *et al.* (2013) based on paleomagnetic data from the intrusive suite (red). Through block rotations and movement along internal strike-slip faults the CACC can be reconstructed as an elongate N-S arc. Figure modified from Lefebvre *et al*. (2011b).

1.8.2 Magmatic origin of the NMC

Petrologic features of the NMC gabbros such as the presence of magmatic hornblende, magnesian orthopyroxene, and calcic plagioclase, as well as the high Mg, low Ti geochemistry are typical of boninitic compositions commonly ascribed to a forearc or "pre-arc" tectonic affinity (Pearce *et al*., 1984a; Bloomer and Hawkins, 1987). Yalınız *et al*. (2008) observed similar compositions for mafic rocks of the Çiçekdağ, Sarıkaraman and Bozkır localities (Fig. 1.1b – localities 3&4) and interpreted a forearc affinity and highly depleted melt source for the CAO. Boninitic magmas are commonly considered to represent the earliest stage of rifting above an intraoceanic subduction zone and their attributes are commonly ascribed to a high degree of melting of depleted mantle in the presence of slab derived fluids and water (Bloomer and Hawkins, 1987). In the case of subduction initiation, shallow levels of depleted mantle are melted to create initial magmas with boninitic compositions, and as the subduction zone matures and melting moves to deeper, less depleted parts of the mantle wedge, magmas with island-arc tholeiite (IAT) affinities are generated (Bloomer and Hawkins, 1987). In other examples, however, the opposite trend occurs and IAT, followed by boninitic magmas are generated; in this case the boninites are inferred to represent shallow melting of lithospheric mantle that has been depleted by the preceding IAT magmatism (e.g. Dilek and Thy, 2009). Gabbro of the NMC, EMC and Northern Region has low high field strength element contents and is depleted in LREE indicating a very depleted mantle source (Figs. 1.11, 1.12). Later diabase and basalt, while also boninitic, appear to come from a slightly more enriched source possibly indicating initial melting of shallow, highly depleted mantle to form the gabbros, followed by deeper melting of less depleted mantle to form the late mafic dikes as in the subduction initiation hypothesis of Bloomer and Hawkins (1987).

1.8.3 Textural and geochemical evaluation of amphibole

Hornblende from mafic rocks in the study area displays a wide range of textures (Fig. 1.7) and chemical compositions (Fig. 1.20). The exact origin of ubiquitous hornblende in the CAO has not been resolved, and in some cases there are multiple

parageneses of hornblende even within individual samples. Depending on textures, mineral compositions and thermobarometric results, three types of amphibole from the field area are distinguished that represent three sets of formation conditions: 1) magmatic crystallization, 2) low-grade, static metamorphism, and 3) medium-grade syn-deformation metamorphism.

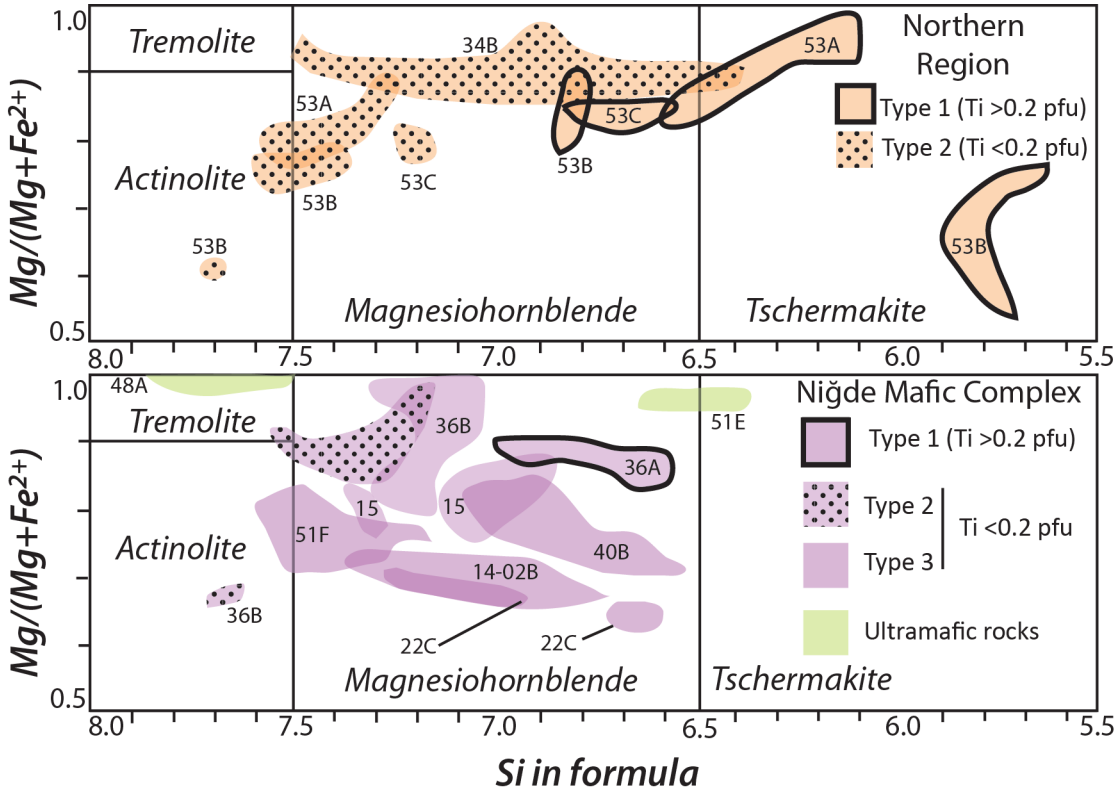

Figure 1.20: Plot of Si vs Mg/(Mg+Fe) pfu for amphibole n the study area. Compositional fields are from Leake *et al*. (1997). Colored fields show the various compositions of amphibole from individual thin sections. Purple indicates Niğde Mafic Complex (NMC) gabbro/diabase, orange indicates Northern Region gabbro/basalt, green indicates ultramafic rock of the NMC. Numbers refer to the sample number. Distinctions between amphibole types 1, 2 and 3 are discussed in Section 1.8.3.

Magmatic amphiboles (Type-1) are best represented by samples 53A, B and C, and are euhedral, randomly oriented, diamond shaped and acicular. They are typically brownish in color. Euhedral amphiboles may be partially or fully pseudomorphed by actinolite (Fig. 1.7c), which only forms during relatively low-grade metamorphism (Deer *et al*., 1992). However, cores of these euhedral grains preserve high Ti tschermakitic hornblende (fields outlined in black, Fig. 1.20). As shown by Otten (1984), higher Ti contents are directly related to temperature of formation, and thus the combined

observations of high Ti content and euhedral texture clearly indicate a magmatic origin for some amphiboles in the field area. In one sample from the Niğde Mafic Complex (36A), brown hornblende has high Ti contents but irregular phase boundaries with pyroxene and plagioclase. In this case the high temperature implied by the Ti, and the interstitial, reactive texture, point toward a late magmatic origin.

Type-2 amphiboles include actinolite and magnesiohornblende but typically compositions fall within or close to the actinolite field (spotted fields, Fig. 1.20). Sample 34B from the Northern Region is different in having amphibole with a wide range of compositions spanning the entire field of magnesiohornblende and into the field of tschermakite. Type-2 amphiboles are unoriented and occur as rims on or blebs within clinopyroxene or magmatic hornblende. In some cases actinolitic amphiboles have developed along grain boundaries or in veins. These commonly have a fibrous or uralitic appearance and are light green in color. Samples containing type-2 amphibole are unfoliated and preserve magmatic minerals such as pyroxene, high Ti tschermakitic hornblende and anorthite. Some phases in type-2 amphibole bearing rocks show evidence of deformation such as cracking, undulose extinction or deformation twins, but lack abundant dynamic recrystallization microstructures or any preferred orientation of the metamorphic amphibole. Features of type-2 amphibole from the field area are similar to those of hydrothermally altered gabbros and dikes from ocean-floor metamorphosed rocks. For example, Mevel (1988) found that gabbros that were hydrothermally metamorphosed under static conditions preserved igneous textures, developed actinolite as rims on clinopyroxene, and contained compositionally heterogeneous amphibole. Alt *et al*. (1996) also found wide ranges of amphibole composition at the thin section scale for hydrothermally altered sheeted dike complexes, similar to what is observed in sample 34b (Fig. 1.20).

Type-3 amphiboles are identified only in the NMC and are low Ti magnesiohornblende with the exception of some analyses from sample 51F, which are actinolitic. These amphiboles are darker green than type-2 and show a foliated or granoblastic texture. A few foliated NMC amphibolites (22A,C; 50A,E) contain low Ti, brown hornblende. The type-3 hornblendes occur in clusters of polygonal textured grains.

In more strongly deformed samples the hornblende is fish shaped indicating syn-kinematic recrystallization. Type-3 hornblende does not occur with high-Ti hornblende and igneous textures are generally not well preserved in these rocks, although igneous phases such as pyroxene are preserved as relicts. The edenite-tremolite thermometer of Holland and Blundy (1994) indicates conditions of ~700°C for type-3 hornblende with the exception of sample 51F (~600°C) (Table 1.2).

The occurrence of two distinct types of metamorphic hornblende in the mafic rocks could imply a metamorphic gradient, since lower temperature type-2 amphiboles are mostly found in the Northern Region and high temperature type-3 amphiboles are observed only from the NMC (Fig. 1.20), or it could imply two separate metamorphic events; for example, an ocean floor metamorphism that affected much of the CAO including the NMC, EMC and Northern Region, but that was overprinted by amphibolite-facies metamorphism that affected the NMC only. Evidence for the latter is the occurrence of type-2 (static, low temperature) amphibole in sample 36A (Fig. 1.7f) from the NMC, which otherwise contains type-3 (synkinematic) amphibole.

1.8.4 Metamorphic grade of the Niğde Mafic Complex and cause of metamorphism

In the NMC, mineral assemblages from all four mafic complex lithologies (gabbro, diabase, plagiogranite and ultramafic rock) reveal amphibolite facies metamorphic conditions for deformation and recrystallization. Gabbro and diabase have developed magnesiohornblende and secondary plagioclase. Plagiogranite shows retrogression of amphibole to biotite and metaperidotite has an isofacial assemblage of talc-tremolite-forsterite. With the exception of the metaperidotite, all of the above assemblages are synkinematic.

The occurrence of the jackstraw-textured metaperidotite is a striking metamorphic feature of the NMC because of the relative rarity of this type of rock. It has been reported from orogenic settings such as the Alps (Evans and Trommsdorff, 1974) and Caledonides (Bakke and Korneliussen, 1986) and in exhumed subduction zones (Trommsdorff *et al*., 1998; Padrón-Navarta *et al*., 2011) as well as contact metamorphic aureoles (Evans and Trommsdorff, 1974). The jackstraw texture is well developed in one sample (48D; Fig.

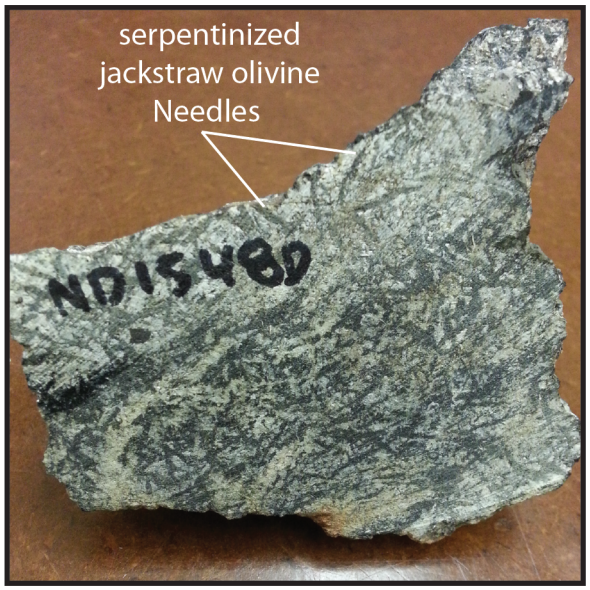

Figure 1.21: Hand sample photo of sample 48D, a metaperidotite from near Özyurt (Fig. 1.2e). The needle-like features are serpentine pseudomorphs of elongate, metamorphic olivine. The light colored matrix is a mixture of talc and tremolite.

1.21), which contains abundant talc, whereas it is somewhat less well developed in a more tremolite rich sample (48A). The elongate shape of the olivine indicates its metamorphic and not relict origin, as elongate igneous olivine is uncommon, aside from in spinifex-textured komatiites (Evans and Trommsdorff, 1974). The development of jackstraw-textured olivine is thought to occur during prograde metamorphism of serpentinite and be a response to the depletion halo developed in serpentine owing to olivine crystallization that results in preferential growth in the direction with the smallest face (in this case (001)) (Bakke and Korneliussen, 1981). The assemblage is stable over a relatively narrow range, indicative of temperatures between 550-650°C (Winter, 2010).

Microstructural evidence, including foliation parallel myrmeckite, dynamic recrystallization of plagioclase, and subgrain rotation suggest deformation conditions in excess of 600°C (Passchier and Trouw, 2005). The above indicators are in agreement with results of plagioclase-hornblende thermometry from the NMC mafic mylonites, which also indicate amphibolite facies conditions for syntectonic assemblages. Overall the evidence overwhelmingly suggests middle-upper amphibolite facies temperatures for metamorphism of the Niğde Mafic Complex.

Although the Northern Region was not mapped in detail, the few samples obtained from this area suggest a lower grade of metamorphism. Cummingtonite in a plagiogranite from the Northern Region (sample 31) is partially replaced by chlorite (typical of greenschist facies), whereas in the NMC it is replaced by biotite and hornblende (typical of amphibolite facies). Gabbro and basalt at Yıldıztepe (Northern

Region) have actinolitic secondary amphibole and preserve igneous textures. Where present, deformation microstructures in the Northern Region also suggest lower grade conditions. Plagiogranite with recrystallized quartz but lack of core-mantle structure in plagioclase suggests temperatures of 400-600°C. Cataclasitized gabbro from Edikli implies brittle conditions, but could also have developed during a different event (i.e. exhumation or later faulting). Uralite gabbros were common in the Northern Region, but foliated amphibolites with recrystallized hornblende and plagioclase were not observed. Assemblages and microstructures from the Northern Region may be compatible with alteration owing to ocean-floor metamorphism and future work could involve evaluation of trace elements, such as chlorine, in amphibole to assess this hypothesis (cf. Coogan *et al*., 2001). The Ecemiş Mafic Complex also lacks a high-grade metamorphic overprint, and it is variably serpentinized or retrograded to greenschist-facies assemblages, potentially also reflecting ocean-floor metamorphism.

The geochemical similarities between the three regions supports that they were derived from the same ophiolite sheet, but the petrologic differences indicate separate metamorphic histories. The apparent metamorphic gradient between the Niğde Mafic Complex and Northern Region can be explained either by considering a buried detachment fault somewhere north of the NMC (Fig. 1.22), or simply broad scale folding, in which case the basement sequence is tilted northward, away from the high grade dome. The preservation of igneous textures and low-grade metamorphic overprint of the Ecemiş Mafic Complex, despite its origin in the lowest section of the ophiolite, suggests that it has become juxtaposed to the high-grade Niğde Massif owing to thrusting that postdated the main metamorphism, potentially related to motion of the nearby Ecemiş Fault.

Amphibolite facies conditions of >700°C are recorded for metasedimentary rocks in the high-grade core of the Niğde Massif (Whitney and Dilek, 1998; Whitney *et al*., 2003, 2007) and thus the Niğde Mafic Complex (recording temperatures of 550-790°C) does not have a significantly lower grade than the metasediments as suggested by Gautier *et al*. (2002, 2008). Preservation of igneous fabrics (such as dike/vein contacts) and coarse grain size is somewhat common in metagabbro because the retrograde reactions that occur (e.g. Cpx→Hbl) require hydration and fluid pathways, which are not always

available (Bucher and Grapes, 2015). There is no evidence from the metamorphic or structural features of the mafic complex that a detachment existed (i.e. near Özyurt; Fig. 1.2a, e) directly between the presently exposed gabbroic units and the metasedimentary rocks as indicated by Gautier *et al.* (2008).

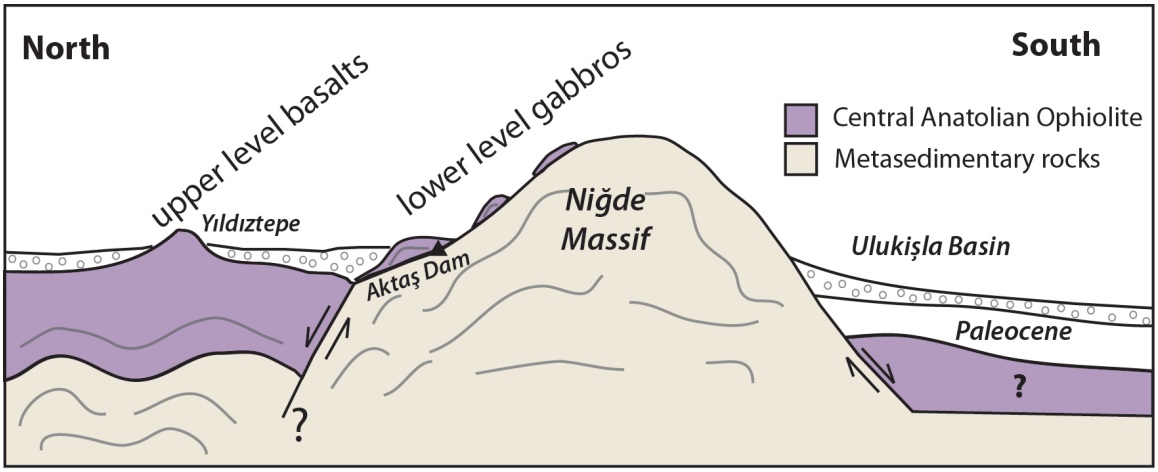

Figure 1.22: Schematic cross section through the study area to explain the metamorphic gradient observed between the Niğde Mafic Complex and the Northern Region. The Niğde Mafic Complex is the lowermost part of the Central Anatolian Ophiolite, in direct contact with the metasedimentary rocks, while areas to the north may be upper levels of the ophiolite. A buried detachment fault may or may not exist north of the Niğde Massif to explain the observed metamorphic difference.

Comparison of the NMC to ophiolite metamorphic soles

Amphibolite in ophiolites may occur as a "metamorphic sole," a feature that develops owing to deformation and heating as a subducting oceanic plate is accreted to the upper plate during the early stages of intra-oceanic subduction and obduction (Williams and Smyth, 1973; Hacker, 1990). Although highly deformed and interpreted as an ophiolite, the NMC is very unlike a metamorphic sole in the following ways: 1) Metamorphic soles are characterized by a variable or inverted metamorphic gradient, from granulite through greenschist facies, whereas similar amphibolite facies conditions were encountered throughout the NMC. Lower grade gabbros of the EMC and Northern Region are relatively undeformed and thus cannot be part of a metamorphic sole. 2) Metamorphic soles occur where the peridotitic mantle of the upper plate is thrust above the upper, basaltic crust of the lower plate; however, the NMC metagabbros are more typical of the lower oceanic crust and there is no evidence that they were or are structurally lower than tectonized peridotites. 3) Greenschist-amphibolite facies

metamorphic soles should have a maximum ~500 m thickness (Hacker, 1990). It is not possible to tell the original orientation and therefore thickness of the NMC, but based on vertical relief within individual gabbro hills (i.e. Özyurt/Değirmenli; Fig. 1.2b-e) it is a minimum of 400 m thick, but almost certainly much thicker based on the high angle of the foliations and lithologic contacts (Fig. 1.16). 4) Finally, metamorphic soles typically consist of multiple lithologies of varying metamorphic grades thrust together during the obduction process (Hacker, 1990), whereas the NMC is overall a coherent but ductilely deformed block of similar grade, lower oceanic crust without major internal thrusts or intercalated metasedimentary units.

Comparison to Ocean Floor Metamorphism

Amphibolite facies conditions occur locally in ocean floor metamorphism (Alt, 1995). However, the ductile, compressional structures observed in the NMC (Figs. 1.14-1.16) are incompatible with ocean floor hydrothermal metamorphism, which requires extension and cracking in order for water to infiltrate the dense oceanic crust (Alt, 1995). Even if the NMC metamorphism was pre-obduction, it would require the complex and coincidental scenario of obducting an amphibolite-facies oceanic terrane onto exhumed, amphibolite facies continental crust with similarly oriented foliations. This is difficult to explain in terms of geochronology, as the exhumation path of the Niğde Massif is well documented (Fig. 1.3) and the ophiolite has been intruded by crustal granites, of which the youngest in the Niğde Massif intruded at ~85 Ma during exhumation (Whitney *et al*., 2003).

Metamorphism in a continental orogen

The simplest and most satisfactory explanation for the metamorphism and deformation of the NMC is regional metamorphism within a dominantly continental orogenic wedge. Therefore, we propose that ophiolite emplacement preceded and was a contributing event in the prograde metamorphic path of the Niğde Massif as a whole. The Niğde Massif was metamorphosed in a transpressional orogen in Late Cretaceous time as evidenced by the long (92-78 Ma) period of high-grade metamorphism and crustal

melting (Whitney *et al*., 2003) and subhorizontal lineations roughly parallel to the Ecemiş (Central Anatolian) Fault (Whitney *et al.,* 2001, 2007). The high-grade, ductile middle crust was exhumed in a transtensional regime and cooled to below ~350°C by 74 Ma (Whitney *et al*., 2007). Based on the age of ophiolite metamorphic soles and arc magmatism, subduction was occurring in the Inner Tauride ocean until at least 92-89 Ma (Dilek *et al*., 1999; Parlak *et al.,* 2013), and along the Izmir-Ankara-Erzincan ocean until Maastrichtian time (Görür *et al*., 1984), thus it is likely that the CACC was still mostly bordered by oceanic crust at ~91 Ma whilst undergoing the main phase of orogenic thickening. This begs the question of whether oblique collision between the CACC and adjacent oceanic plates could cause the metamorphic and deformational features observed in the CACC, and particularly the Niğde Massif.

1.8.5 Tectonic model for the development of the Niğde Mafic Complex

Integrating the above data and interpretations it becomes clear that the presence of amphibolite facies metaophiolite in the Niğde Massif has important implications for the development of Central Anatolia. The main conclusions from this study that must be considered within the tectonic evolution of the CACC are as follows: 1) The Niğde Massif contains fragments of suprasubduction zone metaophiolite derived from the CAO; 2) parts of the Central Anatolian Ophiolite were deformed and metamorphosed in the middle crust along with metasediments (NMC), while other parts of the CAO experienced only low-grade metamorphism (EMC and Northern Region); 3) at the scale of the study area as well as the CAO in general, mantle sections of ophiolite mostly occur in the east, while upper crustal levels are exposed in the west, most consistent with emplacement from the east.

For our model of ophiolite emplacement, we prefer the paleogeographic interpretation of Görür *et al*. (1984) and reconstruction of Lefebvre *et al.* (2013) in which the CACC only attained its triangular shape during latest Cretaceous-Paleocene collision with the Pontides. In this reconstruction, ophiolites of the CAO are arranged in a linear, nearly N-S belt that would imply obduction from either the west or east, rather than from the Izmir-Ankara-Erzincan suture to the north (Fig. 1.19). In pre-Maastrichtian time the

CACC may have been an elongate, roughly N-S microcontinent, pinned at the Izmir-Ankara-Erzincan suture in the north (Görür *et al.,* 1984) and bordered by oceanic crust to the south, east and west (Fig. 1.23b). Based on the age and geochemistry of magmatism within the CACC (Kadıoğlu *et al.,* 2003; Whitney *et al.,* 2003, 2007; İlbeyli, 2005), and the age of ophiolites in the Tauride belt (Dilek *et al*., 1999; Parlak *et al*., 2013) it is likely that there was an Inner Tauride subduction zone dipping northward and/or eastward beneath the CACC during Turonian-Campanian time (Dilek and Whitney, 1997; Lefebvre *et al*., 2013). It is possible that this subduction zone could also have generated, at an earlier stage, the forearc magmas that would later be obducted as the CAO. Because Tethyan-style ophiolites are thought to be emplaced when a continental margin is dragged into a subduction zone (Wakabayashi and Dilek, 2003) this would require that either 1) the Inner Tauride subduction zone had a switch in polarity to generate ophiolites that became obducted onto both the CACC and Tauride blocks or 2) the eastward dipping subduction zone initially occupied a position to the east of the CACC to generate the CAO (Fig. 1.23a), and that it then jumped back or was reinitiated to the south and west of the CACC after obduction of the CAO (Fig. 1.23b). Scenario 2 is the preferred interpretation, as it requires no major change in kinematics and because the obduction may have been from the east, as discussed above.

Regardless of the originating suture zone, the relationship between ophiolite obduction and metamorphism of the CACC must be reevaluated in light of the finding that some parts of the CAO have themselves been metamorphosed at high temperatures. Based on the absence of thick mantle sequences in the CAO, it is likely that it was not a particularly thick ophiolite. Typical SSZ-type ophiolites have crustal thicknesses of only 2-6 km (Pearce *et al.,* 1984a), far too thin to be the sole cause of ~20 km of burial experienced by the Niğde Massif metasediments (Fig. 1.3). The presence of amphibolite-facies metaophiolite in the Niğde Massif requires that crustal thickening continued after ophiolite obduction. This crustal thickening apparently occurred in the absence of continental collision, based on the age of subduction-related magmatism within the CACC and Pontides.

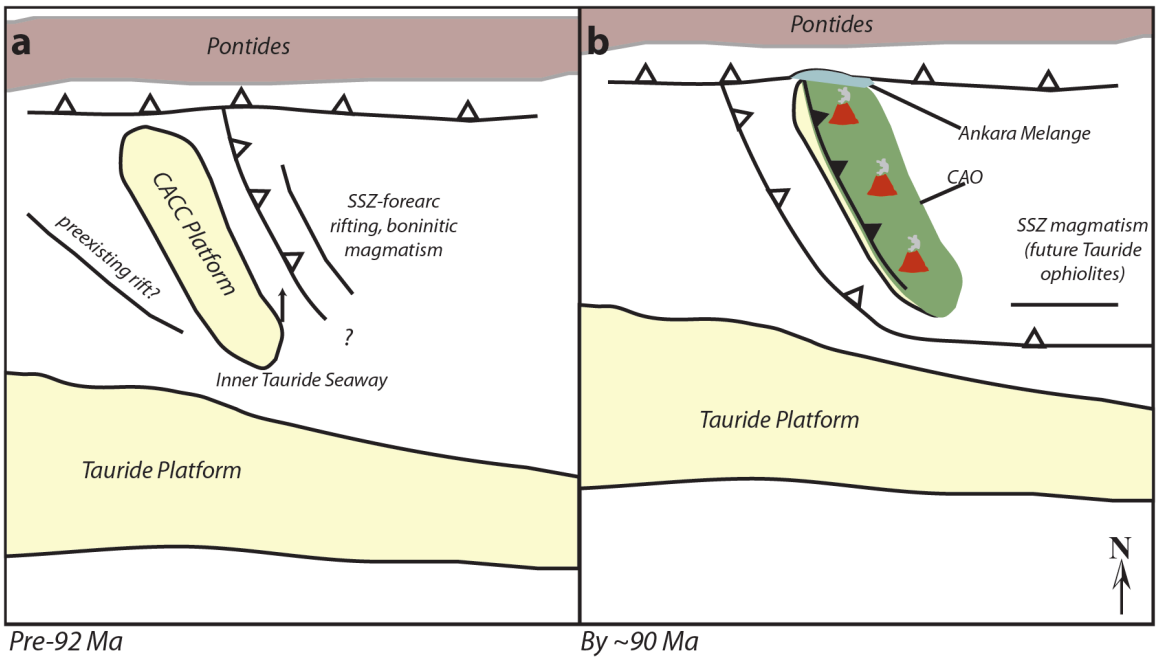

Figure 1.23: Schematic sketch of the development of the CACC before and after ophiolite emplacement. **a)** A newly established subduction zone develops in a N-S orientation, above which boninitic magmas are generated in the forearc rift. The CACC, separated from the Tauride Platform, obliquely approaches the N-S subduction zone. **b)** As the subduction zone becomes clogged by the CACC, a new subduction zone forms westward of the underthrust continent. Continued collision causes crustal thickening in the CACC and CAO. At the same time subduction initiates in the Inner Tauride seaway that will eventually form the Tauride Ophiolites.

Structural analysis of high-grade fabrics in the Niğde Massif indicate that orogeny occurred owing to oblique collision (Whitney *et al.,* 2007). In one potential scenario that accounts for the structural and petrologic observations within the Niğde Massif area, forearc magmatism above an eastward dipping subduction zone generated the rocks of the CAO (Fig. 1.24a). The CACC platform was underthrust beneath the CAO, and the subduction zone renewed in a position westward of the CACC (Fig. 1.24b). Continued oblique collision along the Inner Tauride subduction zone caused crustal thickening through folding and imbrication (Fig. 1.24c). Doming in the mid-crust generated the high-grade structure preserved in the Niğde Massif (Fig. 1.24d). Granitoids then intruded the deformed CACC and ophiolite, and ultimately the mid-crustal rocks were exhumed through upper crustal detachment faults that juxtapose higher structural levels of low-grade ophiolite with the high-grade NMC.

The issue of timing is problematic: detailed geo- and thermochronology from the Niğde Massif indicate high temperature, mid-crustal conditions from ~92-78 Ma

(Whitney *et al*., 2003, 2007). Turonian faunal ages from epi-ophiolitic sediments (Yalınız *et al*., 2000) and U/Pb zircon ages of plagiogranite at Sarıkaraman indicate generation of the ophiolite crust at ~91 Ma (van Hinsbergen *et al*., 2016), leaving essentially no time for ophiolite obduction and crustal thickening. For the Late Cretaceous Tauride ophiolites, obduction apparently closely followed formation of the oceanic crust and metamorphic sole, within ~10 Ma (Dilek *et al*., 1999) or 13-22 Ma (Parlak *et al*., 2013). The timing of collision could have been somewhat diachronous, as Niğde and Sarıkaraman are presently separated by ~100 km (Fig. 1.1b); however even with these caveats, the burial rate would need to be abnormally high to result in the apparently coincident ages of crustal anatexis and ophiolite generation.

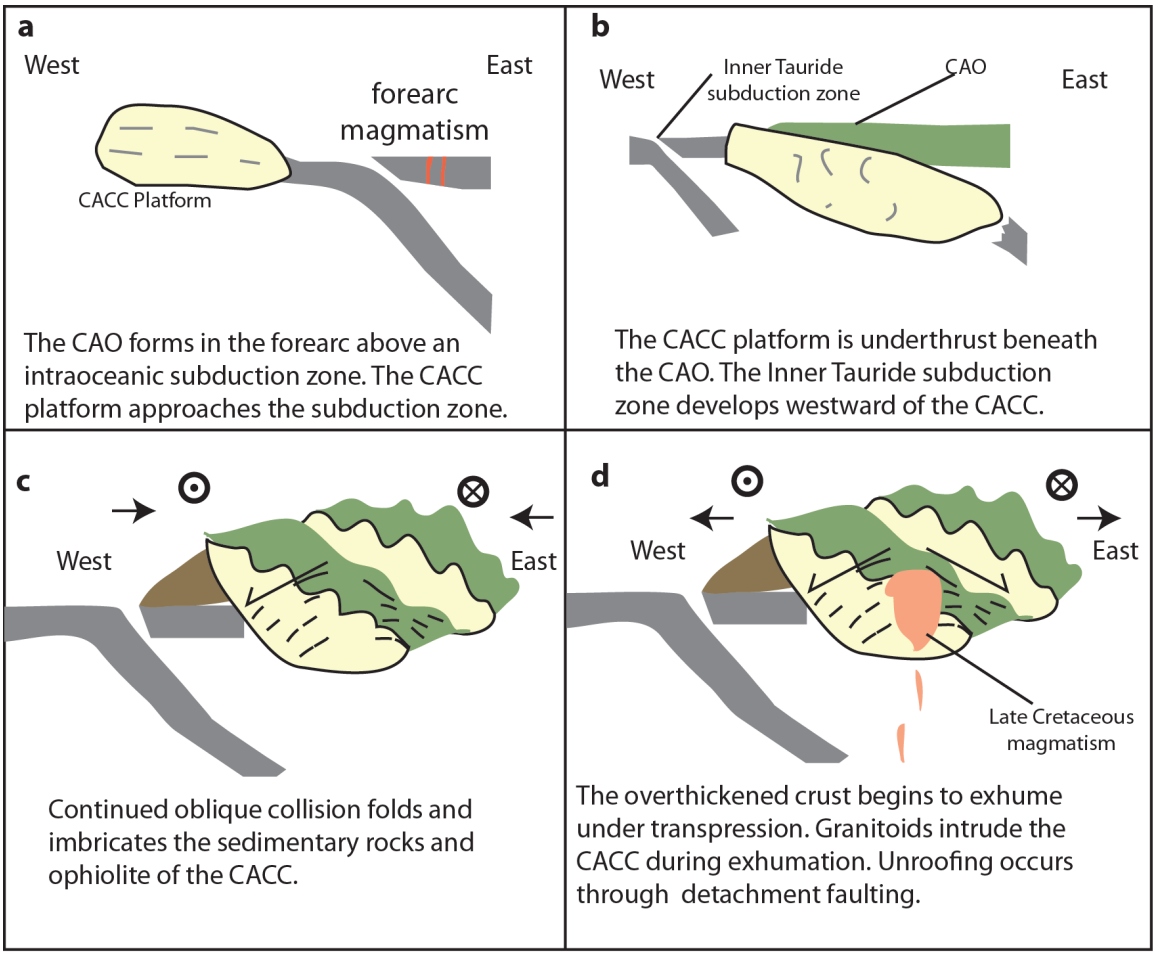

Figure 1.24: Schematic to explain the metamorphic and structural features of the CACC in the Niğde region with respect to the Central Anatolian Ophiolite (CAO).

The evidence from Niğde, where metaophiolite is deformed with metasediments, and from several localities of the CAO, where ophiolitic rocks are also intruded by Late Cretaceous granitoids (Yalınız *et al.,* 1996; Yılmaz and Boztuğ, 1998; this study) requires a pre-91 Ma obduction. More geochronologic data from the Central Anatolian Ophiolites will be necessary to understand the exact timing and rate of burial/crustal thickening, however a (pre-91 Ma) Cretaceous age is likely if obduction directly preceded peak metamorphism and because other Tethyan SSZ ophiolites are consistently Late Cretaceous in age.

Resolution of the timing and kinematics of emplacement of the Central Anatolian Ophiolite is critical to our understanding of the mechanisms and rates of tectonic processes in collision zones. The total distance of obduction for the CAO varies by an order of magnitude depending on whether it was emplaced via an Izmir-Ankara-Erzincan or Inner Tauride subduction zone. Establishing an age for the Central Anatolian Ophiolite that is consistent with the observed field relations will provide a constraint on the rate of burial and crustal thickening in the CACC in addition to its well-constrained exhumation path. Finally, elucidation of the relationship between obduction of the CAO and metamorphism will provide insight into how crystalline terranes can develop prior to continent-continent collision, which has relevance to geologic interpretation of orogenic belts in general.

1.9 Conclusions

Petrologic, geochemical, and structural data obtained in this study confirm that the NMC originated as part of the larger Central Anatolian Ophiolite in a suprasubduction zone, forearc setting, possibly associated with the earliest stages of subduction. The mafic, ultramafic and plagiogranitic rocks of the Niğde Mafic Complex are in tectonic (thrust) contact with the high-grade metasedimentary rocks of the Niğde Massif and contain deformational features and mineral assemblages consistent with amphibolite-facies metamorphism in a transpressional, continental orogen. Lower grade assemblages and textures are preserved north and east of the Niğde Massif, indicating that amphibolite-facies deformation did not affect all levels of the ophiolite, and that

these parts of the ophiolite have become juxtaposed by either thrust or detachment faulting.

Chapter 2

Provenance analysis of gabbro conglomerates in basins surrounding the Niğde Massif

2.1 Introduction

Gabbro cobbles are a puzzling component in Tertiary sedimentary rocks and terraces surrounding the Niğde Massif. Gabbro cobbles are found in both Paleogene and Neogene conglomerates of the Ecemiş and Ulukışla Basins (Fig. 2.1b) as well as in conglomerates of likely Neogene age north of the Niğde Massif. The provenance of gabbro clasts in the Ulukışla/Ecemiş Basins is not obvious, as gabbro occurs as part of ophiolites in both the Niğde Massif to the north and the Taurides to the south (Fig. 2.1b) and because significant topographic barriers presently separate these possible sources from the basins where gabbro is found as clasts. The provenance of these sediments is of interest because the Ecemiş and Ulukışla Basins are deposited on a major suture zone between the Central Anatolian Crystalline Complex (CACC) and Tauride terranes (Fig. 2.1a, b). The purpose of this supplement is to provide preliminary data on the petrographic and geochemical features of gabbro cobbles from these basins in order to suggest the most likely source regions. These results will be applicable to interpretations of paleodrainage, paleotopography, and Tertiary extent of ophiolite exposure, all of which are of interest to understanding the surficial response to continental collision in Central Anatolia.

2.2 Regional Geology

The Ulukışla and Ecemiş basins coincide with the Inner Tauride suture zone, which separates two major Anatolian terranes – the Central Anatolian Crystalline Complex and the Taurides (Fig. 2.1a, b). Collision between the two terranes occurred in latest Cretaceous time (Clark and Robertson, 2002; Parlak *et al*., 2013). Both terranes are overlain by ophiolites, but the CACC is made up of metasedimentary rocks and granitic intrusions, while the Tauride platform is dominantly composed of limestone and dolostone (Balci, 2010).

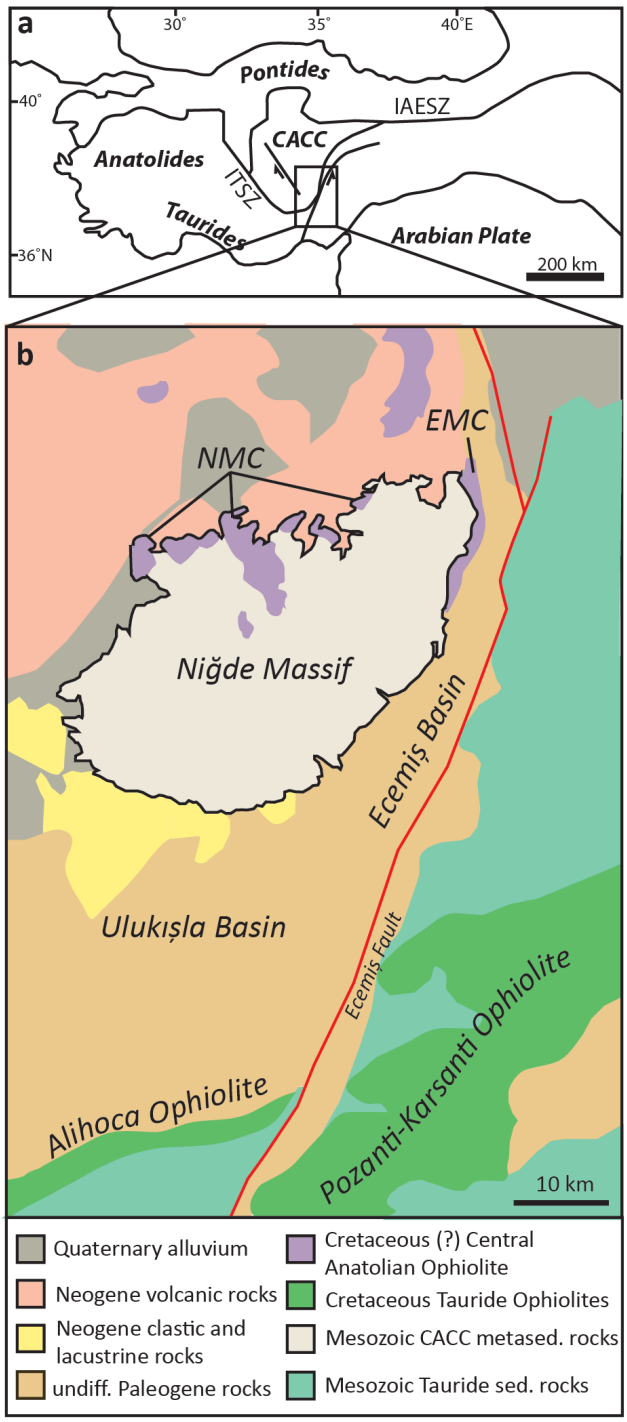

Figure 2.1: a) Regional map showing the location of the Niğde Massif anad surrounding basins. **b)** Generalized geologic map of the Niğde Massif, basins and nearby ophiolites. CACC: Central Anatolian Crystalline Complex, EMC: Ecemiş Mafic Complex, IAESZ: Izmir-Ankara-Erzincan suture zone, ITSZ: Inner Tauride suture zone, NMC: Niğde Mafic Complex.

The Niğde Massif is a metamorphic dome consisting of high-grade (amphibolite facies) metasedimentary rocks and granite and is located in the southernmost region of the CACC (Figs. 2.1, 2.2). Metamorphosed gabbro and related rocks of the Niğde Mafic Complex (NMC) structurally overly the Niğde Massif metasediments and are fragments of the Central Anatolian Ophiolite, which may have once covered much of the CACC (Floyd *et al*., 2000; this study). The Taurides are structurally overlain by ophiolites derived from the Inner Tauride suture zone (Dilek and Whitney, 1997; Dilek *et al*., 1999), including the Pozanti-Karsanti and Alihoca ophiolites (Fig. 2.1b). The crystalline bedrock of the Niğde Massif has allowed previous provenance studies to readily identify it as a source area, based on the occurrence of metamorphic and granitic clasts in some sedimentary rocks (Gautier *et al*., 2002; Clark and Robertson, 2005; Jaffey and Robertson, 2005). Based on the presence of ophiolite klippen of the NMC, metagabbro may have also

been a major lithologic component of the Niğde Massif during its exhumation and unroofing. The former extent of ophiolite and metaophiolite in the Niğde Massif are important to understanding the crustal architecture of the CACC during collision and exhumation.

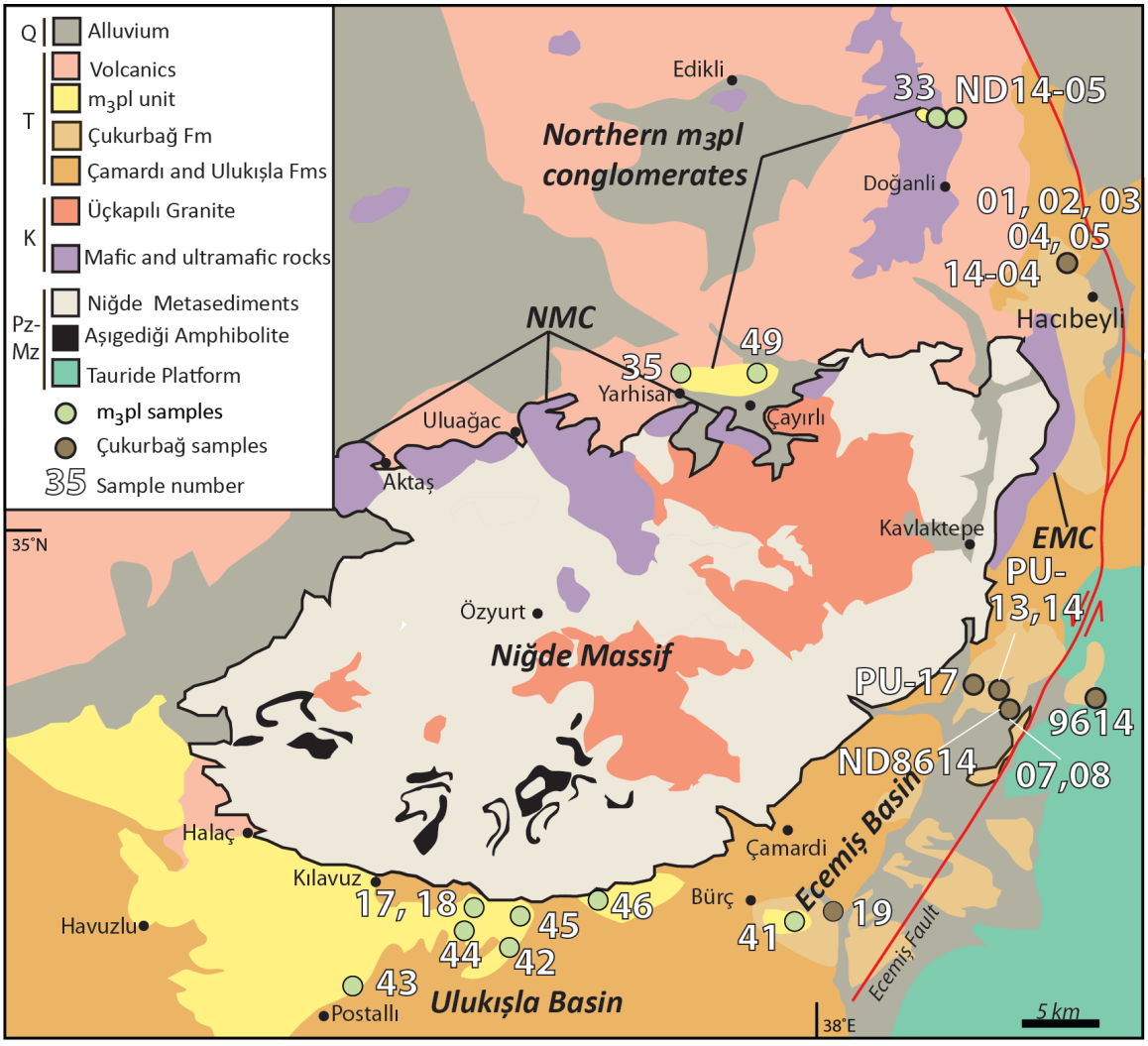

Figure 2.2: Cobble sample locations from the Ecemiş and Ulukışla basins and from conglomerates north of the Niğde Massif. EMC: Ecemiş Mafic Complex, NMC: Niğde Mafic Complex.

2.3 Description of Çukurbağ, m_3pl and northern conglomerate units

The Ecemiş Basin is continuous with the Ulukışla Basin and coincides with the Ecemiş Fault (Fig. 2.2). Gabbro cobbles were sampled from the Paleogene Çukurbağ Formation in the Ecemiş Basin and the Miocene 'm_3pl' unit in the Ulukışla Basin (Fig.

2.2). Gabbro cobbles were also obtained from conglomerates north of the Niğde Massif and are tentatively correlated to the $m_3$pl unit.

2.3.1 Çukurbağ Formation

The Oligocene Çukurbağ Formation is mostly exposed in the Ecemiş Basin and is a well-lithified sequence of fluvial clastics that were folded due to mid-Miocene transpression on the Ecemiş Fault (Fig. 2.3a; Jaffey and Robertson, 2001). Clast counts reveal that gabbro cobbles are associated with variable lithologies including granite, volcanic rocks, limestone, and marble (Fig. 2.4; Appendix 5). Clast size data for conglomerates from 4 sites of the Çukurbağ Formation is provided in Table 2.1, full clast counts are provided in Appendix 5.

Sample locality no.	Average clast size (all lithologies)	Average clast size (gabbro)	Percent gabbro
01	7.4 cm	7.9 cm	65
08	5.5 cm	5.0 cm	22
19	6.3 cm	5.9 cm	51
PU-14	6.7 cm	6.1 cm	30

Table 2.1: Size data from clast counts performed on gabbro-bearing conglomerates of the Çukurbağ Formation in the Ecemiş Basin. 100 clasts were counted for each analysis, clasts under 2 cm were not counted thus averages in the above table are for the sediment fraction >2 cm in diameter only. Refer to Fig. 2.4 for locations and lithologies. See Appendix 5 for all clast count data.

2.3.2 M_3pl conglomerate – Ulukışla Basin

In the Ulukışla Basin, the $m_3$pl unit is unconformable on Paleogene rocks (Fig. 2.3b) and is composed of lacustrine sediments with intercalations of volcanic tuff and fluvial conglomerate (MTA, 2002). A volcanic tuff in the $m_3$pl unit, near sample locality 43 (Fig. 2.2), was dated at 6.2 ± 0.12 Ma ($^{40}Ar/^{39}Ar$; M. Meijers & G. Brocard, pers. comm.). A poorly lithified conglomerate, locally containing abundant gabbro, occurs above the 6.2 Ma tuff and is locally interfingering with travertine (G. Brocard, pers. comm.). Travertine covers much of the $m_3$pl surface southwest of the Niğde Massif in the vicinity of Postallı, Havuzlu and Kılavuz but is discontinuous or absent northeast of Postallı, along the southern edge of the Niğde Massif. The lack of travertine capping the $m_3$pl east of Postallı has led to incision and dissection of the $m_3$pl deposits resulting in a series of terraces, atop which gabbro cobbles and boulders are abundant. Two samples

were obtained from intact outcrops displaying stratigraphy (Sample localities 43, 46 – Fig. 2.2), however the remaining 6 Ulukışla Basin samples were obtained from the ground surface, without observable stratigraphy. Cobbles littering the terrace surfaces are interpreted as erosional remnants of the $m_3$pl conglomerate, and cobbles at lower elevations (i.e. at base of terraces) were transported by downslope processes from the terrace tops (Fig. 2.3c). Gabbro cobbles from the $m_3$pl terraces are typically >50 cm, while those from outcrops of the $m_3$pl conglomerate are generally <30 cm (Table 2.2). The occurrence of such coarse cobbles/boulders on terrace surfaces as opposed to in outcrops may be an effect of weathering whereby smaller clasts were transported by runoff or broken down and incorporated into soil, thus concentrating large boulder size particles on terrace surfaces and in adjacent gullies.

Sample Locality no.	Max. clast size (gabbro)	% gabbro	Other lithologies
41	60 cm	90	Granite, marble
42	60 cm	30	Limestone, granite, marble
43	10 cm	30	Granite, volcanic, schist
44	110 cm	30	Marble
45	60 cm	10	Marble
46	30 cm	50	Marble, volcanic

Table 2.2: Features of the $m_3$pl conglomerate in the Ulukışla Basin.

2.3.3 M_3pl conglomerate – North of Niğde Massif

In several locations north of the Niğde Massif, (sample localities 33, 35, 49 – Fig. 2.2) gabbro conglomerates were observed to form small hills, locally capped by ignimbrite. These are tentatively correlated to the $m_3$pl conglomerate known from the Ulukışla Basin, because of the similarity in probable age (the northern conglomerates are locally capped by upper Miocene or Pliocene ignimbrite) and appearance (poorly lithified and intercalated with red sandstone). North of the villages of Çayırlı and Yarhisar (Fig. 2.2) in an area mapped as gabbro on MTA geologic maps (Atabey, 1989) thick sequences of gabbro-dominated conglomerate were observed rather than gabbro bedrock. The conglomerate is locally overlain by Cappadocian ignimbrite, which may have formed an erosional cap, allowing the conglomerate to underlie small hills, despite its high erosivity (Fig. 2.3d). Clast size in the Çayırlı-Yarhisar conglomerates ranges from a few cm to >1

m in diameter and the lithologies observed as clasts are similar to the bedrock exposed in the Niğde Mafic Complex (NMC) - gabbro, diabase and plagiogranite. Another conglomerate hill was observed in the Doğanlı valley (sample locality 33 – Fig. 2.2) in which boulders up to 50 cm in diameter are present. Lithologies observed in this conglomerate include ultramafic rocks, gabbro, granite, and basalt.

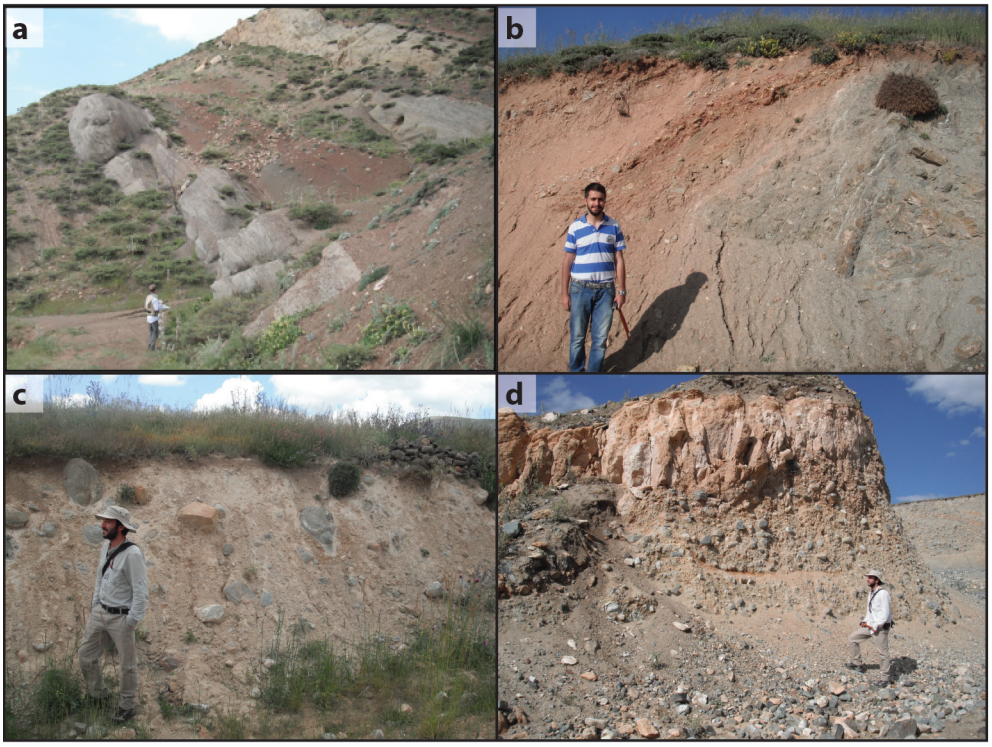

Figure 2.3: Field photos from the various conglomerate units sampled for this study. **a)** Gabbro-bearing conglomerate in the tilted Çukurbağ Formation (sample locality 07). **b)** Unconformity between gray Paleogene volcanics and red $m_3$pl clastics in the Ulukışla Basin (sample locality 46). **c)** Colluvium near terrace containing abundant gray gabbro boulders in the Ulukışla Basin (sample locality 18). **d)** Northern conglomerate comprised of ~90% gabbro overlain by ignimbrite of late Miocene or Pliocene age (sample locality 35).

2.4 Petrography of gabbro cobbles

2.4.1 Çukurbağ Formation – Ecemiş Basin

Seventeen gabbro and one plagiogranite cobbles were sampled from the Çukurbağ Formation in the Ecemiş Basin and analyzed petrographically for textural features and mineral assemblages. A variety of mineral assemblages and textures were observed in the Çukurbağ Formation cobbles and are described in Appendix 1. Gabbro types include clinopyroxene gabbro, olivine gabbro and hornblende gabbro. Features common to all of

the Çukurbağ cobbles are the lack of ductile deformation and a greenschist-facies overprint represented by uralite, actinolite and/or chlorite. Hornblende occurs in eight of the Çukurbağ cobbles (1 plagiogranite, 1 diabase, and 6 gabbros). Four samples (ND15-07, PU15-14, PU15-17 and ND9614) have hornblende that may be metamorphic, but textures are obscured by alteration. The textures of the Çukurbağ cobbles in general are magmatic and overprinted by low-grade alteration and weathering. Flow textures were observed in two samples from Hacıbeyli (ND14-04A, ND15-03).

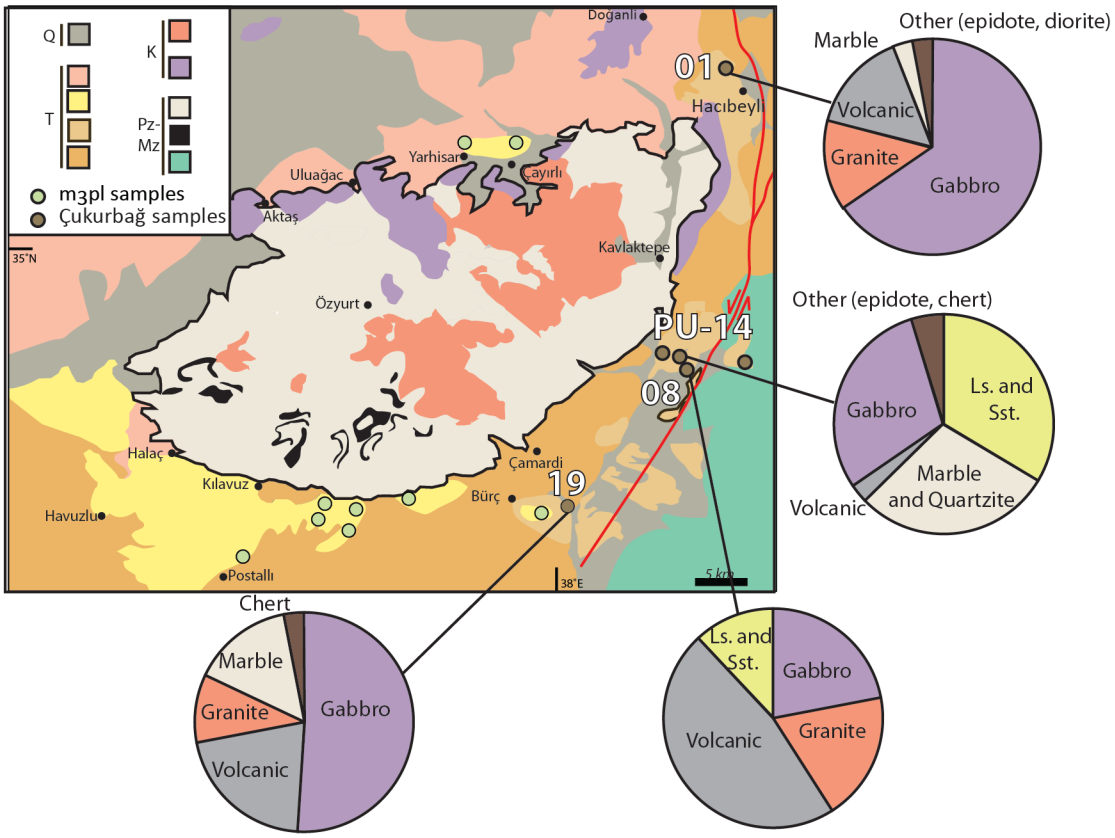

Figure 2.4: Results of clast counts in the Çukurbağ Formation of the Ecemiş Basin. For each analysis, 100 grains > 2 cm in diameter were counted. Sample localities are given for each clast count and size data are given in Table 2.1.

2.4.2 M₃pl conglomerate – Ulukışla Basin

Nine gabbro cobbles were analyzed petrographically from the m₃pl unit in the Ulukışla Basin. These show a variety of mineral assemblages and textures, reported in Appendix 1. Five of the Ulukışla Basin gabbros are igneous-textured olivine gabbros (17A, 18 and 44) or clinopyroxene gabbros (17B, 45) with greenschist-facies overprints

of chlorite, uralite or epidote, and accessory green spinel. Of these, samples 18 and 45 have a magmatic flow texture. Three of the Ulukışla Basin gabbro cobbles are hornblende metagabbros with plagioclase that is irregularly shaped and poorly twinned, hornblende that is poikilitic or polygonal textured, and relict clinopyroxene (samples 42, 43 and 46). Sample 41 is a hornblende metadiabase with similar texture to metadiabase of the Nigde Mafic Complex (Fig. 2.5). Of these, samples 41 and 46 also have a greenschist-facies overprint of chlorite or epidote.

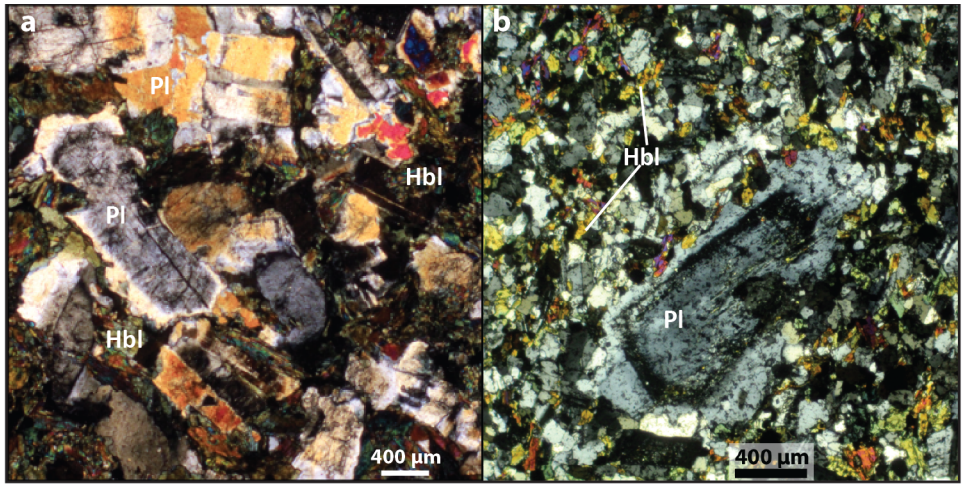

Figure 2.5: Comparison of petrographic features in cobbles from the $m_3$pl unit and the Niğde Mafic Complex bedrock. a) Metadiabase cobble from the $m_3$pl unit with zoned plagioclase and irregular grain boundaries with hornblende (sample 41). b) Metadiabase from the Niğde Mafic Complex (sample 29).

2.4.3 M_3pl conglomerate – North of Niğde Massif

Five gabbro and two diabase cobbles were sampled from conglomerates north of the Niğde Massif, descriptions are given in Appendix 1. One diabase (49B) has a porphyritic texture with plagioclase and hornblende phenocrysts and is unmetamorphosed. The other diabase (ND14-05B) has a similar porphyritic texture but has cracked plagioclase phenocrysts and an overprint of secondary chlorite. Sample 49A is a clinopyroxene gabbro that has been ~70% altered to uralite. The remaining four samples are hornblende metagabbro. Sample 33A contains brown, poikilitic hornblende with inclusions of plagioclase and clinopyroxene that have preferred orientation (flow texture). The brown hornblende has irregular grain boundaries with feldspar and pyroxene and does not have a preferred orientation like the enclosed chadacrysts, thus it is considered to be metamorphic. Feldspar in this sample is cracked and has undulose

extinction and deformation twins. Samples 33B, 35 and ND14-05A are composed of plagioclase and metamorphic hornblende, with or without relict Cpx. Hornblende in these metagabbro cobbles has a polygonal texture. Sample ND14-05A has a slight fabric defined by foliated hornblende.

2.5 Geochemical features of gabbro cobbles

Four cobbles from the Çukurbağ Formation in the Ecemiş Basin and four cobbles from the $m_3$pl unit in the Ulukışla Basin were analyzed for whole-rock geochemistry using XRF at Macalester College. Geochemical data are provided in Appendix 3.

2.5.1 Ecemiş Basin – Çukurbağ Formation cobbles

The geochemical results from the Çukurbağ Formation indicate two distinct groups of gabbro. Samples ND14-04B and PU15-14, which are from the northern part of the Ecemiş basin (on the western side) have SiO_2 contents of 50.26 and 53.03 wt. %, respectively, fairly high TiO_2 (0.68-0.98 wt. %), Zr (55-63 ppm) and Y (16-22 ppm) contents, and Ti/V ratios of 21 and 23, respectively. These two samples have the general geochemical characteristics of island-arc tholeiites (Fig. 2.6a, b). The second group of Çukurbağ cobbles (08A and 19B) are from conglomerate south of the other two analyzed samples, on the western side of the basin, and have lower SiO_2 contents of 48.38 and 46.94 wt. %, respectively, low TiO_2 (0.10-0.16 wt. %), Zr (1-2 ppm) and Y (2-4 ppm) contents, and Ti/V ratios of 4-6 - characteristic of boninites (Fig. 2.6a, b).

2.5.2 Ulukışla – $m_3$pl cobbles

The $m_3$pl cobbles include 3 gabbros of basaltic composition (samples 43, 44, and 46) with SiO_2 from 46.95-50.04 wt. % and one andesitic diabase (sample 41) with SiO_2 content of 57.26 wt. %. All of the $m_3$pl cobbles have low TiO_2 (0.12-0.49 wt. %), Zr (1-23 ppm) and Y (3-13 ppm) contents, and Ti/V ratios of 7-10. Thus the $m_3$pl cobbles in general have the geochemical characteristics of boninites (Fig. 2.6a, b).

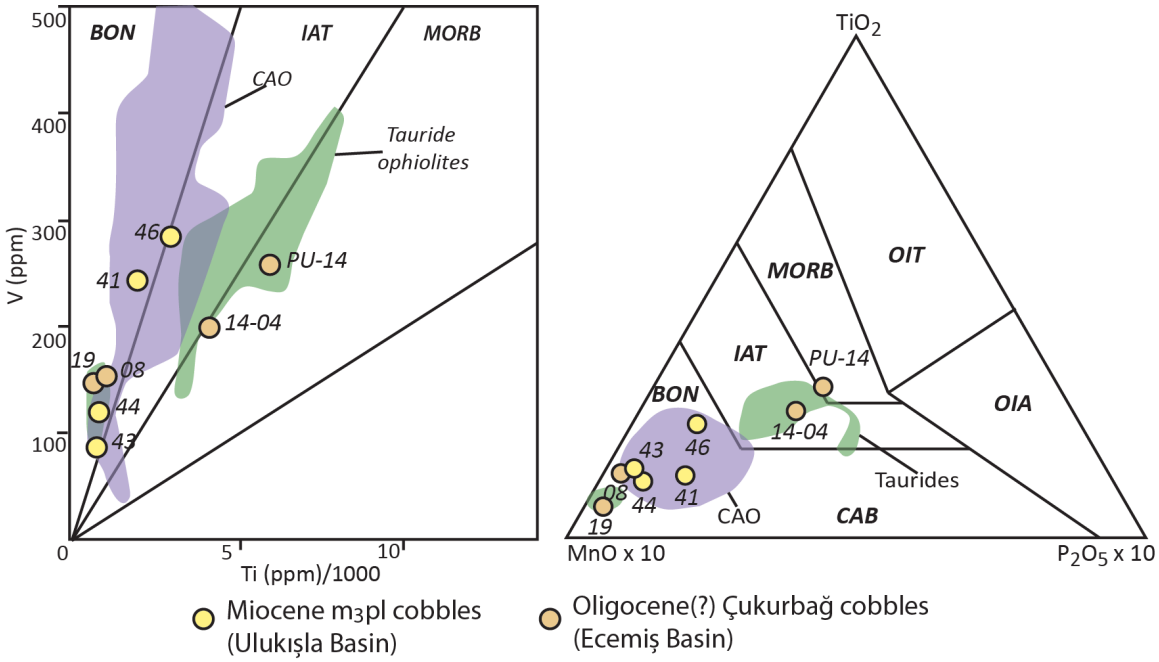

Figure 2.6: Tectonic discrimination diagrams for the gabbroic cobbles of the Çukurbağ and $m_3$pl units. Purple fields are for the Central Anatolian Ophiolite (CAO) and encompass data from Kocak *et al.* (2005), Yalınız (2008), Yılmaz and Boztuğ (1998), and this study (Ray MS thesis). Greenfields are for the Tauride ophiolites and emcompass data from Dilek *et al.* (1999) Parlak *et al.* (2000) and Sarıfakıoğlu *et al.* (2013). **a)** V vs Ti diagram from Shervais (1982). BON: boninite, IAT: island-arc tholeiite, MORB: mid-ocean ridge basalt. **b)** MnO-TiO_2-P_2O_5 ternary diagram with tectonic fields from Mullen (1983). CAB: calc-alkaline basalt, OIA: ocean-island alkali basalt, OIT: ocean-island tholeiite.

2.6 Discussion

2.6.1 Features of gabbro source areas in the CACC and Taurides

The main question to be assessed is whether the Niğde Mafic Complex (NMC), in the northern part of the Niğde Massif (Fig. 2.1b, 2.2), could have been a source area for cobbles in the Çukurbağ and $m_3$pl units. The Niğde Mafic Complex is a fairly unique source area in that it is variably deformed and has a high-grade metamorphic overprint represented by metamorphic hornblende and plagioclase (this study). Gabbro from elsewhere in the CAO, including the Ecemiş Mafic Complex (this study) and parts of the Northern Region (see Fig. 1.2) has a lower grade, greenschist-facies overprint or is unmetamorphosed. Most gabbro of the Alihoca and Pozanti-Karsanti ophiolites is undeformed but may have a greenschist-amphibolite facies overprint resulting from hydrothermal alteration (Parlak *et al.,* 2000; Sarıfakıoğlu *et al.,* 2013).

Because of weathering, petrographic features are obscured in many of the cobbles, and metamorphic hornblende may be retrograded to low-grade assemblages of chlorite, uralite, actinolite or other minerals. For this reason, geochemistry is an important addition to the assessment of provenance. Geochemically, the NMC and CAO in general are distinguished by having features of boninites such as high MgO, low TiO_2, Y and Zr, and Ti/V ratios of less than 10. Boninitic gabbros occur in both the CAO and the Taurides, however they appear to make up the vast majority of gabbros in the CAO, whereas in the Taurides they are subsidiary to gabbros with island-arc tholeiite affinities (Fig. 2.6).

Table 2.3 shows general guidelines suggested for ascertaining the provenance of gabbroic clasts in the Ulukışla and Ecemiş basins. In general, where the majority of cobbles have metamorphic hornblende with or without a foliation and boninitic geochemistry, the NMC is the most likely source area. Where the majority of cobbles have boninitic geochemistry and a greenschist-facies overprint, other parts of the CAO – such as the Ecemiş Mafic Complex and Northern Region – may be the source area. Where a significant portion of gabbro cobbles has IAT or MORB geochemistry and a greenschist-facies overprint, a Tauride ophiolite source is suggested. There is heterogeneity of geochemistry and mineral assemblages within each of the suggested source areas (NMC, CAO and Taurides), thus a reasonable assessment should be made based on the majority of samples. A mixture of characteristics may indicate multiple source areas.

Secondary mineral assemblage	Geochemical affinity	Likely source area
Hbl + Pl	BON	Niğde Mafic Complex
Act ± Hbl ± Chl ± Ep	BON	Central Anatolian Ophiolite
Act ± Hbl ± Chl ± Ep	IAT or MORB	Tauride ophiolites

Table 2.3: Suggested guidelines for distinguishing between the Niğde Mafic Complex (NMC), Central Anatolian Ophiolite (CAO) and Tauride ophiolites as source areas for gabbro cobbles in the Ulukışla and Ecemiş Basins. BON: boninite, IAT: island-arc tholeiite, MORB: mid-ocean ridge basalt.

2.6.2 Assessment of provenance for Çukurbağ, $m_3$pl and northern conglomerates

Gabbro cobbles from the Ecemiş and Ulukışla Basins have ambiguous provenance due to their location on the suture zone between the CACC and Tauride terranes, distal from any presently exposed gabbro source. The northern $m_3$pl

conglomerates (Fig. 2.2) are almost certainly derived from the CAO, as they are comprised exclusively of ophiolitic lithologies (gabbro, diabase, plagiogranite, basalt and ultramafic rock) and occur within a few kilometers of exposed ophiolite bedrock. All but two of the northern conglomerate cobbles have metamorphic hornblende suggesting the NMC and/or other parts of the CAO are the source area. Of the two that do not have metamorphic hornblende, one (49B) is an igneous-textured diabase and the other (49A) is severely retrograded to uralite. Only one of the northern $m_3$pl samples (ND14-05A) has a ductile deformation fabric, suggesting that most of these gabbros were derived from higher levels of the CAO than what is presently exposed in the Niğde Mafic Complex, where a foliation is common.

Samples from the Ulukışla Basin $m_3$pl conglomerates in general have characteristics of the CAO (Table 2.4). The Ulukışla Basin sample suite includes three hornblende metagabbro cobbles (42, 43 and 46) and one metadiabase (41) that are texturally similar to bedrock in the Niğde Mafic Complex (Fig. 2.5). Geochemically, all four of the cobbles analyzed from the Ulukışla Basin sediments have boninitic affinities similar to the NMC and CAO. Based on these criteria, it seems likely that gabbro cobbles of the Ulukışla Basin $m_3$pl conglomerate are at least partially sourced in the NMC, possibly with input from the Ecemiş Mafic Complex, based on the presence of olivine-gabbro cobbles (17A, 18, 44).

Unit	% clasts with metamorphic Hbl	% Boninite	Likely source area
Çukurbağ	24% (4/17)	50% (n=4)	Taurides or mixed
$m_3$pl (south)	44% (4/9)	100% (n=4)	NMC + CAO (EMC?)
$m_3$pl (north)	71% (5/7)	Not analyzed	NMC + CAO

Table 2.4: Analysis of gabbro provenance using the criteria discussed above and outlined in Table 2.3. M_3pl (south) refers to the $m_3$pl conglomerate in the Ulukışla Basin, while $m_3$pl (north) indicates $m_3$pl conglomerates north of the Niğde Massif. CAO: Central Anatolian Ophiolite, EMC: Ecemiş Mafic Complex, NMC: Niğde Mafic Complex.

Provenance analysis of the Çukurbağ Formation returns more ambiguous results. Many of the Çukurbağ cobbles were severely altered, thus the 24% with metamorphic hornblende is a minimum. Two of the four cobbles analyzed for geochemistry have IAT affinities (Fig. 2.6) thus the Çukurbağ gabbro cobbles were probably in part sourced from the Tauride ophiolites. A mixture of Tauride and CAO source regions is also possible

based on the presence of two boninitic cobbles and four cobbles with metamorphic hornblende (Table 2.4).

2.6.3 Future work and geomorphic implications

The results from the Çukurbağ Formation are unclear at this point, but with a larger sample suite it may be possible to suggest that there were either multiple gabbro source regions in the Tauride and Central Anatolian ophiolites or that the Tauride ophiolites were the main source area for the Çukurbağ gabbro cobbles. It would also be of interest to analyze several cobbles from different parts of the Çukurbağ to determine if there are lateral or vertical changes in gabbro provenance.

The presence of thick, incised gabbro conglomerates north of the Nigde Massif has implications for the tectonic and geomorphic evolution of the CACC. These conglomerates could record the widespread denudation of the Central Anatolian Ophiolite, which apparently covered the entire CACC, but is now sparsely exposed. If exhumation of the metamorphic massifs of the CACC was even partially controlled by erosion, sediments with CAO affinity should be voluminous.

The Ulukışla Basin $m_3$pl conglomerates contain coarse, boulder-size gabbro clasts that appear to have been sourced in large part from the CAO. Three scenarios can be considered to account for CAO-derived cobbles in the upper Miocene Ulukışla Basin: 1) The Niğde Mafic Complex was more extensive in late Miocene time and gabbro boulders were sourced locally, from gabbro outcropping along the southern margin of the Niğde Massif – although there are no remnant NMC klippen presently exposed south of Özyurt; 2) Gabbro of the $m_3$pl unit was derived from NMC/CAO bedrock on the northern side or north of the Niğde Massif and transported via some fluvial system that either went through or around the Niğde Massif; and 3) It may be that gabbro conglomerates north of the Niğde Massif are older than the $m_3$pl conglomerate of the Ulukışla Basin and that the southern $m_3$pl sediments are recycled from earlier conglomerates deposited north of the Niğde Massif. This too would require a fluvial system connecting the northern and southern margins of the Niğde Massif. Both scenarios 2 and 3 require significant post-Miocene differential uplift between the northern and southern margin of the Niğde

Massif, as the $m_3$pl terraces are at ~1900 m in the Ulukışla Basin, and with the exception of the southernmost parts of the NMC, all of the CAO is presently at elevations below 1900 m.

References

Akıman, O., Erler, A., Göncüoğlu, M.C., Güleç, N., Geven, A., Türeli, T.K. and Kadıoğlu, Y.K., 1993, *Geochemical characteristics of granitoids along the western margin of the Central Anatolian Crystalline Complex and their tectonic implications*, Geological Journal, Vol. 28, p. 371-382

Alt, J.C., 1995, *Subseafloor processes in mid-ocean ridge hydrothermal systems*, in Humphris, S.E., Zierenberg, R.A., Mullineaux, L.S., and Thomspon, R.E., *Seafloor Hydrothermal Systems*, AGU Geophysical Monograph 91,p. 85-114

Alt, J.C., Laverne, C., Vanko, D.A., Tartarotti, P., Teagle, D.A.H., Bach, W., Zuleger, E., Erzinger, J., Honnorez, J., Pezard, P.A., Becker, K., Salisbury, M.H., and Wilkins, R.H., 1996, *Hydrothermal alteration of a section of upper oceanic crust in the eastern equatorial Pacific: a synthesis of results from site 504 (DSDP Legs 69, 70, and 83, and ODP Legs 111, 137, 140, and 148),* Proceedings of the Ocean Drilling Program, Scientific Results, Vol. 148, p. 417-434

Atabey, E., 1989, *Geologic Map of the Kayseri-I19 Quadrangle*, Ankara, General Directorate of Mineral Research and Exploration

Atabey, E., Göncüoğlu, M.C. and Turhan, N., 1990, *Geologic Map of the Kozan-J19 Quadrangle*, Ankara, General Directorate of Mineral Research and Exploration

Bakke, S., and Korneliussen, A., 1986, *Jack-straw-textured olivines in some Norwegian metaperidotites*, Norsk Geologisk Tidsskrift, Vol. 66, p. 271-276

Balci, V., 2010, *Geologic map of the Adana-M34 Quadrangle*, Ankara, General Directorate of Mineral Research and Exploration

Beccaluva, L., Macciotta, G., Piccardo, G.B., and Zeda, O., 1989, *Clinopyroxene composition of ophiolite basalts as petrogenetic indicator*, Chemical Geology, Vol. 77, p. 165-182

Bloomer, S.H., and Hawkins, J.W., 1987, *Petrology and geochemistry of boninite series volcanic rocks from the Mariana Trench*, Contributions to Mineralogy and Petrology, Vol. 97, p. 361-377

Burns, L.E., 1985, *The Border Ranges ultramafic and mafic complex, south central Alaska, cumulate fractionates of island-arc volcanics*, Canadian Journal of Earth Science, Vol. 22, p. 1020-1038

Clark, M., and Robertson, A., 2002, *The role of the Early Tertiary Ulukışla Basin, southern Turkey, in suturing of the Mesozoic Tethys ocean*, Journal of the Geological Society, London, Vol. 159, p. 673-690

Clark, M., and Robertson, A., 2005, *Uppermost Cretaceous-Lower Tertiary Ulukışla Basin, south-central Turkey: sedimentary evolution of part of a unified basin complex within an evolving Neotethyan suture zone*, Sedimentary Geology, Vol. 173, p. 15-51

Coogan, L.A., Wilson, R.N., Gillis, K.M., and MacLeod, C.J., 2001, *Near-solidus evolution of oceanic gabbros: insights from amphibole geochemistry*, Geochimica et Cosmochimica Acta, Vol. 65, no. 23, p. 4339-4357

Deer, W.A., Howie, R.A., and Zussman, J., 1992, An introduction to the rock forming minerals, 2nd ed., Longman, London

Dilek, Y., and Whitney, D.L., 1997, Counterclockwise P-T-t trajectory from the metamorphic sole of a Neo-Tethyan ophiolite (Turkey), Tectonophysics, Vol. 280, p. 295-310

Dilek, Y., Thy, P., Hacker, B., and Grundvig, S., 1999, *Structure and petrology of Tauride ophiolites and mafic dike intrusions (Turkey): implications for the Neotethyan ocean*, Bulletin of the Geological Society of America, Vol. 111, no. 8, p. 1192-1216

Dilek, Y., and Thy, P., 2009, *Island arc tholeiite to boninitic melt evolution of the Cretaceous Kizildag (Turkey) ophiolite: model for multi-stage early arc-forearc magmatism in Tethyan subduction factories*, Lithos, Vol. 113, p. 68-87

Dilek, Y., and Furnes, H., 2014, *Ophiolites and their origins*, Elements, Vol. 10, no. 2, p. 93-100

Evans, B.E., and Trommsdorff, V., 1974, On elongate olivine of metamorphic origin, Geology, Vol. 2, no. 3, p. 131-132

Fayon, A.K., Whitney, D.L., Teyssier, C., Garver, J.I., and Dilek, Y., 2001, *Effects of plate convergence obliquity on timing and mechanisms of exhumation of a mid-crustal terrain, the Central Anatolian Crystalline Complex*, Earth and Planetary Science Letters, Vol. 192, p. 191-205

Fayon, A.K., and Whitney, D.L., 2007, *Interpretation of tectonic versus magmatic processes for resetting apatite fission track ages in the Niğde Massif, Turkey*, Tectonophysics, Vol 434, p. 1-13

Floyd, P.A., Yalınız, M.K, and Göncüoğlu, M.C., 1998, *Geochemistry and petrogenesis of intrusive and extrusive ophiolitic plagiogranites, Central Anatolian Crystalline Complex, Turkey*, Lithos, Vol. 42, p. 225-241

Floyd, P.A., Göncüoğlu, M.C., Winchester, J.A., and Yalınız, M.K, 2000, *Geochemical character and tectonic environment of the Neotethyan ophiolitic fragments and*

metabasites in the Central Anatolian Crystalline Complex, Turkey, in Bozkurt, E., Winchester, J.A, and Piper, J.D.A., *Tectonics and magmatism in Turkey and the surrounding area*, Geological Society of London, Special Publications, 173, p. 183-202

Freund, S., Haase, K.M., Keith, M., Beier, C., and Garbe-Schönberg, D., 2014, *Constraints on the formation of geochemically variable plagiogranite intrusions in the Troodos Ophiolite, Cyprus*, Contributions to Mineralogy and Petrology, Vol. 167, no. 978

Frost, B.R., 2001, *A geochemical classification for granitic rocks*, Journal of Petrology, Vol. 42, no. 11, p. 2033-2048

Gautier, P., Bozkurt, E., Hallot, E., and Dirik, K., 2002, *Dating the exhumation of a metamorphic dome: geological evidence for pre-Eocene unroofing of the Niğde Massif (Central Anatolia, Turkey),* Geological Magazine, Vol. 139, no. 5, p. 559-576

Gautier, P., Bozkurt, E., Bosse, V., Hallot, E. and Dirik, K., 2008, *Coeval extensional shearing and lateral underflow during Late Cretaceous core complex development in the Niğde Massif, Central Anatolia, Turkey*, Tectonics, Vol. 27, TC1003

Görür, N., Oktay, F.Y., Seymen İ. and Şengör, A.M.C., 1984, *Palaeotectonic evolution of the Tuzgölü basin complex, Central Turkey: sedimentary record of a Neo-Tethyan closure*, in Dixon, D.E. and Robertson, A.H.F., *The Geological Evolution of the Eastern Mediterranean*, Geological Society of London, Special Publications, 17, p. 467-482

Hacker, B.R., 1990, *Simulation of the metamorphic and deformational history of the metamorphic sole of the Oman Ophiolite*, Journal of Geophysical Research, Vol. 95, no. B4, p. 4895-4907

Holland, T., and Blundy, J., 1994, *Non-ideal interactions in calcic amphiboles and their bearing on amphibole-plagioclase thermometry*, Contributions to Mineralogy and Petrology, Vol. 116, p. 433-447

Idleman, L., Cosca, M.A., Heizler, M.T., Thomson, S.N., Teyssier, C., and Whitney, D.L., 2014, *Tectonic burial and exhumation cycles tracked by muscovite and K-feldspar $^{40}Ar/^{39}Ar$ thermochronology in a strike-slip fault zone, central Turkey*, Tectonophysics, Vol. 612-613, p. 134-146

İlbeyli, N., 2005, *Mineralogical-geochemical constraints on intrusives in central Anatolia, Turkey: tectono-magmatic evolution and characteristics of mantle source*, Geological Magazine, Vol. 142, no. 2, p. 187-207

İlbeyli, N., 2008, *Geochemical comparison of ultramafic-mafic cumulate rocks from the Central Anatolian Ophiolites, Turkey*, International Geology Review, Vol. 50, p. 810-825

Irvine, T.N. and Barager, W.R.A., 1971, *A guide to the chemical classification of the common volcanic rocks*, Canadian Journal of Earth Science, Vol. 8, p. 523-548

Jaffey, N., and Robertson, A., 2001, *New sedimentological and structural data from the Ecemiş Fault Zone, southern Turkey: implications for its timing and offset and the Cenozoic tectonic escape of Anatolia*, Journal of the Geological Society, London, Vol. 158, p. 367-378

Jaffey, N., and Robertson, A., 2005, *Non-marine sedimentation associated with Oligocene-Recent exhumation and uplift of the central Taurus Mountains, S Turkey*, Sedimentary Geology, Vol. 173, p. 53-89

Kadıoğlu, Y.K., Dilek, Y., Güleç, N., and Foland, K.A., 2003, *Tectonomagmatic evolution of bimodal plutons in the Central Anatolian Crystalline Complex, Turkey*, The Journal of Geology, Vol. 113, no. 4, p. 671-690

Keskin, H., Dönmez, M., Akçay, A.E., 2010, Geological Map of the Kayseri L34 Quadrangle, Ankara, General Directorate of Mineral Research and Exploration

Kocak, K., and Leake, B.E., 1994, *The petrology of the Ortakoy district and its ophiolite at the western edge of the Middle Anatolian Massif*, Turkey, Journal of African Earth Sciences, Vol. 18, no. 2, p. 163-174

Kocak, K., Işik, F., Arslan, M., and Zedef, V., 2005, *Petrological and source region characteristics of ophiolitic hornblende gabbros from the Aksaray and Kayseri regions, central Anatolian crystalline complex, Turkey*, Journal of Asian Earth Sciences, Vol. 25, p. 883-891

Kocak, K., Kurt, H., Zedef, V., and Ferré, E.C., 2007, *Characteristics of the amphibolites from Niğde metamorphics (Central Turkey), deduced from whole rock and mineral chemistry,* Geochemical Journal, Vol. 41, p. 241-257

Leake, B.E., Woolley, A.R., Arps, C.E.S., Birch, W.D., Gilbert, M.C., Grice, J.D., Hawthorne, F.C., Kato, A., Kisch, H.J., Krivovichev, V.G., Linthout, K., Laird, J., Mandarino, J.A., Maresch, W.V., Nickel, E.H., Rock, N.M.S., Schumacher, J.C., Smith, D.C., Stephenson, N.C.N., Ungaretti, L., Whittaker, E.J.W., and Youzhi, G., 1997, *Nomenclature of amphiboles: report of the subcommittee on amphiboles of the international mineralogical association, commission on new minerals and mineral names*, The Canadian Mineralogist, Vol. 35, p. 219-246

Lefebvre, C., Barnhoorn, A., van Hinsbergen, D.J.J., Kaymakçı, N., and Vissers, R.L.M., 2011a, *Late Cretaceous extensional denudation along a marble detachment fault zone in the Kırşehir Massif near Kaman, central Turkey*, Journal of Structural Geology, Vol. 33, p. 1220-1236

Lefebvre, C., 2011b, *The tectonics of the Central Anatolian Crystalline Complex a structural, metamorphic and paleomagnetic study*, PhD dissertation, Utrecht Studies in Earth Sciences, Utrecht

Lefebvre, C., Meijers, M.J.M., Kaymakçı, N., Peynircioğlu, A., Langereis, C.G., and van Hinsbergen, D.J.J., 2013, *Reconstructing the geometry of central Anatolia during the late Cretaceous: Large-scale Cenozoic rotations and deformation between the Pontides and Taurides*, Earth and Planetary Science Letters, Vol. 366, p. 83-98

Lockock, A., 2014, *An Excel spreadsheet to classify chemical analyses of amphiboles following the IMA 2012 recommendations*, Computers and Geosciences, Vol. 62, p. 1-11

Maniar, P.D., and Piccoli, P.M., 1989, *Tectonic discrimination of granitoids*, Geological Society of America Bulletin, Vol. 101, p. 635-643

Mevel, C., 1988, *Metamorphism in oceanic layer 3, Gorringe Bank, Eastern Atlantic*, Contributions to Mineralogy and Petrology, Vol. 100, p. 496-509

Moores, E.M., 1982, Origin and emplacement of ophiolites, Reviews of Geophysics, Vol. 20, no. 4, p. 735-760

MTA (2002), *Geological Map of Turkey-Kayseri*, Ankara, General Directorate of Mineral Research and Exploration

Mullen, E.D., 1983, *$MnO/TiO_2/P_2O_5$: a minor element discriminant for basaltic rocks of oceanic environments and its implications for petrogenesis*, Earth Planetary and Science Letters, Vol. 62, p. 53-62

Otten, M.T., 1984, *The origin of brown hornblende in the Artfjället gabbro and dolerites*, Contributions to Mineralogy and Petrology, Vol. 86, p. 189-199

Padrón-Navarta, J.A., Sánchez-Vizcaíno, V.L., Garrido, C.J., and Gómez-Pugnaire, M.T., 2011, *Metamorphic record of high-pressure dehydration of antigorite serpentinite to chlorite harzburgite in a subduction setting (Cerro del Almirez, Nevado-Filábride Complex, Southern Spain),* Journal of Petrology, Vol. 52, p. 2047-2078

Parlak, O., Delaloye, M., and Bíngöl, E., 1996, *Mineral chemistry of ultramafic and mafic cumulates as an indicator of the arc-related origin of the Mersin ophiolite (southern Turkey),* Geologische Rundschau, Vol. 85, p. 647-661

Parlak, O., Höck, V., and Delaloye, M., 2000, *Suprasubduction zone origin of the Pozantı-Karsantı Ophiolite (southern Turkey) deduced from whole-rock and mineral chemistry of the gabbroic cumulates*, in Bozkurt, E., Winchester, J.A., and Piper, J.D.A. *Tectonics and magmatism in Turkey and the Surrounding Area*, Geological Society of London, Special Publications 173, p. 219-234

Parlak, O., Karaoğlan, F., Rizaoğlu, T., Klötzli, U., Koller, F., and Billor, Z., 2013, *U-Pb and ^{40}Ar-^{39}Ar geochronology of the ophiolites and granitoids from the Tauride belt: Implications for the evolution of the Inner Tauride suture*, Journal of Geodynamics, Vol. 65, p. 22-37

Passchier, C.W., and Trouw, R.A.J., 2005, *Microtectonics*, Springer, Berlin

Pearce, J.A., 1982, *Trace element characteristics of lavas from destructive plate boundaries*, in Thorpe, R.S., *Andesites: orogenic andesites and related rocks,* p. 525-548

Pearce, J.A., Lippard, S.J., and Roberts, S., 1984a, *Characteristics and tectonic significance of supra-subduction zone ophiolites*, in Kokelaar, B.P., and Howells, M.F., *Marginal Basin Geology: volcanic and associated sedimentary and tectonic processes in modern and ancient marginal basins*, Vol. 16, p. 77-94

Pearce, J.A., Harris, N.B.W., and Tindle, A.G., 1984b, *Trace element discrimination diagrams for the tectonic interpretation of granitic rocks*, Journal of Petrology, Vol. 25, p. 956-983

Pearce, J.A., 1996, *A user's guide to basalt discrimination diagrams,* in Wyman, D.A., *Trace element geochemistry of volcanic rocks: applications for massive sulphide exploration*, Geological Association of Canada, Short Course Notes, Vol. 12, p. 79-113

Pearce, J.A., 2008, *Geochemical fingerprinting of oceanic basalts with applications to ophiolite classification and the search for Archean oceanic crust*, Lithos, Vol. 100, p. 14-48

Robertson, A.H.F, Parlak, O. and Ustaömer, T., 2013, *Late Palaeozoic-Early Cenozoic tectonic development of Southern Turkey and the easternmost Mediterranean region: evidence from the inter-relations of continental and oceanic units*, in Robertson, A.H.F., Parlak, O. And Ünlügenç, U.C., *Geological development of Anatolia and the easternmost Mediterranean region*, Geological Society of London, Special Publications, 372, p. 9-48

Sarıfakıoğlu, E., Dilek, Y., and Winchester, J.A., 2013, *Late Cretaceous subduction initiation and Palaeocene-Eocene slab breakoff magmatism in South-Central Anatolia, Turkey*, International Geology Review, Vol. 55, no. 1, p. 66-87

Schmidt, M.W., 1992, *Amphibole composition in tonalite as a function of pressure: an experimental calibration of the Al-in-hornblende barometer*, Contributions to Mineralogy and Petrology, Vol. 293, p. 304-310

Şengör, A.M.C. and Yılmaz, Y. 1981, *Tethyan evolution of Turkey: a plate tectonic approach*, Tectonophysics, Vol. 75, p. 181-241

Shervais, J.W., 1982, *Ti-V plots and the petrogenesis of modern and ophiolitic lavas,* Earth and Planetary Science Letters, Vol. 59, p. 101-118

Sun, S.-s., and McDonough, W.F., 1989, *Chemical and isotopic systematics of oceanic basalts: implications for mantle composition and processes*, Geological Society of London Special Publications, Vol. 42, p. 313-345

Toksoy-Köksal, F., and Göncüoğlu, M.C., 2001, *Petrology of the Kurancali phlogopitic metagabbro: an island arc type ophiolitic sliver in the Central Anatolian Crystalline Complex*, International Geology Review, Vol. 43, p. 624-639

Toksoy-Köksal, F., Oberhaensli, R., and Göncüoğlu, M.C., 2009, *Hydrous aluminosilicate metasomatism in an intra-oceanic subduction zone: implications from the Kurancali (Turkey) ultramafic-mafic cumulates within the Alpine Neotethys Ocean*, Mineralogy and Petrology, Vol. 95, p. 273-290

Trommsdorff, V., Sánchez-Vizcaíno, L., Gómez-Pugnaire, M.T., and Müntener, O., 1998, *High pressure breakdown of antigorite to spinifex-textured olivine and orthopyroxene, SE Spain*, Contributions to Mineralogy and Petrology, Vol. 132, p. 139-148

Umhoefer, P.J., Whitney, D.L., Teyssier, C., Fayon, A.K., Casale, G., and Heizler, M., 2007, *Yo-yo tectonics in a wrench zone, Central Anatolian fault zone, Turkey*, in Till, A.B., Roeske, S.M., Sample, J.C., and Foster, D.A., *Exhumation associated with continental strike-slip fault systems*, Geological Society of America Special Paper 434, p. 35-57

van Hinsbergen, D.J.J., Maffione, M., Plunder, A., Kaymakçı, N., Ganerod, M., Hendriks, B.W.H., Corfu, F., Gürer, D., de Gelder, G.I.N.O., Peters, K., McPhee, P.J., Brouwer, F.M., Advokaat, E.L., and Vissers, R.L.M., 2016, *Tectonic evolution and paleogeography of the Kırşehir Block and the Central Anatolian Ophiolites, Turkey*, Tectonics, Vol. 35, TC004018

Vervoort, J.D., Wirth, K., Kennedy, B., Sandland, T., and Harpp, K.S., 2007, *The magmatic evolution of hte Midcontinent rift: New geochronologic and geochemical evidence from felsic magmatism*, Precambrian Research, Vol. 157, p. 235-268

Wakabayashi, J., and Dilek, Y., 2003, *What constitutes 'emplacement' of an ophiolite?: Mechanisms and relationship to subduction initiation and formation of metamorphic soles*, in Dilek, Y., and Robertson, P.T., *Ophiolites in Earth history*, Geological Society of London, Special Publications, 218, p. 427-447

Wells, P.R.A., *Pyroxene thermometry in simple and complex systems*, Contributions to Mineralogy and Petrology, Vol. 62, p. 129-139

Whitney, D.L., and Dilek, Y., 1997, *Core complex development in central Anatolia*, Geology, Vol. 25, p. 1023-1026

Whitney, D.L., and Dilek, Y., 1998, *Metamorphism during Alpine crustal thickening and extension in Central Anatolia, Turkey: the Niğde metamorphic core complex*, Journal of Petrology, Vol. 39, p. 1385-1403

Whitney, D.L., Teyssier, C., Dilek, Y., and Fayon, A.K., 2001, *Metamorphism of the Central Anatolian Crystalline Complex, Turkey: influence of orogen-normal vs. wrench dominated tectonics on P-T-t paths*, Journal of Metamorphic Geology, Vol. 19, p. 411-432

Whitney, D.L., Teyssier, C., Fayon, A.K., Hamilton, M.A. and Heizler, M., 2003, *Tectonic controls on metamorphism, partial melting and intrusion: timing and duration of regional metamorphism and magmatism in the Niğde Massif, Turkey*, Tectonophysics, Vol. 376, p. 37-60

Whitney, D.L., Teyssier, C., and Heizler, M., 2007, *Gneiss domes, metamorphic core complexes, and wrench zones: thermal and structural evolution of the Niğde Massif, central Anatolia*, Tectonics, Vol. 26, TC5002

Whitney, D.L., Umhoefer, P.J., Teyssier, C., and Fayon, A.K., 2008, *Yo-yo tectonics of the Niğde Massif during wrenching in Central Anatolia*, Turkish journal of Earth Sciences, Vol. 17, p. 209-217

Whitney, D.L., and Evans, B.W., 2010, *Abbreviations for names of rock-forming minerals*, American Mineralogist, Vol. 95, p. 185-187
Winter, J.D., 2010, *Principles of igneous and metamorphic petrology*, 2nd ed., Pearson, New York (?)

Williams, H., and Smyth, R., 1973, *Metamorphic aureoles beneath ophiolite suites and Alpine peridotites: Tectonic implications with west Newfoundland examples*, American Journal of Science, Vol. 273, p. 594-621

Winter, J.D., 2010, *Principles of igneous and metamorphic petrology*, Prentice Hall, New York

Yalınız, M.K., Floyd, P.A. and Göncüoğlu, M.C., 1996 *Supra-subduction zone ophiolites of Central Anatolia: geochemical evidence from the Sarikaraman Ophiolite, Aksaray, Turkey*, Mineralogical Magazine, Vol. 60, no. 402, p. 697-710

Yalınız, M.K., and Göncüoğlu, M.C., 1998, General geological characteristics and distribution of the Central Anatolian Ophiolites, Bulletin of Earth Sciences Application and Research Centre of Hacettepe University, Vol. 20, p. 19-30

Yalınız, M.K., and Göncüoğlu, M.C., 1999, *Clinopyroxene compositions of the isotropic gabbros from the Sarıkaraman Ophiolite: new evidence on supra-subduction zone type magma genesis in Central Anatolia*, Turkish Journal of Earth Sciences, Vol. 8, p. 103-111

Yalınız, M.K., Aydın, N.S., Göncüoğlu, M.C., and Parlak, O., 1999, *Terlemez quartz monzonite of Central Anatolia (Aksaray-Sarıkaraman): age, petrogenesis and geotectonic implications for ophiolite emplacement*, Geological Journal, Vol. 34, no. 3, p. 233-242

Yalınız, M.K., Göncüoğlu, M.C. and Özkan-Altiner, S., 2000, *Formation and emplacement ages of the SSZ-type Neotethyan ophiolites in Central Anatolia, Turkey: palaeotectonic implications*, Geological Journal, Vol. 35, p. 35-68

Yalınız, M.K, 2008, *A geochemical attempt to distinguish forearc and back arc ophiolites from the "supra-subduction" Central Anatolian Ophiolites (Turkey) by comparison with modern oceanic analogues*, Ofioliti, Vol. 33, no. 2, p. 119-129

Yılmaz, S., and Boztuğ, D., 1998, *Petrogenesis of the Çiçekdağ Igneous Complex, N of Kırşehir, Central Anatolia, Turkey*, Turkish Journal of Earth Sciences, Vol. 7, p. 185-199

Appendix 1

Sample Descriptions

Table 1: Petrographic descriptions of all hand samples obtained as a part of this study. Samples that were analyzed for whole-rock or mineral chemistry are indicated in columns 4-6. Mineral abbreviations are from Whitney and Evans (2010). In column 7, bold font indicates the mineral was analyzed by WDS, while italic font indicates it was analyzed by EDS. Quantitative data for analyzed minerals is given in Appendix 4.
Abbreviations: EMC: Ecemiş Mafic Complex, EPMA: electron probe microanalysis; ICP-MS: inductively coupled plasma mass spectrometry, NMC: Niğde Mafic Complex, XRF: X-ray fluorescence. M_3pl (N): northern conglomerates tentatively correlated to the upper Miocene $m_3$pl unit. M_3pl (S): upper Miocene conglomerates in the Ulukışla Basin.

Table 1: Sample descriptions

Sample Number	Unit	Lithology	XRF	ICP-MS	EPMA	Mineral Assemblage	Texture	Coordinates (Lat, Long)
ND01-17A	Aşıgediği	Amphibolite	X			Hbl + Pl + Qz + Bt		37.8465 N, 34.8360 E
ND01-32B	Gümüşler	Amphibolite	X	X		Hbl + Pl + Qz + Bt		37.9500 N, 34.8124 E
ND14-01	Float, NMC	Cobble (gabbro)				Pl + Hbl	Disequilibrium, amphibole overprinting plagioclase	38.03224 N, 34.74825 E
ND14-02A	NMC	Metagabbro				Pl + Hbl + Cpx + Ttn	Porphyroclastic with synkinematic hornblende and plagioclase	38.01018 N, 34.75679 E
ND14-02B	NMC	Metagabbro			X	**Pl** + **Cpx** + **Hbl** + Ttn	Porphyroclastic with synkinematic hornblende and plagioclase	38.01018 N, 34.75679 E
ND14-02C	NMC	Protomylonite				Pl + Hbl + Qz + Ttn	Porphyroclastic- mylonitic. Synkinematic Qz, Pl, Hbl	38.01018 N, 34.75679 E
ND14-02D	NMC	Protomylonite				Pl + Qz + Bt + Afs	Porphyroclastic with minor myrmeckite on secondary alkali feldspar	38.01018 N, 34.75679 E
ND14-02E	NMC	Protomylonite				Pl + Qz + Hbl + Bt + Zr	Porphyroclastic with minor skeletal hornblende	38.01018 N, 34.75679 E
ND14-03A	EMC	Gabbro				Ol + Cpx + Pl + Srp	Strongly serpentinized, plagioclase poor.	38.0764 N, 35.12908 E
ND14-03B	EMC	Ultramafic				Srp + Mag	Bastite texture reflects relict Opx cumulate. Interstices dominated by oxides. Cut by Srp vein.	38.0764 N, 35.12908 E
ND14-04A	Çukurbağ	Cobble (gabbro)				Ol + Cpx + Pl + Srp + Act	Flow texture. Igneous textured with minor alteration to Srp, Act and iddingsite.	38.14707 N, 35.13839 E
ND14-04B	Çukurbağ	Cobble (diabase)	**X**			Pl + Hbl + Ttn + Chl + uralite	Nice interstitial titanite, cross-cutting carbonate vein. Hbl looks secondary. Bimodal grain size in Pl.	38.14707 N, 35.13839 E
ND14-05A	M_3pl (N)	Float (metagabbro)				Pl + Hbl	Polygonal textured hornblende and zoned plagioclase. Weakly developed fabric.	38.2215 N, 35.0612 E

Sample Number	Unit	Lithology	XRF	ICP-MS	EPMA	Mineral Assemblage	Texture	Coordinates (Lat, Long)
ND14-05B	M_3pl (N)	Float (diabase)				Pl + Hbl	Hbl mats have replaced primary mafic phase. Coarse, cracked & zoned Pl. Unique texture.	38.2215 N, 35.0612 E
ND14-06A	EMC	Gabbro	X			Cpx + Pl + Ac	Needly actinolite aggregates along grain boundaries. Pervasive alteration.	38.01138 N, 35.10219 E
ND14-06B	EMC	Gabbro				Ol + Cpx + Pl + Srp	Very anhedral grain shapes, cracking in feldspar due to expansion of olivine.	38.01138 N, 35.10219 E
ND14-06C	EMC	Ultramafic				Srp + Cpx + Pl	Mesh texture and relict cpx replaced by optically indiscernable aggregate.	38.01138 N, 35.10219 E
ND14-06D	EMC	Gabbro				Ol + Cpx + Srp + Pl	Serpentinized	38.01138 N, 35.10219 E
ND14-07A	EMC	Gabbro	X	X	X	**Ol** + **Cpx** + **Pl** + Ac + Srp	Altering along grain boundaries, strongly seriticized feldspar	37.9924 N, 35.1039 E
ND14-08A	Aladağ Ophiolite?	Ultramafic				Ol + Opx + Srp + Chr	Olivine in mesh texture being replaced by iddingsite and serpentine. Large amount of Opx	37.78225 N, 35.07171 E
ND15-01	Çukurbağ	cobble (gabbro)				Pl + Cpx + uralite	Undeformed, coarse grained. Alteration to uralite.	38.14685 N, 35.13848 E
ND15-02	Çukurbağ	cobble (gabbro)				Pl + Hbl + Chl	Plagioclase cumulate with poikilitic intercumulus hornblende. Secondary chlorite.	38.14685 N, 35.13848 E
ND15-03	Çukurbağ	cobble (gabbro)				Pl + Cpx + Chl	Magmatic flow texture, overprinted by feathery chlorite.	38.14685 N, 35.13848 E
ND15-04	Çukurbağ	cobble (gabbro)				Pl + Cpx + Act + Sp	Equigranular, altered. Poikilitic-reactive Cpx-Pl phase boundaries.	38.14772 N, 35.1388 E
ND15-05	Çukurbağ	cobble (gabbro)				Pl + Cpx + Act + Chl + Sp	Equigranular, strongly altered to actinolite and chlorite. Spinel occurs with secondary assemblage.	38.14772 N, 35.1388 E
ND15-06	EMC	Gabbro	X	X		Pl + Cpx + Ol	Equigranular, pristine	37.99448 N, 35.10757 E

Sample Number	Unit	Lithology	XRF	ICP-MS	EPMA	Mineral Assemblage	Texture	Coordinates (Lat, Long)
ND15-07	Çukurbağ	Cobble (gabbro)				Pl + Hbl + Chl	Inequigranular, porphyritic. Zoned plagioclase and metamorphic? hornblende.	37.89441 N, 35.09982 E
ND15-08A	Çukurbağ	cobble (gabbro)	X			Pl + Cpx + Ol + uralite	Strongly altered.	37.89448 N, 35.09982 E
ND15-08B	Çukurbağ	cobble (plagiogranite)				Pl + Qz + Hbl + Afs	Undeformed, slightly undulose quartz.	37.89448 N, 35.09982 E
ND15-09A	NMC	Gabbro				Pl + Hbl + Bt + Qz + Afs + Cpx	Mylonitic, granitic segregation	38.00996 N, 34.75678 E
ND15-09B	NMC	Gabbro				Pl + Hbl	Mylonitic, porphyroclastic	38.00996 N, 34.75678 E
ND15-09C	NMC	Plagiogranite				Pl + Qz	True mylonite	38.00996 N, 34.75678 E
ND15-09D	NMC	Gabbro				Pl + Hbl + Cpx	Hornblende moat texture	38.00996 N, 34.75678 E
ND15-09E	NMC	Gabbro				Pl + Hbl + Cpx	Coarse grained clinopyroxene	38.00996 N, 34.75678 E
ND15-09F	NMC	Gabbro				Pl + Hbl + Cpx	Undeformed to mylonitic	38.00996 N, 34.75678 E
ND15-09G	NMC	Gabbro				Pl + Hbl	Mylonitic, porphyroclastic	38.00996 N, 34.75678 E
ND15-09H	NMC	Gabbro				Pl + Hbl + Bt	Undeformed to mylonitic	38.00996 N, 34.75678 E
ND15-09I	NMC	Granitoid				Qz + Pl + Afs + Bt + Zr	Mylonitic, porphyroclastic	38.00996 N, 34.75678 E
ND15-09J	NMC	Gabbro	X			Pl + Hbl + Cpx + opaques	Coarse grained undeformed	38.00996 N, 34.75678 E

Sample Number	Unit	Lithology	XRF	ICP-MS	EPMA	Mineral Assemblage	Texture	Coordinates (Lat, Long)
ND15-10	NMC	Gabbro				Pl + Hbl	Lightly deformed	38.02005 N, 34.76472 E
ND15-11A	NMC	Gabbro				Pl + Hbl + Qz	Undeformed	38.02184 N, 34.76223 E
ND15-11B	NMC	Gabbro	X			Pl + Hbl	Slight fabric	38.02184 N, 34.76223 E
ND15-12	NMC	Plagiogranite				Pl + Hbl + Qz	Protomylonitic, possibly cummingtonite cores in hornblende	38.02209 N, 34.76722 E
ND15-13	NMC	Plagiogranite				Pl + Hbl + Qz	Mylonitic	38.01467 N, 34.74663 E
ND15-14	NMC	Diabase	X			Hbl + Pl + Bt		38.02942 N, 34.74106 E
ND15-15	NMC	Gabbro	X	X	X	**Pl** + **Hbl** + **Opx** + **Cpx**	Slight fabric	38.02942 N, 34.74106 E
ND15-16	NMC	Gabbro	X	X		Pl + Hbl + Cpx	Undeformed	38.02942 N, 34.74106 E
ND15-17A	M_3pl (S)	cobble (gabbro)				Pl + Cpx + Ol + Chl + Sp	Cumulate, with alteration halos around olivine.	37.79285 N, 34.83465 E
ND15-17B	M_3pl (S)	cobble (gabbro)				Pl + Cpx + uralite + Sp + Chl	Altered ~80%	37.79285 N, 34.83465 E
ND15-18	M_3pl (S)	cobble (gabbro)				Pl + Cpx + Ol + uralite + Sp	Flow fabric. Alteration haloes around olivine.	37.79166 N, 34.82545 E
ND15-19A	Çukurbağ	cobble (limestone)				Cal		37.7886 N, 35.00814 E
ND15-19B	Çukurbağ	cobble (gabbro)	X			Pl + Cpx + Chl + uralite	Strongly altered	37.7886 N, 35.00814 E

Sample Number	Unit	Lithology	XRF	ICP-MS	EPMA	Mineral Assemblage	Texture	Coordinates (Lat, Long)
ND15-19C	Çukurbağ	cobble (gabbro)				Pl + Cpx + Ttn + Chl + uralite	Strongly altered	37.7886 N, 35.00814 E
ND15-20	NMC	Diabase				Pl + Hbl + Cpx	Acicular plagioclase with flow texture, hornblende partially replacing clinopyroxene	38.04366 N, 34.83705 E
ND15-21A	NMC	Granitoid				Qz + Hbl + Pl	Mylonitic, porphyroclastic	38.04189 N, 34.83964 E
ND15-21B	NMC	Plagiogranite	X			Qz + Hbl + Pl	Mylonitic	38.04189 N, 34.83964 E
ND15-22A	NMC	amphibolite				Qz + Pl + Hbl	Mylonitic	38.03722 N, 34.8397 E
ND15-22B	NMC	granitic gneiss				Bt + Qz + Pl	Mylonite	38.03722 N, 34.8397 E
ND15-22C	NMC	Amphibolite			X	**Hbl** + Qz + **Pl**	Mylonitic	38.03722 N, 34.8397 E
ND15-22D	Üçkapılı	Pegmatite				Qz + Fsp	Undeformed	38.03722 N, 34.8397 E
ND15-23	NMC	Gabbro				Pl + Hbl + Cpx + Qz	Pegmatitic replacive	38.03455 N, 34.85101 E
ND15-24	NMC	Gabbro	X			Pl + Cpx + uralite	Undeformed with uralite clusters replacing unknown mineral(s).	38.03522 N, 34.85263 E
ND15-25	NMC	Rhyolite	X			Pl + Qz + Bt + Ms	Slightly deformed, devitrified, porphyritic	38.03675 N, 34.8521 E
ND15-26	NMC	gneiss				Pl + Qz + Bt + Ms	Gneissose	38.00586 N, 34.85191 E
ND15-27	NMC	Gabbro				Pl + Hbl + Qz + Cpx + Cal	Amphibolitized, pseudomorphed pegmatitic texture	38.03478 N, 34.8903 E

Sample Number	Unit	Lithology	XRF	ICP-MS	EPMA	Mineral Assemblage	Texture	Coordinates (Lat, Long)
ND15-28	NMC	Diabase	X	X		Pl + Hbl + Qz	Fine grained igneous texure completely amphibolitized	38.04575 N, 34.87593 E
ND15-29	NMC	Diabase	X			Pl + Qz + Hbl	Porphyritic	38.02634 N, 34.89849 E
ND15-30A	N. Region	Gabbro				Pl + Hbl + Qz	Protomylonitic	38.19878 N, 35.06535 E
ND15-30B	N. Region	ultramafic				Srp	Bastite textured and mesh textured serpentine as well as darker amorphous material.	38.19878 N, 35.06535 E
ND15-31	N. Region	Plagiogranite	X		X	*Pl* + Qz + *Cum* + *Chl*	Porphyroclastic	38.19944 N, 35.06783 E
ND15-32	N. Region	Diabase	X			Pl + Hbl + Qz	Undeformed, amphibolitized	38.20171 N, 35.06634 E
ND15-33A	M_3pl (N)	cobble (metagabbro)				Pl + Hbl + Opx + Cpx	Undeformed, poikilitic hornblende overprinting flow/cumulus texture.	38.22279 N, 35.05791 E
ND15-33B	M_3pl (N)	cobble (metagabbro)				Pl + Hbl + Cpx	Plagioclase is undeformed. Cpx partially replaced by Hbl. Polygonal Hbl mats after Cpx	38.22279 N, 35.05791 E
ND15-34A	N. Region	Gabbro				Pl + Hbl + Qz + Cpx	Veins of fibrous amphibole .	38.22818 N, 34.95158 E
ND15-34B	N. Region	Gabbro	X	X	X	**Pl** + **Ol** + **Cpx** + **Opx** + **Hbl**	Equigranular, igneous textured	38.22818 N, 34.95158 E
ND15-34C	N. Region	Gabbro				Pl + Ol + Cpx + Ac + iddingsite	Equigranular, igneous textured	38.22818 N, 34.95158 E
ND15-34D	N. Region	Gabbro				Pl + Hbl	Cataclastic	38.22818 N, 34.95158 E
ND15-35	M_3pl (N)	cobble (metagabbro)				Pl + Hbl	Most plagioclase is euhedral, but some is recrystallized. Hbl alone or in mats.	38.07973 N, 34.93031 E

Sample Number	**Unit**	**Lithology**	**XRF**	**ICP-MS**	**EPMA**	**Mineral Assemblage**	**Texture**	**Coordinates (Lat, Long)**
ND15-36A	NMC	Gabbro			X	**Pl** + **Opx** + **Cpx** + **Hbl**	Undeformed, very coarse	38.04772 N, 34.91239 E
ND15-36B	NMC	Gabbro	X	X	X	**Pl** + **Opx** + **Cpx** + **Hbl**	Poikilitic, Undeformed	38.04772 N, 34.91239 E
ND15-37	NMC	Gabbro				Pl + Hbl + Qz	Undeformed	37.9606 N, 34.8655 E
ND15-38A	NMC	Gabbro	X			Amp + Cb + Cpx	Cumulate	37.96175 N, 34.87276 E
ND15-38B	NMC	Hornblendite			X	**Amp** + Cb + **Cpx**	Cumulate	37.96175 N, 34.87276 E
ND15-38C	Aşıgediği	Quartzite				Qz	Deformed	37.96175 N, 34.87276 E
ND15-39	Gümüşler	Gneiss				Qz + Bt + Fsp	Gneissose	37.96257 N, 34.88025 E
ND15-40A	NMC	Plagiogranite	X		X	Qz + *Pl* + *Bt* + *Cum* + *Hbl*	Recrystallized	38.02985 N, 34.74078 E
ND15-40B	NMC	Diabase	X	X	X	**Pl** + **Hbl** + Bt + Qz + **Afs**	Amphibolitized	38.02985 N, 34.74078 E
ND15-40C	Üçkapılı	Pegmatite				Afs + Qz	Granophyre	38.02985 N, 34.74078 E
ND15-41	M_3pl (S)	cobble (metadiabase)	X			Pl + Hbl + Qz + Chl	Porphyritic, amphibolitized	37.78354 N, 34.97796 E
ND15-42	M_3pl (S)	cobble (metagabbro)				Pl + Hbl + Cpx + Ep	Coarse, twinned, poikilitic hornblende. Polygonal textured mats enclosing Pl + Cpx.	37.77607 N, 34.83318 E
ND15-43	M_3pl (S)	cobble (gabbro)	X			Pl + Hbl + Cpx	Hornblende or uralite metagabbro	37.74267 N, 34.7411 E

Sample Number	Unit	Lithology	XRF	ICP-MS	EPMA	Mineral Assemblage	Texture	Coordinates (Lat, Long)
ND15-44	M_3pl (S)	cobble (gabbro)	X			Pl + Ep + Cpx + Ol	Moats of epidote	37.78556 N, 34.8151 E
ND15-45	M_3pl (S)	cobble (diabase)				Pl + Cpx + Sp + Chl + uralite	Flow texture of Cpx and Pl. Overprinted ~50% by replacement assemblage	37.79258 N, 34.83747 E
ND15-46	M_3pl (S)	cobble (metagabbro)	X			Pl + Hbl + Cpx	Cpx cores with hornblende mats.	37.79528 N, 34.87641 E
ND15-47A	Aşıgediği	gneiss				Pl + Qz + Hbl	Gneissose	37.87794 N, 34.8921 E
ND15-47B	Aşıgediği	amphibolite	X	X		Cpx + Hbl + Pl + Ep + Cb	Gneissose	37.87794 N, 34.8921 E
ND15-47C	Aşıgediği	eclogite				Gt + Cpx + Ep		37.87794 N, 34.8921 E
ND15-47D	Aşıgediği	amphibolite				Hbl + Qz + Gt		37.87794 N, 34.8921 E
ND15-47E	Aşıgediği	amphibolite				Hbl + Cb + Ep	Strongly foliated	37.87794 N, 34.8921 E
ND15-48A	NMC	metaperidotite			X	**Ol** + **Tr** + Tlc + Srp	Spinifex texture of Ol + Tr + Tlc, overprinted by Srp.	37.98822 N, 34.89011 E
ND15-48B	NMC	serpentinite				Chl + Srp	chlorite overprinting serpentine, chlorite is kinked	37.98822 N, 34.89011 E
ND15-48C	NMC	Diabase				Pl + Hbl	Porphyritic, amphibolitized, altered	37.98822 N, 34.89011 E
ND15-48D	NMC	metaperidotite				Ol + Tlc + Tr + Srp	Spinifex textured olivine that has been retrograded to serpentine.	37.98822 N, 34.89011 E
ND15-48E	NMC	Gabbro	X		X	**Pl** + **Opx** + **Cpx** + Hbl	Igneous, equigranular, pristine. Somewhat layered.	37.98822 N, 34.89011 E

Sample Number	Unit	Lithology	XRF	ICP-MS	EPMA	Mineral Assemblage	Texture	Coordinates (Lat, Long)
ND15-48F	Üçkapılı	Aplite Dike	X			Ab + Qz + Bt + Gt + Ms	xenomorphic granular/aplitic	37.98822 N, 34.89011 E
ND15-48G	NMC	Gabbro	X	X		Pl + Cpx + Opx + Hbl	Replacive	37.98822 N, 34.89011 E
ND15-49A	M_3pl (N)	cobble (gabbro)				Pl + Cpx + uralite	~70 % replaced by uralite.	38.07938 N, 34.97025 E
ND15-49B	M_3pl (N)	cobble (diabase)				Pl + Hbl	Porphyritic, igneous textured.	38.07938 N, 34.97025 E
ND15-50A	NMC	Amphibolite				Hbl + Qz + Pl	Deformed	38.06963 N, 35.00359 E
ND15-50B	NMC	ultramafic				Srp + Mag	Bastite and meshwork textured serpentine. Magnetite forms walls of meshwork.	38.06963 N, 35.00359 E
ND15-50C	NMC	Gabbro	X			Pl + Hbl	Undeformed	38.06963 N, 35.00359 E
ND15-50D	NMC	Plagiogranite	X			Pl + Qz	Lightly deformed, recrystallized	38.06963 N, 35.00359 E
ND15-50E	NMC	Amphibolite				Hbl + Cal + Qz + Pl	Slight fabric	38.06963 N, 35.00359 E
ND15-51A	NMC	Gabbro (?)				Chl + Ep + Cal + Qz		38.03359 N, 34.82002 E
ND15-51B	NMC	Unknown				Chl + Cal +Act	Metaultramafic or metsomatic	38.03359 N, 34.82002 E
ND15-51C	NMC	ultramafic				Srp + Chr + Hc	Bastite textures, serpentine veins.	38.03359 N, 34.82002 E
ND15-51D	NMC	Gabbro				Hbl + Pl + Qz	Protomylonitic	38.03359 N, 34.82002 E

Sample Number	Unit	Lithology	XRF	ICP-MS	EPMA	Mineral Assemblage	Texture	Coordinates (Lat, Long)
ND15-51E	NMC	hornblende-chlorite schist			X	**Hbl** + Chl + Qz + Pl	Strong foliation defined by fibrous chlorite.	38.03359 N, 34.82002 E
ND15-51F	NMC	Gabbro or diabase			X	**Hbl** + **Pl** + Qz + Ms(Tlc?)	Porphyroclastic, Mylonitic	38.03359 N, 34.82002 E
ND15-52	Aşıgediği	Amphibolite	X			Hbl + Cal + Ep + Pl	Strongly deformed	37.89328 N, 34.71012 E
ND15-53A	N. Region	Gabbro			X	**Ts** + **Ac** + **Pl** + Qz	Metamorphic overprint	38.16915 N, 34.75048 E
ND15-53B	N. Region	Basalt	X	X	X	**Amp (Ts, Ac, Mhb)** + **Pl** + Qz	Fine grained	38.16915 N, 34.75048 E
ND15-53C	N. Region	Gabbro			X	**Hbl** + **Pl**	Pegmatitic upper, Gabbroic lower	38.16915 N, 34.75048 E
PU15-13A	Çukurbağ	Cobble (sandstone)				Qz + Fsp + Cal	Fairly angular grains, non-undulose quartz	37.90568 N, 35.0994 E
PU15-13B	Çukurbağ	Cobble (diabase)				Hbl + Pl + Chl + ur	Acicular plagioclase with zoning. Brown Hbl is weathered but appears primary. Similar to NMC.	37.90568 N, 35.0994 E
PU15-13C	Çukurbağ	Cobble (micrite?)				N/A	Cryptocrystalline, but layering is apparent and some carbonate veins	37.90568 N, 35.0994 E
PU15-13D	Çukurbağ	Cobble (granite)				Qz + Fsp	Fine-grained quartz and feldspar without mafic mineral. Non undulose quartz.	37.90568 N, 35.0994 E
PU15-14	Çukurbağ	Cobble (gabbro)	X			Pl + Cpx + Hbl + Ch	Euhedral, zoned plagioclase. Chl overgrowths on Cpx. Cracked cores in Pl. Hbl primary?	37.90568 N, 35.0994 E
PU15-17	Çukurbağ	Cobble (gabbro)				Pl + Ol + Hbl + Chl	Gorgeous euhedral Ol (110) face. Abundant secondary chlorite. Zoned euhedral plagioclase.	37.91304 N, 35.08693 E
ND8614	Çukurbağ	Cobble (gabbro)				Cpx + Pl + Act	Undeformed, igneous textured Cpx gabbro. Rounded grains.	37.90668 N, 35.09982 E
ND9614	Çukurbağ	Cobble (gabbro)				Hbl + Pl	Twinned hbl, unclear whether primary or secondary. Plag weathered to isotropic material.	37.90714 N, 35.15305 E

Appendix 2

Mineral Compositions

Table 1: Clinopyroxene compositions obtained using wavelength dispersive analysis (WDS) on a Jeol JXA-8900R electron microprobe at the University of Minnesota. Components (En: enstatite, Fs: ferrosilite, Wo: wollastonite) were calculated using atomic proportions.

Table 2: Orthopyroxene compositions obtained using WDS on a Jeol JXA-8900R electron microprobe at the University of Minnesota. Components (En: enstatite, Fs: ferrosilite, Wo: wollastonite) were calculated using atomic proportions.

Table 3: Olivine compositions obtained using WDS on a Jeol JXA-8900R electron microprobe at the University of Minnesota. Components (Fo: forsterite, Fa: fayalite) were calculated using atomic proportions.

Table 4: Amphibole compositions obtained using WDS on a Jeol JXA-8900R electron microprobe at the University of Minnesota.

Table 5: Feldspar compositions obtained using WDS on a Jeol JXA-8900R electron microprobe at the University of Minnesota. Components (An: anorthite, Ab: albite, Or: orthoclase) were calculated using atomic proportions.

Table 6: Approximate mineral compositions of assemblages in plagiogranite obtained using energy dispersive spectroscopy (EDS) on a Jeol JXA-8900R electron microprobe at the University of Minnesota. Amphibole names were determined using the spreadsheet of Locock (2014).

Table 1: Clinopyroxene compositions obtained using wavelength dispersive analysis

Sample no.	**ND14-02B**	**ND14-02B**	**ND14-02B**	**ND14-02B**	**ND14-02B**	**ND14-02B**	**ND14-02B**	**ND14-02B**	**ND14-02B**	**ND14-02B**	**ND14-02B**
Lithology	Metagabbro	Metagabbro	Metagabbro	Metagabbro	Metagabbro	Metagabbro	Metagabbro	Metagabbro	Metagabbro	Metagabbro	Metagabbro
Unit	NMC	NMC	NMC	NMC	NMC	NMC	NMC	NMC	NMC	NMC	NMC
Analysis no.	112	113	114	115	116	117	118	119	120	136	137
SiO_2	52.22	53.24	53.15	53.26	53.14	53.26	53.12	53.19	53.11	53.15	53.27
TiO_2	0.14	0.11	0.12	0.14	0.16	0.09	0.08	0.03	0.20	0.03	0.05
Al_2O_3	1.05	0.92	0.96	0.96	0.86	0.94	0.85	0.81	1.14	0.81	0.87
Cr_2O_3	0.00	0.09	0.08	0.01	0.06	0.02	0.05	0.02	0.00	0.07	0.06
FeO	8.50	6.98	6.93	6.86	6.76	7.08	8.36	8.22	7.35	8.58	8.41
MnO	0.33	0.29	0.30	0.24	0.26	0.30	0.28	0.35	0.26	0.32	0.28
MgO	13.19	14.28	14.28	14.30	13.71	14.30	13.17	13.69	13.73	13.40	13.35
CaO	24.18	24.59	24.43	24.48	23.61	24.45	24.19	24.43	24.57	24.45	24.41
Na_2O	0.28	0.27	0.30	0.28	0.27	0.32	0.24	0.27	0.33	0.32	0.24
K_2O	0.00	0.00	0.02	0.00	0.00	0.01	0.01	0.00	0.00	0.01	0.00
Total	99.88	100.78	100.58	100.53	98.82	100.78	100.36	101.03	100.69	101.14	100.94
En	44	40	40	40	40	40	37	38	39	37	37
Fs	7	11	11	11	11	11	14	13	12	14	14
Wo	49	49	49	49	49	49	49	49	49	49	49

Table 1 (ctd.): Clinopyroxene compositions obtained using wavelength dispersive analysis

Sample no.	**ND14-02B**	**ND14-02B**	**ND14-02B**	**ND14-02B**	**ND14-02B**	**ND14-02B**	**ND14-02B**	**ND14-02B**	**ND14-02B**	**ND14-07**	**ND14-07**
Lithology	Metagabbro	Metagabbro	Metagabbro	Metagabbro	Metagabbro	Metagabbro	Metagabbro	Metagabbro	Metagabbro	Gabbro	Gabbro
Unit	NMC	NMC	NMC	NMC	NMC	NMC	NMC	NMC	NMC	EMC	EMC
Analysis no.	138	142	143	145	147	149	150	151	152	297	298
SiO_2	53.25	53.47	53.32	52.98	53.23	52.65	53.17	53.33	52.96	52.26	52.50
TiO_2	0.06	0.10	0.12	0.22	0.00	0.08	0.06	0.09	0.24	0.32	0.33
Al_2O_3	0.61	0.81	0.95	1.16	0.92	1.47	1.06	0.94	1.27	2.68	2.44
Cr_2O_3	0.04	0.01	0.01	0.02	0.06	0.05	0.00	0.02	0.03	0.47	0.43
FeO	8.75	8.18	7.79	8.58	8.58	9.14	9.02	8.68	8.73	5.02	5.37
MnO	0.35	0.34	0.26	0.29	0.29	0.33	0.31	0.36	0.29	0.13	0.14
MgO	13.05	13.41	13.52	13.28	13.24	12.65	13.03	13.14	13.12	17.54	18.07
CaO	24.76	24.48	24.51	24.26	24.42	24.07	24.16	24.13	24.36	21.58	20.27
Na_2O	0.24	0.27	0.28	0.30	0.30	0.31	0.28	0.31	0.28	0.21	0.19
K_2O	0.00	0.00	0.00	0.01	0.01	0.02	0.00	0.00	0.02	0.00	0.02
Total	101.12	101.07	100.75	101.08	101.02	100.76	101.08	100.99	101.30	100.23	99.77
En	37	37	38	37	37	36	37	37	37	49	51
Fs	14	13	13	14	14	15	15	14	14	8	9
Wo	49	49	49	49	49	49	49	49	49	43	41

Table 1 (ctd.): Clinopyroxene compositions obtained using wavelength dispersive analysis

Sample no.	**ND14-07**	**ND14-07**	**ND14-07**	**ND14-07**	**ND14-07**	**ND14-07**	**ND14-07**	**ND15-15**	**ND15-15**	**ND15-15**	**ND15-15**
Lithology	Gabbro	Gabbro	Gabbro	Gabbro	Gabbro	Gabbro	Gabbro	Metagabbro	Metagabbro	Metagabbro	Metagabbro
Unit	EMC	EMC	EMC	EMC	EMC	EMC	EMC	NMC	NMC	NMC	NMC
Analysis no.	299	300	301	311	312	313	314	242	243	244	245
SiO_2	52.40	52.85	52.15	52.06	52.39	52.43	52.90	52.31	51.95	52.80	52.71
TiO_2	0.35	0.36	0.30	0.36	0.28	0.32	0.32	0.20	0.31	0.16	0.17
Al_2O_3	2.67	2.61	2.60	2.75	2.30	2.67	2.56	1.54	1.73	1.24	1.43
Cr_2O_3	0.46	0.46	0.40	0.43	0.38	0.47	0.52	0.04	0.01	0.09	0.02
FeO	4.68	4.69	4.45	4.72	5.23	4.68	4.70	7.78	7.96	7.51	7.60
MnO	0.18	0.15	0.14	0.13	0.26	0.13	0.12	0.25	0.27	0.32	0.27
MgO	17.06	17.15	17.08	16.95	16.76	17.69	17.26	15.02	14.90	14.63	14.72
CaO	22.60	22.57	22.91	22.12	22.36	21.75	22.34	22.78	22.72	23.25	22.67
Na_2O	0.23	0.23	0.25	0.23	0.23	0.26	0.22	0.26	0.30	0.28	0.29
K_2O	0.00	0.00	0.00	0.00	0.02	0.01	0.01	0.00	0.00	0.01	0.02
Total	100.63	101.06	100.28	99.74	100.21	100.42	100.95	100.18	100.15	100.28	99.90
En	47	48	47	48	47	49	48	42	42	41	42
Fs	8	8	7	8	9	7	8	13	13	12	12
Wo	45	45	46	45	45	43	45	46	46	47	46

Table 1 (ctd.): Clinopyroxene compositions obtained using wavelength dispersive analysis

Sample no.	**ND15-15**	**ND15-15**	**ND15-15**	**ND15-15**	**ND15-15**	**ND15-15**	**ND15-15**	**ND15-15**	**ND15-15**	**ND15-15**	**ND15-15**
Lithology	Metagabbro	Metagabbro	Metagabbro	Metagabbro	Metagabbro	Metagabbro	Metagabbro	Metagabbro	Metagabbro	Metagabbro	Metagabbro
Unit	NMC	NMC	NMC	NMC	NMC	NMC	NMC	NMC	NMC	NMC	NMC
Analysis no.	246	247	248	249	278	279	280	281	282	283	256
SiO_2	51.85	53.03	52.27	52.46	52.72	52.92	52.79	52.37	53.23	52.78	52.52
TiO_2	0.30	0.18	0.28	0.19	0.20	0.14	0.18	0.21	0.15	0.14	0.15
Al_2O_3	1.98	1.17	1.71	1.53	1.24	1.25	1.13	1.45	1.02	1.16	1.37
Cr_2O_3	0.02	0.05	0.05	0.03	0.02	0.01	0.03	0.01	0.07	0.01	0.05
FeO	7.49	7.82	7.72	7.75	8.11	8.23	8.02	8.25	7.91	8.20	7.92
MnO	0.19	0.28	0.19	0.25	0.33	0.27	0.26	0.27	0.34	0.26	0.29
MgO	15.04	14.96	15.14	14.76	14.86	14.61	14.57	14.85	14.54	14.49	14.75
CaO	23.04	22.94	22.54	22.56	22.77	23.18	23.49	22.50	23.40	22.96	23.08
Na_2O	0.29	0.27	0.30	0.27	0.24	0.26	0.22	0.24	0.23	0.25	0.31
K_2O	0.00	0.01	0.01	0.02	0.00	0.00	0.00	0.01	0.00	0.00	0.00
Total	100.18	100.72	100.21	99.80	100.51	100.86	100.69	100.15	100.89	100.27	100.43
En	42	42	42	42	41	41	40	41	40	41	41
Fs	12	13	12	13	13	13	13	13	13	13	13
Wo	46	46	45	46	46	46	47	45	47	46	46

Table 1 (ctd.): Clinopyroxene compositions obtained using wavelength dispersive analysis

Sample no.	**ND15-34B**	**ND15-34B**	**ND15-34B**	**ND15-34B**	**ND15-34B**	**ND15-34B**	**ND15-34B**	**ND15-34B**	**ND15-34B**	**ND15-34B**	**ND15-34B**
Lithology	Gabbro	Gabbro	Gabbro	Gabbro	Gabbro	Gabbro	Gabbro	Gabbro	Gabbro	Gabbro	Gabbro
Unit	N. Region	N. Region	N. Region	N. Region	N. Region	N. Region	N. Region	N. Region	N. Region	N. Region	N. Region
Analysis no.	164	165	166	167	168	169	187	188	189	190	205
SiO_2	52.44	52.62	52.24	53.73	53.34	52.71	54.02	53.07	53.30	53.18	53.48
TiO_2	0.31	0.26	0.33	0.14	0.21	0.22	0.08	0.15	0.18	0.11	0.12
Al_2O_3	2.83	3.13	2.68	1.40	1.86	2.44	1.06	1.70	1.67	1.37	1.12
Cr_2O_3	0.30	0.47	0.26	0.11	0.20	0.28	0.07	0.16	0.17	0.18	0.11
FeO	5.27	5.84	6.10	4.98	5.04	5.60	3.85	4.74	4.25	4.27	4.06
MnO	0.17	0.17	0.19	0.17	0.19	0.20	0.17	0.13	0.15	0.16	0.16
MgO	15.52	15.48	15.49	15.93	15.65	15.36	16.10	15.97	15.91	15.73	15.99
CaO	23.45	23.12	23.14	24.42	23.87	23.28	24.84	23.45	24.61	24.36	24.45
Na_2O	0.17	0.22	0.14	0.10	0.15	0.17	0.09	0.16	0.11	0.09	0.07
K_2O	0.00	0.00	0.00	0.00	0.00	0.03	0.01	0.00	0.00	0.00	0.02
Total	100.46	101.30	100.58	100.98	100.54	100.29	100.30	99.54	100.35	99.46	99.60
En	44	44	43	44	44	43	44	45	44	44	44
Fs	9	9	10	8	8	9	6	8	7	7	7
Wo	48	47	47	48	48	47	49	47	49	49	49

Table 1 (ctd.): Clinopyroxene compositions obtained using wavelength dispersive analysis

Sample no.	**ND15-34B**	**ND15-34B**	**ND15-34B**	**ND15-34B**	**ND15-34B**	**ND15-34B**	**ND15-36A**	**ND15-36A**	**ND15-36A**	**ND15-36A**	**ND15-36A**
Lithology	Gabbro	Gabbro	Gabbro	Gabbro	Gabbro	Gabbro	Metagabbro	Metagabbro	Metagabbro	Metagabbro	Metagabbro
Unit	N. Region	N. Region	N. Region	N. Region	N. Region	N. Region	NMC	NMC	NMC	NMC	NMC
Analysis no.	211	212	213	214	215	217	174	177	207	208	209
SiO_2	53.56	52.53	53.79	52.72	53.00	52.86	50.84	51.96	51.87	52.20	52.37
TiO_2	0.18	0.20	0.09	0.26	0.13	0.17	0.36	0.32	0.40	0.28	0.37
Al_2O_3	1.59	2.20	1.34	2.10	1.64	1.66	1.63	2.10	2.92	2.75	2.26
Cr_2O_3	0.20	0.24	0.16	0.25	0.18	0.26	0.19	0.17	0.81	0.63	0.22
FeO	4.54	4.87	4.35	4.47	4.82	4.48	7.01	7.40	6.95	7.14	7.43
MnO	0.15	0.16	0.17	0.16	0.14	0.10	0.21	0.19	0.19	0.15	0.23
MgO	15.79	15.78	16.28	15.65	16.07	15.73	15.13	14.86	15.23	14.76	15.16
CaO	23.85	23.69	23.51	23.79	23.53	24.28	22.80	22.63	21.95	22.38	22.64
Na_2O	0.11	0.18	0.15	0.13	0.11	0.11	0.51	0.71	0.81	0.56	0.41
K_2O	0.00	0.00	0.00	0.00	0.03	0.00	0.00	0.00	0.01	0.00	0.00
Total	99.97	99.83	99.83	99.54	99.65	99.66	98.67	100.35	101.15	100.86	101.09
En	44	44	46	44	45	44	42	42	43	42	42
Fs	7	8	7	7	8	7	11	12	11	12	12
Wo	48	48	47	48	47	49	46	46	45	46	46

Table 1 (ctd.): Clinopyroxene compositions obtained using wavelength dispersive analysis

Sample no.	**ND15-36A**	**ND15-36A**	**ND15-36A**	**ND15-36A**	**ND15-36A**	**ND15-36A**	**ND15-36B**	**ND15-36B**	**ND15-36B**	**ND15-36B**	**ND15-36B**
Lithology	Metagabbro	Metagabbro	Metagabbro	Metagabbro	Metagabbro	Metagabbro	Metagabbro	Metagabbro	Metagabbro	Metagabbro	Metagabbro
Unit	NMC	NMC	NMC	NMC	NMC	NMC	NMC	NMC	NMC	NMC	NMC
Analysis no.	210	211	213	214	215	216	239	242	243	244	246
SiO_2	52.11	52.50	51.80	52.90	52.24	52.53	53.28	52.78	52.85	53.17	53.24
TiO_2	0.23	0.26	0.19	0.44	0.19	0.36	0.23	0.28	0.27	0.26	0.27
Al_2O_3	2.69	2.48	2.99	1.94	2.87	2.10	1.50	1.77	1.68	2.30	1.58
Cr_2O_3	0.56	0.68	0.81	0.16	0.76	0.16	0.04	0.04	0.00	0.04	0.06
FeO	7.87	8.12	7.18	7.22	6.52	7.44	8.58	8.91	9.03	9.26	9.00
MnO	0.23	0.23	0.21	0.20	0.18	0.19	0.29	0.31	0.27	0.21	0.26
MgO	14.94	15.57	14.74	15.28	15.10	15.35	15.12	14.79	14.73	15.27	14.85
CaO	21.82	20.53	22.82	22.65	22.68	22.10	22.05	22.03	22.42	19.06	22.12
Na_2O	0.34	0.33	0.74	0.27	0.31	0.00	0.09	0.96	0.29	0.51	0.37
K_2O	0.00	0.00	0.00	0.02	0.00	0.02	0.01	0.01	0.00	0.07	0.02
Total	100.80	100.70	101.48	101.09	100.83	100.25	101.19	101.88	101.53	100.15	101.78
En	42	44	42	43	43	43	42	41	41	45	41
Fs	13	13	12	12	11	12	14	15	14	16	14
Wo	45	42	47	46	46	45	44	44	45	40	44

Table 1 (ctd.): Clinopyroxene compositions obtained using wavelength dispersive analysis

Sample no.	**ND15-36B**	**ND15-36B**	**ND15-36B**	**ND15-36B**	**ND15-36B**	**ND15-36B**	**ND15-38A**	**ND15-38A**	**ND15-48E**	**ND15-48E**	**ND15-48E**
Lithology	Metagabbro	Metagabbro	Metagabbro	Metagabbro	Metagabbro	Metagabbro	Hornblendite	Hornblendite	Gabbro	Gabbro	Gabbro
Unit	NMC	NMC	NMC	NMC	NMC	NMC	NMC	NMC	NMC	NMC	NMC
Analysis no.	247	248	249	260	261	265	52	53	109	110	111
SiO_2	53.04	53.62	53.10	53.79	53.42	54.13	52.37	52.50	52.13	52.76	52.66
TiO_2	0.32	0.17	0.17	0.13	0.26	0.07	0.09	0.08	0.26	0.26	0.30
Al_2O_3	1.72	1.16	1.39	1.32	1.56	1.09	1.43	1.10	2.58	2.70	2.67
Cr_2O_3	0.06	0.00	0.01	0.00	0.00	0.00	0.22	0.20	0.22	0.24	0.17
FeO	8.73	12.36	8.24	8.72	8.77	9.05	6.04	6.01	6.25	6.10	6.80
MnO	0.30	0.32	0.28	0.31	0.28	0.30	0.28	0.20	0.20	0.19	0.22
MgO	14.70	17.35	15.42	14.89	14.73	15.05	14.60	14.91	15.89	15.44	16.02
CaO	22.18	16.08	22.28	22.80	22.49	22.51	24.54	24.83	22.64	23.24	21.89
Na_2O	1.03	0.46	0.18	0.31	0.14	0.00	0.23	0.00	0.31	0.34	0.32
K_2O	0.01	0.01	0.02	0.00	0.00	0.00	0.00	0.01	0.02	0.01	0.01
Total	102.09	101.53	101.10	102.27	101.64	102.20	99.80	99.85	100.50	101.29	101.06
En	41	48	43	41	41	41	41	41	44	43	45
Fs	14	20	13	14	14	14	10	10	10	10	11
Wo	45	32	44	45	45	44	49	49	45	47	44

Table 1 (ctd.): Clinopyroxene compositions obtained using wavelength dispersive analysis

Sample no.	**ND15-48E**	**ND15-48E**	**ND15-48E**	**ND15-48E**	**ND15-48E**	**ND15-48E**	**ND15-48E**	**ND15-48E**	**ND15-48E**	**ND15-48E**	**ND15-48E**
Lithology	Gabbro	Gabbro	Gabbro	Gabbro	Gabbro	Gabbro	Gabbro	Gabbro	Gabbro	Gabbro	Gabbro
Unit	NMC	NMC	NMC	NMC	NMC	NMC	NMC	NMC	NMC	NMC	NMC
Analysis no.	112	113	114	115	116	117	124	125	126	129	130
SiO_2	52.23	52.19	52.05	51.34	51.93	52.14	51.77	52.53	51.43	51.91	52.25
TiO_2	0.27	0.21	0.25	0.19	0.23	0.28	0.25	0.24	0.28	0.26	0.26
Al_2O_3	2.63	2.32	2.70	2.48	2.80	2.87	2.39	2.65	2.45	2.78	2.49
Cr_2O_3	0.25	0.14	0.26	0.25	0.30	0.21	0.16	0.19	0.18	0.28	0.29
FeO	5.85	5.85	5.78	5.94	6.03	5.95	6.27	6.15	6.23	5.99	5.96
MnO	0.20	0.14	0.16	0.23	0.16	0.19	0.22	0.15	0.19	0.17	0.19
MgO	15.72	15.97	15.61	15.77	15.66	15.73	16.13	15.69	15.77	15.47	15.48
CaO	23.39	23.41	23.16	23.09	23.04	23.03	22.70	23.03	22.91	23.38	23.25
Na_2O	0.31	0.29	0.36	0.33	0.33	0.32	0.32	0.37	0.36	0.35	0.31
K_2O	0.00	0.00	0.00	0.00	0.01	0.00	0.01	0.00	0.01	0.01	0.00
Total	100.85	100.52	100.33	99.62	100.50	100.72	100.22	101.00	99.81	100.61	100.47
En	44	44	44	44	44	44	45	44	44	43	43
Fs	9	9	9	10	10	10	10	10	10	10	10
Wo	47	47	47	46	46	46	45	46	46	47	47

Table 1 (ctd.): Clinopyroxene compositions obtained using wavelength dispersive analysis

Sample no.	**ND15-48E**	**ND15-48E**	**ND15-48E**	**ND15-48E**	**ND15-48E**	**ND15-48E**	**ND15-48E**
Lithology	Gabbro	Gabbro	Gabbro	Gabbro	Gabbro	Gabbro	Gabbro
Unit	NMC	NMC	NMC	NMC	NMC	NMC	NMC
Analysis no.	131	132	133	147	148	149	150
SiO_2	52.62	52.42	52.07	52.06	51.62	51.54	52.43
TiO_2	0.22	0.24	0.28	0.17	0.17	0.16	0.23
Al_2O_3	2.27	2.40	2.65	2.65	2.30	2.45	2.15
Cr_2O_3	0.14	0.13	0.13	0.19	0.23	0.28	0.20
FeO	6.02	6.22	6.70	5.87	5.62	6.03	5.59
MnO	0.23	0.19	0.21	0.16	0.19	0.20	0.16
MgO	16.01	15.87	16.24	15.99	15.98	15.82	15.84
CaO	22.90	22.71	22.04	23.17	22.81	23.16	23.47
Na_2O	0.35	0.34	0.31	0.33	0.37	0.32	0.27
K_2O	0.01	0.00	0.02	0.00	0.02	0.02	0.00
Total	100.77	100.54	100.64	100.60	99.32	99.99	100.34
En	45	44	45	44	45	44	44
Fs	10	10	11	9	9	10	9
Wo	46	46	44	46	46	46	47

Table 2: Orthopyroxene compositions obtained using wavelength dispersive analysis

Sample no.	**ND15-15**	**ND15-15**	**ND15-15**	**ND15-15**	**ND15-15**	**ND15-15**	**ND15-15**	**ND15-15**	**ND15-15**	**ND15-15**	**ND15-15**
Lithology	Metagabbro	Metagabbro	Metagabbro	Metagabbro	Metagabbro	Metagabbro	Metagabbro	Metagabbro	Metagabbro	Metagabbro	Metagabbro
Unit	NMC	NMC	NMC	NMC	NMC	NMC	NMC	NMC	NMC	NMC	NMC
Analysis no.	226	227	228	229	230	284	285	286	287	289	290
SiO_2	52.34	52.65	52.12	52.89	52.07	53.06	53.29	53.19	52.89	53.53	52.73
TiO_2	0.07	0.08	0.05	0.06	0.07	0.03	0.05	0.05	0.07	0.04	0.07
Al_2O_3	0.79	0.92	0.89	0.98	0.90	1.65	1.43	1.52	1.61	1.36	1.72
Cr_2O_3	0.03	0.00	0.05	0.00	0.05	0.05	0.03	0.00	0.00	0.03	0.00
FeO	22.33	22.06	22.58	21.92	22.02	18.74	18.97	18.63	18.83	18.58	18.75
MnO	0.66	0.71	0.78	0.71	0.75	0.50	0.43	0.48	0.53	0.44	0.46
MgO	23.25	23.15	23.08	23.42	23.22	26.00	25.97	25.95	25.96	25.81	25.69
CaO	0.51	0.66	0.63	0.65	0.66	0.55	0.53	0.54	0.54	0.64	0.49
Na_2O	0.00	0.00	0.00	0.00	0.02	0.00	0.01	0.01	0.00	0.00	0.01
K_2O	0.01	0.00	0.00	0.01	0.02	0.00	0.00	0.00	0.00	0.00	0.00
Total	99.99	100.23	100.18	100.67	99.76	100.57	100.71	100.38	100.43	100.42	99.93
En	64	64	63	64	64	70	70	70	70	70	70
Fs	35	35	36	35	35	29	29	29	29	29	29
Wo	1	1	1	1	1	1	1	1	1	1	1

Table 2 (ctd): Orthopyroxene compositions obtained using wavelength dispersive analysis

Sample no.	**ND15-34B**	**ND15-34B**	**ND15-34B**	**ND15-34B**	**ND15-36A**	**ND15-36A**	**ND15-36A**	**ND15-36B**	**ND15-36B**	**ND15-36B**	**ND15-36B**
Lithology	Gabbro	Gabbro	Gabbro	Gabbro	Metagabbro	Metagabbro	Metagabbro	Metagabbro	Metagabbro	Metagabbro	Metagabbro
Unit	N. Region	N. Region	N. Region	N. Region	NMC	NMC	NMC	NMC	NMC	NMC	NMC
Analysis no.	208	209	210	216	171	172	217	238	241	245	250
SiO_2	55.01	54.94	54.56	53.85	53.29	53.07	54.35	53.38	53.27	53.08	53.43
TiO_2	0.18	0.14	0.17	0.12	0.17	0.10	0.19	0.11	0.13	0.15	0.17
Al_2O_3	1.88	1.74	1.92	1.64	1.03	1.06	1.01	0.79	0.84	1.06	0.91
Cr_2O_3	0.13	0.17	0.16	0.16	0.09	0.05	0.07	0.00	0.00	0.02	0.03
FeO	12.77	11.96	11.93	13.87	18.86	18.56	18.46	22.09	22.23	22.40	21.93
MnO	0.28	0.19	0.26	0.31	0.43	0.41	0.42	0.62	0.66	0.65	0.62
MgO	29.28	28.53	28.63	27.46	25.23	26.07	25.96	23.47	23.49	23.07	23.51
CaO	0.87	2.49	2.05	1.09	0.86	0.82	0.77	0.85	0.77	0.96	0.96
Na_2O	0.00	0.00	0.00	0.01	0.00	0.00	0.00	0.00	0.47	0.01	0.00
K_2O	0.02	0.00	0.00	0.01	0.00	0.00	0.01	0.01	0.01	0.00	0.00
Total	100.42	100.16	99.68	98.53	99.97	100.14	101.24	101.32	101.86	101.38	101.56
En	79	77	77	76	69	70	70	64	64	63	64
Fs	20	18	19	22	30	29	29	35	35	35	34
Wo	2	5	4	2	2	2	2	2	2	2	2

Table 2 (ctd.): Orthopyroxene compositions obtained using wavelength dispersive analysis

Sample no.	**ND15-36B**	**ND15-36B**	**ND15-36B**	**ND15-48E**	**ND15-48E**
Lithology	Metagabbro	Metagabbro	Metagabbro	Gabbro	Gabbro
Unit	NMC	NMC	NMC	NMC	NMC
Analysis no.	262	263	264	127	128
SiO_2	53.29	53.51	53.61	53.76	52.63
TiO_2	0.04	0.15	0.18	0.07	0.13
Al_2O_3	1.19	1.01	1.00	1.93	1.79
Cr_2O_3	0.00	0.01	0.01	0.13	0.10
FeO	22.12	22.11	22.12	15.77	15.89
MnO	0.57	0.66	0.56	0.44	0.37
MgO	22.72	22.87	22.89	28.12	28.09
CaO	1.02	1.09	1.10	0.46	0.71
Na_2O	0.00	0.00	0.00	0.00	0.01
K_2O	0.01	0.00	0.02	0.02	0.03
Total	100.94	101.41	101.48	100.71	99.75
En	63	63	63	78	79
Fs	35	35	35	21	19
Wo	2	2	2	1	1

Table 3: Olivine compositions obtained using wavelength dispersive analysis

Sample no.	**ND14-07**	**ND14-07**	**ND14-07**	**ND15-34B**	**ND15-34B**	**ND15-34B**	**ND15-34B**	**ND15-48A**	**ND15-48A**
Lithology	Gabbro	Gabbro	Gabbro	Gabbro	Gabbro	Gabbro	Gabbro	Metaperidotite	Metaperidotite
Unit	EMC	EMC	EMC	N. Region	N. Region	N. Region	N. Region	NMC	NMC
Analysis no.	294	295	296	177	178	195	196	41	42
SiO_2	39.02	38.78	39.30	39.00	38.94	39.14	38.71	39.43	39.38
TiO_2	0.00	0.02	0.01	0.00	0.00	0.00	0.01	0.00	0.00
Al_2O_3	0.00	0.00	0.01	0.01	0.00	0.02	0.02	0.00	0.00
Cr_2O_3	0.04	0.00	0.03	0.00	0.05	0.01	0.00	0.00	0.00
FeO	16.44	16.59	16.28	20.94	20.86	19.36	18.95	10.77	10.82
MnO	0.24	0.24	0.23	0.33	0.37	0.30	0.28	0.27	0.23
MgO	45.58	45.35	45.35	40.55	40.55	40.99	40.97	48.66	48.76
CaO	0.06	0.03	0.01	0.01	0.00	0.01	0.04	0.01	0.00
Na_2O	0.02	0.01	0.01	0.00	0.00	0.00	0.02	0.00	0.01
K_2O	0.01	0.01	0.00	0.00	0.01	0.00	0.02	0.00	0.00
Total	101.41	101.02	101.24	100.84	100.78	99.83	99.02	99.14	99.21
Fo	83	83	83	78	78	79	79	89	89
Fa	17	17	17	22	22	21	21	11	11

Table 3: Olivine compositions obtained using wavelength dispersive analysis

Sample no.	**ND15-48A**	**ND15-48A**	**ND15-48A**	**ND15-48A**	**ND15-48A**	**ND15-48A**
Lithology	Metaperidotite	Metaperidotite	Metaperidotite	Metaperidotite	Metaperidotite	Metaperidotite
Unit	NMC	NMC	NMC	NMC	NMC	NMC
Analysis no.	43	44	57	58	59	60
SiO_2	39.81	39.58	40.22	39.85	40.27	39.87
TiO_2	0.05	0.00	0.00	0.01	0.03	0.00
Al_2O_3	0.00	0.00	0.00	0.02	0.00	0.02
Cr_2O_3	0.00	0.02	0.00	0.00	0.00	0.00
FeO	10.90	11.00	11.79	11.81	11.48	11.63
MnO	0.27	0.26	0.24	0.34	0.30	0.29
MgO	48.32	48.64	48.11	47.93	48.18	48.37
CaO	0.02	0.00	0.01	0.00	0.01	0.01
Na_2O	0.00	0.01	0.00	0.00	0.00	0.00
K_2O	0.00	0.01	0.00	0.00	0.02	0.02
Total						
Fo	89	89	88	88	88	88
Fa	11	11	12	12	12	12

Table 4: Amphibole compositions obtained using wavelength dispersive analysis

Sample no.	**ND14-02B**	**ND14-02B**	**ND14-02B**	**ND14-02B**	**ND14-02B**	**ND14-02B**	**ND14-02B**	**ND14-02B**	**ND14-02B**	**ND14-02B**	**ND14-02B**
Lithology	Metagabbro	Metagabbro	Metagabbro	Metagabbro	Metagabbro	Metagabbro	Metagabbro	Metagabbro	Metagabbro	Metagabbro	Metagabbro
Unit	NMC	NMC	NMC	NMC	NMC	NMC	NMC	NMC	NMC	NMC	NMC
Analysis no.	75	76	77	78	79	80	81	82	83	84	85
SiO_2	47.41	46.46	46.97	47.74	46.69	47.55	46.35	46.45	45.81	45.78	48.37
TiO_2	0.48	0.78	0.60	0.75	0.82	0.72	0.41	0.71	0.82	0.85	0.57
Al_2O_3	7.79	9.10	8.36	7.71	8.42	8.18	8.77	8.84	9.09	9.15	7.46
Cr_2O_3	0.01	0.01	0.00	0.09	0.01	0.03	0.03	0.05	0.08	0.04	0.08
FeO	14.57	15.33	14.79	14.79	15.54	14.71	15.48	15.18	15.15	15.40	14.27
MnO	0.30	0.30	0.30	0.35	0.32	0.27	0.26	0.28	0.24	0.27	0.29
MgO	13.16	12.50	12.92	13.06	12.53	13.12	12.48	12.72	12.25	12.35	13.24
CaO	12.62	12.34	12.37	12.26	12.26	12.43	12.53	12.19	12.32	12.18	12.34
Na_2O	0.73	0.92	0.90	0.92	0.83	0.82	0.89	0.94	0.85	0.98	0.77
K_2O	0.51	0.73	0.58	0.43	0.70	0.59	0.63	0.67	0.71	0.79	0.46
Total	97.59	98.48	97.79	98.11	98.13	98.42	97.82	98.03	97.33	97.78	97.86

Table 4 (ctd.): Amphibole compositions obtained using wavelength dispersive analysis

Sample no.	**ND14-02B**	**ND14-02B**	**ND14-02B**	**ND14-02B**	**ND14-02B**	**ND14-02B**	**ND14-02B**	**ND14-02B**	**ND14-02B**	**ND14-02B**	**ND14-02B**
Lithology	Metagabbro	Metagabbro	Metagabbro	Metagabbro	Metagabbro	Metagabbro	Metagabbro	Metagabbro	Metagabbro	Metagabbro	Metagabbro
Unit	NMC	NMC	NMC	NMC	NMC	NMC	NMC	NMC	NMC	NMC	NMC
Analysis no.	100	102	103	104	105	106	107	108	109	110	111
SiO_2	47.81	48.02	48.73	48.04	50.75	49.98	48.31	49.93	48.26	48.20	48.71
TiO_2	0.55	0.96	0.75	0.54	0.31	0.30	0.60	0.39	0.48	0.51	0.53
Al_2O_3	7.52	7.45	6.89	7.43	4.92	5.60	7.35	6.19	7.21	7.06	6.88
Cr_2O_3	0.03	0.09	0.06	0.05	0.01	0.09	0.06	0.05	0.08	0.09	0.02
FeO	14.71	13.38	13.45	14.34	13.65	13.91	13.90	13.67	14.23	14.35	13.86
MnO	0.28	0.24	0.23	0.25	0.31	0.22	0.28	0.21	0.23	0.25	0.28
MgO	13.01	13.98	13.88	13.48	14.77	14.12	13.59	14.27	13.61	13.59	13.76
CaO	12.57	12.73	12.70	12.48	12.75	12.71	12.50	12.60	12.75	12.20	12.59
Na_2O	0.70	0.72	0.64	0.59	0.53	0.47	0.67	0.65	0.64	0.74	0.72
K_2O	0.56	0.50	0.47	0.51	0.26	0.30	0.54	0.40	0.49	0.49	0.48
Total	97.74	98.08	97.81	97.70	98.25	97.69	97.81	98.36	97.98	97.49	97.82

Table 4 (ctd.): Amphibole compositions obtained using wavelength dispersive analysis

Sample no.	**ND14-02B**	**ND14-02B**	**ND14-02B**	**ND14-02B**	**ND14-02B**	**ND14-02B**	**ND14-02B**	**ND14-02B**	**ND14-02B**	**ND14-02B**	**ND14-02B**
Lithology	Metagabbro	Metagabbro	Metagabbro	Metagabbro	Metagabbro	Metagabbro	Metagabbro	Metagabbro	Metagabbro	Metagabbro	Metagabbro
Unit	NMC	NMC	NMC	NMC	NMC	NMC	NMC	NMC	NMC	NMC	NMC
Analysis no.	121	122	123	124	139	140	141	144	146	148	153
SiO_2	48.61	48.42	48.50	48.91	50.03	47.54	51.34	48.34	47.97	48.26	47.57
TiO_2	0.50	0.56	0.49	0.61	0.39	0.56	0.24	0.50	0.63	0.42	0.55
Al_2O_3	7.00	7.16	7.18	6.62	5.53	7.60	4.40	7.08	7.28	7.09	7.86
Cr_2O_3	0.08	0.03	0.09	0.20	0.04	0.11	0.03	0.09	0.20	0.00	0.09
FeO	14.13	14.26	14.64	13.72	14.42	15.29	13.56	14.76	14.54	15.38	15.22
MnO	0.25	0.23	0.24	0.25	0.25	0.27	0.21	0.28	0.22	0.22	0.24
MgO	13.80	13.59	13.61	13.85	14.18	12.66	15.07	13.23	12.80	12.69	12.60
CaO	12.50	12.63	12.48	12.54	12.60	12.55	12.72	12.30	13.65	12.60	12.53
Na_2O	0.64	0.67	0.73	0.69	0.53	0.66	0.38	0.74	0.66	0.68	0.70
K_2O	0.50	0.51	0.48	0.46	0.33	0.55	0.25	0.47	0.53	0.52	0.56
Total	98.00	98.05	98.45	97.85	98.29	97.79	98.20	97.79	98.49	97.87	97.92

Table 4 (ctd.): Amphibole compositions obtained using wavelength dispersive analysis

Sample no.	**ND15-15**	**ND15-15**	**ND15-15**	**ND15-15**	**ND15-15**	**ND15-15**	**ND15-15**	**ND15-15**	**ND15-15**	**ND15-15**	**ND15-15**
Lithology	Metagabbro	Metagabbro	Metagabbro	Metagabbro	Metagabbro	Metagabbro	Metagabbro	Metagabbro	Metagabbro	Metagabbro	Metagabbro
Unit	NMC	NMC	NMC	NMC	NMC	NMC	NMC	NMC	NMC	NMC	NMC
Analysis no.	237	239	240	241	250	251	252	253	254	255	273
SiO_2	48.59	48.18	50.44	49.54	52.06	48.90	48.77	48.50	48.70	49.01	48.90
TiO_2	0.81	0.78	0.31	0.77	0.50	1.15	1.09	1.15	0.92	0.92	0.97
Al_2O_3	7.71	7.37	6.38	5.97	3.98	6.90	6.81	6.75	6.75	6.48	7.19
Cr_2O_3	0.17	0.12	0.02	0.17	0.08	0.11	0.10	0.11	0.07	0.07	0.13
FeO	11.47	11.93	10.97	11.63	10.75	11.91	11.95	11.96	12.24	12.23	12.47
MnO	0.23	0.23	0.24	0.25	0.15	0.15	0.17	0.23	0.25	0.23	0.19
MgO	15.89	15.81	16.92	16.51	17.11	15.76	15.47	15.49	15.18	15.51	14.57
CaO	11.62	11.38	11.52	11.48	12.59	11.68	11.95	12.07	12.18	12.07	11.88
Na_2O	1.01	0.99	0.81	0.82	0.37	0.89	0.88	0.93	0.86	0.86	0.91
K_2O	0.12	0.09	0.05	0.07	0.03	0.12	0.11	0.08	0.09	0.08	0.10
Total	97.61	96.88	97.67	97.21	97.63	97.57	97.29	97.27	97.26	97.46	97.31

Table 4 (ctd.): Amphibole compositions obtained using wavelength dispersive analysis

Sample no.	**ND15-15**	**ND15-15**	**ND15-15**	**ND15-15**	**ND15-15**	**ND15-15**	**ND15-22C**	**ND15-22C**	**ND15-22C**	**ND15-22C**	**ND15-22C**
Lithology	Metagabbro	Metagabbro	Metagabbro	Metagabbro	Metagabbro	Metagabbro	Metagabbro	Metagabbro	Metagabbro	Metagabbro	Metagabbro
Unit	NMC	NMC	NMC	NMC	NMC	NMC	NMC	NMC	NMC	NMC	NMC
Analysis no.	274	275	276	235	258	288	67	68	69	77	78
SiO_2	49.14	51.21	49.44	48.28	48.91	48.27	44.87	47.15	49.50	44.71	44.51
TiO_2	1.04	0.46	0.96	0.53	1.03	0.42	1.25	0.80	0.42	1.57	1.52
Al_2O_3	6.44	4.93	6.48	7.88	6.83	8.67	9.94	8.00	5.82	10.68	10.63
Cr_2O_3	0.08	0.00	0.04	0.13	0.12	0.03	0.07	0.06	0.06	0.15	0.10
FeO	12.75	13.00	12.26	11.28	11.67	9.98	14.46	13.68	13.09	13.58	13.95
MnO	0.24	0.22	0.20	0.22	0.15	0.15	0.23	0.18	0.20	0.17	0.19
MgO	15.27	15.65	15.22	16.21	15.35	16.98	11.99	13.20	14.21	12.16	11.97
CaO	11.79	11.88	11.71	11.41	12.42	11.63	12.19	12.50	12.42	12.12	12.07
Na_2O	0.83	0.65	0.90	1.02	0.84	1.19	1.41	1.28	0.84	1.64	1.69
K_2O	0.09	0.06	0.10	0.08	0.11	0.07	0.35	0.23	0.15	0.38	0.35
Total	97.67	98.07	97.32	97.04	97.43	97.40	96.76	97.08	96.69	97.15	96.99

Table 4 (ctd.): Amphibole compositions obtained using wavelength dispersive analysis

Sample no.	**ND15-34B**	**ND15-34B**	**ND15-34B**	**ND15-34B**	**ND15-34B**	**ND15-34B**	**ND15-34B**	**ND15-34B**	**ND15-34B**	**ND15-34B**	**ND15-34B**
Lithology	Gabbro	Gabbro	Gabbro	Gabbro	Gabbro	Gabbro	Gabbro	Gabbro	Gabbro	Gabbro	Gabbro
Unit	N. Region	N. Region	N. Region	N. Region	N. Region	N. Region	N. Region	N. Region	N. Region	N. Region	N. Region
Analysis no.	154	155	156	157	158	159	160	161	162	163	179
SiO_2	51.10	50.66	46.85	50.59	49.75	48.91	52.62	47.44	47.79	49.67	47.14
TiO_2	0.32	0.28	0.78	0.32	0.35	0.53	0.25	0.45	0.61	0.34	0.52
Al_2O_3	6.57	7.08	10.06	7.38	7.97	8.27	5.19	10.04	9.35	7.82	10.36
Cr_2O_3	0.20	0.11	0.19	0.06	0.23	0.15	0.16	0.25	0.25	0.28	0.51
FeO	8.05	8.27	9.56	8.34	8.37	8.52	6.52	8.90	8.59	7.93	7.98
MnO	0.13	0.13	0.13	0.15	0.13	0.13	0.13	0.11	0.15	0.14	0.09
MgO	18.13	18.16	16.25	17.82	17.73	17.56	19.24	16.56	16.99	17.46	16.80
CaO	12.69	12.38	12.44	12.46	12.23	12.37	12.91	12.53	12.56	12.69	12.55
Na_2O	0.90	0.92	1.38	0.98	1.10	1.06	0.67	1.36	1.36	1.05	1.39
K_2O	0.05	0.04	0.17	0.04	0.03	0.02	0.00	0.05	0.05	0.03	0.09
Total	98.14	98.04	97.81	98.14	97.88	97.54	97.69	97.68	97.71	97.40	97.43

Table 4 (ctd.): Amphibole compositions obtained using wavelength dispersive analysis

Sample no.	**ND15-34B**	**ND15-34B**	**ND15-34B**	**ND15-34B**	**ND15-34B**	**ND15-34B**	**ND15-34B**	**ND15-34B**	**ND15-34B**	**ND15-34B**	**ND15-34B**
Lithology	Gabbro	Gabbro	Gabbro	Gabbro	Gabbro	Gabbro	Gabbro	Gabbro	Gabbro	Gabbro	Gabbro
Unit	N. Region	N. Region	N. Region	N. Region	N. Region	N. Region	N. Region	N. Region	N. Region	N. Region	N. Region
Analysis no.	180	181	182	183	184	185	186	197	198	199	200
SiO_2	48.16	46.30	44.22	45.86	52.87	48.57	48.03	44.95	49.35	48.47	49.87
TiO_2	0.39	0.55	0.94	0.70	0.16	0.38	0.41	1.03	0.68	0.44	0.24
Al_2O_3	9.57	11.24	11.93	11.54	5.17	8.51	9.35	11.70	8.24	8.43	7.10
Cr_2O_3	0.16	0.40	0.72	0.36	0.16	0.18	0.31	0.70	0.53	0.38	0.22
FeO	7.50	8.44	8.42	8.32	5.94	7.40	8.14	8.75	7.46	7.69	7.02
MnO	0.12	0.08	0.09	0.12	0.11	0.11	0.08	0.11	0.09	0.14	0.15
MgO	17.19	16.41	15.60	16.32	19.65	17.60	17.17	15.91	17.86	17.35	18.41
CaO	12.85	12.58	12.50	12.51	12.90	12.56	12.43	12.41	12.72	12.62	12.29
Na_2O	1.30	1.57	1.72	1.52	0.66	1.19	1.35	1.63	1.11	1.09	1.01
K_2O	0.08	0.19	0.24	0.18	0.03	0.05	0.06	0.23	0.13	0.09	0.05
Total	97.33	97.78	96.38	97.42	97.65	96.55	97.33	97.43	98.16	96.70	96.36

Table 4 (ctd.): Amphibole compositions obtained using wavelength dispersive analysis

Sample no.	**ND15-34B**	**ND15-34B**	**ND15-34B**	**ND15-34B**	**ND15-34B**	**ND15-34B**	**ND15-36A**	**ND15-36A**	**ND15-36A**	**ND15-36A**	**ND15-36A**
Lithology	Gabbro	Gabbro	Gabbro	Gabbro	Gabbro	Gabbro	Metagabbro	Metagabbro	Metagabbro	Metagabbro	Metagabbro
Unit	N. Region	N. Region	N. Region	N. Region	N. Region	N. Region	NMC	NMC	NMC	NMC	NMC
Analysis no.	201	202	203	204	206	207	173	175	176	178	179
SiO_2	50.20	48.72	53.73	49.05	55.38	48.63	45.81	46.02	46.91	46.12	49.62
TiO_2	0.29	0.13	0.11	0.18	0.05	0.36	2.22	2.26	1.86	2.13	1.23
Al_2O_3	6.94	9.75	3.97	8.13	1.83	8.68	9.04	8.92	7.98	8.94	6.33
Cr_2O_3	0.27	0.08	0.14	0.18	0.16	0.27	0.45	0.46	0.41	0.46	0.28
FeO	7.21	7.06	5.67	7.49	7.62	7.92	11.57	11.39	11.15	11.36	10.47
MnO	0.17	0.13	0.11	0.21	0.33	0.09	0.15	0.18	0.14	0.16	0.11
MgO	18.43	17.63	20.35	18.75	22.72	16.91	14.87	15.03	15.77	14.88	16.90
CaO	12.45	12.59	12.47	11.56	8.63	12.66	11.43	11.44	11.68	11.55	11.79
Na_2O	1.00	1.37	0.51	1.01	0.20	1.15	1.23	1.62	1.35	0.92	1.07
K_2O	0.02	0.04	0.01	0.02	0.02	0.06	0.08	0.08	0.12	0.07	0.06
Total	96.99	97.50	97.07	96.58	96.95	96.73	96.85	97.39	97.35	96.59	97.87

Table 4 (ctd.): Amphibole compositions obtained using wavelength dispersive analysis

Sample no.	**ND15-36A**	**ND15-36A**	**ND15-36A**	**ND15-36A**	**ND15-36A**	**ND15-36A**	**ND15-36A**	**ND15-36A**	**ND15-36A**	**ND15-36A**	**ND15-36A**
Lithology	Metagabbro	Metagabbro	Metagabbro	Metagabbro	Metagabbro	Metagabbro	Metagabbro	Metagabbro	Metagabbro	Metagabbro	Metagabbro
Unit	NMC	NMC	NMC	NMC	NMC	NMC	NMC	NMC	NMC	NMC	NMC
Analysis no.	180	181	186	187	188	189	190	196	197	198	199
SiO_2	48.00	46.03	51.37	51.59	51.66	51.35	50.10	51.72	51.57	52.72	51.83
TiO_2	1.71	2.24	0.49	0.43	0.37	0.37	0.88	0.57	0.26	0.24	0.26
Al_2O_3	7.24	8.88	5.11	4.86	4.76	4.95	6.14	4.39	4.47	3.96	4.71
Cr_2O_3	0.32	0.42	0.17	0.13	0.11	0.09	0.48	0.24	0.16	0.31	0.02
FeO	11.36	11.31	10.93	10.09	10.76	10.09	10.45	10.33	12.09	11.12	12.04
MnO	0.17	0.14	0.18	0.14	0.18	0.16	0.10	0.12	0.26	0.21	0.22
MgO	16.00	14.98	16.32	17.58	17.31	18.02	16.88	16.98	16.53	17.20	16.54
CaO	11.59	11.42	11.80	11.75	11.58	11.34	11.65	12.32	11.15	11.68	11.50
Na_2O	0.93	1.57	0.57	0.83	0.76	0.89	0.51	0.36	0.35	0.43	0.42
K_2O	0.09	0.08	0.05	0.08	0.05	0.06	0.08	0.08	0.10	0.09	0.16
Total	97.41	97.07	96.98	97.48	97.55	97.31	97.29	97.11	96.94	97.98	97.71

Table 4 (ctd.): Amphibole compositions obtained using wavelength dispersive analysis

Sample no.	**ND15-36A**	**ND15-36A**	**ND15-36B**	**ND15-36B**	**ND15-36B**	**ND15-36B**	**ND15-36B**	**ND15-36B**	**ND15-36B**	**ND15-36B**	**ND15-36B**
Lithology	Metagabbro	Metagabbro	Metagabbro	Metagabbro	Metagabbro	Metagabbro	Metagabbro	Metagabbro	Metagabbro	Metagabbro	Metagabbro
Unit	NMC	NMC	NMC	NMC	NMC	NMC	NMC	NMC	NMC	NMC	NMC
Analysis no.	200	201	221	222	223	224	225	226	256	257	258
SiO_2	53.05	54.20	51.34	52.92	50.61	51.16	50.04	50.98	51.00	50.88	50.24
TiO_2	0.21	0.18	0.24	0.17	0.26	0.23	0.26	0.25	0.73	0.71	0.77
Al_2O_3	3.26	2.49	5.12	3.70	5.67	4.97	5.21	5.19	5.89	5.86	6.07
Cr_2O_3	0.23	0.01	0.01	0.01	0.00	0.04	0.00	0.00	0.04	0.04	0.00
FeO	11.01	11.99	12.21	11.50	12.82	11.49	12.39	12.64	12.12	12.22	12.01
MnO	0.22	0.28	0.21	0.24	0.20	0.27	0.21	0.22	0.20	0.17	0.22
MgO	17.29	17.43	17.10	18.10	16.41	17.09	17.03	16.51	16.56	16.59	16.36
CaO	11.78	11.19	11.54	11.41	11.44	11.38	11.08	11.45	11.48	11.35	11.26
Na_2O	0.45	0.34	0.11	0.45	0.42	0.57	0.74	0.28	0.83	0.89	0.61
K_2O	0.09	0.15	0.06	0.04	0.10	0.09	0.06	0.07	0.04	0.05	0.05
Total	97.60	98.26	97.95	98.53	97.93	97.27	97.02	97.59	98.90	98.77	97.60

Table 4 (ctd.): Amphibole compositions obtained using wavelength dispersive analysis

Sample no.	**ND15-36B**	**ND15-36B**	**ND15-36B**	**ND15-36B**	**ND15-36B**	**ND15-36B**	**ND15-36B**	**ND15-36B**	**ND15-36B**	**ND15-36B**	**ND15-36B**
Lithology	Metagabbro	Metagabbro	Metagabbro	Metagabbro	Metagabbro	Metagabbro	Metagabbro	Metagabbro	Metagabbro	Metagabbro	Metagabbro
Unit	NMC	NMC	NMC	NMC	NMC	NMC	NMC	NMC	NMC	NMC	NMC
Analysis no.	259	266	267	268	269	270	271	272	273	274	275
SiO_2	50.98	52.16	52.13	53.77	53.70	54.12	51.05	51.35	51.37	51.63	51.99
TiO_2	0.59	0.34	0.39	0.29	0.06	0.05	0.59	0.50	0.48	0.48	0.44
Al_2O_3	5.69	4.97	5.01	3.59	2.69	2.40	5.79	5.68	5.80	5.34	4.96
Cr_2O_3	0.01	0.00	0.02	0.02	0.00	0.04	0.04	0.00	0.00	0.05	0.00
FeO	12.30	12.75	12.67	12.37	15.19	15.32	12.78	12.59	12.16	12.21	13.00
MnO	0.21	0.24	0.21	0.19	0.27	0.37	0.22	0.22	0.22	0.23	0.24
MgO	16.75	16.19	16.23	16.67	14.41	14.24	16.40	16.36	16.24	16.67	15.91
CaO	11.28	11.81	11.83	12.33	12.68	12.47	11.58	11.47	11.78	11.60	11.93
Na_2O	0.67	0.78	0.40	0.58	0.16	0.23	0.80	0.82	1.68	0.79	0.65
K_2O	0.07	0.10	0.13	0.11	0.05	0.08	0.08	0.08	0.12	0.10	0.10
Total	98.54	99.34	99.02	99.92	99.21	99.31	99.32	99.07	99.84	99.11	99.23

Table 4 (ctd.): Amphibole compositions obtained using wavelength dispersive analysis

Sample no.	**ND15-38B**	**ND15-38B**	**ND15-38B**	**ND15-38B**	**ND15-38B**	**ND15-40B**	**ND15-40B**	**ND15-40B**	**ND15-40B**	**ND15-40B**	**ND15-40B**
Lithology	Hornblendite	Hornblendite	Hornblendite	Hornblendite	Hornblendite	Diabase	Diabase	Diabase	Diabase	Diabase	Diabase
Unit	NMC	NMC	NMC	NMC	NMC	NMC	NMC	NMC	NMC	NMC	NMC
Analysis no.	49	50	51	54	55	111	112	113	114	115	116
SiO_2	46.92	50.47	44.38	49.09	50.72	47.45	47.75	48.06	47.94	45.19	44.73
TiO_2	0.64	0.53	0.87	0.38	0.30	0.66	0.60	0.52	0.45	0.89	0.92
Al_2O_3	9.10	5.61	11.81	7.58	5.24	7.61	7.54	7.05	7.39	9.63	10.26
Cr_2O_3	0.22	0.30	0.62	0.32	0.17	0.01	0.01	0.00	0.06	0.00	0.00
FeO	9.29	10.40	9.90	8.85	8.67	14.15	13.80	13.56	13.75	14.75	15.25
MnO	0.19	0.22	0.12	0.14	0.20	0.29	0.28	0.31	0.28	0.28	0.25
MgO	15.87	15.94	14.46	16.31	17.16	14.14	14.35	14.75	14.21	12.56	12.32
CaO	12.62	12.69	12.33	12.74	12.75	11.68	11.95	11.73	11.95	11.88	11.86
Na_2O	1.16	0.38	1.62	0.71	0.50	0.58	0.74	0.55	0.56	1.03	1.13
K_2O	0.40	0.27	0.60	0.45	0.32	0.42	0.39	0.31	0.27	0.60	0.63
Total	96.41	96.81	96.71	96.57	96.03	96.99	97.41	96.84	96.85	96.82	97.34

Table 4 (ctd.): Amphibole compositions obtained using wavelength dispersive analysis

Sample no.	**ND15-40B**	**ND15-40B**	**ND15-40B**	**ND15-40B**	**ND15-40B**	**ND15-40B**	**ND15-40B**	**ND15-40B**	**ND15-40B**	**ND15-40B**	**ND15-40B**
Lithology	Diabase	Diabase	Diabase	Diabase	Diabase	Diabase	Diabase	Diabase	Diabase	Diabase	Diabase
Unit	NMC	NMC	NMC	NMC	NMC	NMC	NMC	NMC	NMC	NMC	NMC
Analysis no.	117	128	129	130	131	132	133	134	135	136	137
SiO_2	47.72	46.89	48.09	46.62	47.32	47.85	47.12	47.36	46.82	48.16	45.71
TiO_2	0.44	0.62	0.50	0.72	0.66	0.59	0.67	0.63	0.68	0.48	0.77
Al_2O_3	7.50	8.28	7.28	8.91	8.22	7.60	8.31	8.26	8.78	7.51	9.34
Cr_2O_3	0.02	0.00	0.05	0.02	0.01	0.05	0.02	0.00	0.01	0.00	0.00
FeO	13.83	14.05	13.67	14.29	14.04	13.99	14.41	14.15	14.52	13.82	15.11
MnO	0.29	0.31	0.30	0.29	0.31	0.32	0.30	0.33	0.28	0.23	0.23
MgO	14.10	13.53	14.07	13.24	13.62	14.07	13.58	13.56	13.23	14.03	12.81
CaO	12.07	11.64	11.74	11.96	12.01	11.79	11.72	12.01	11.80	11.91	11.75
Na_2O	0.66	0.80	0.80	0.75	0.67	0.77	0.66	0.80	0.70	0.62	0.82
K_2O	0.26	0.43	0.36	0.46	0.38	0.39	0.42	0.41	0.50	0.20	0.55
Total	96.89	96.54	96.85	97.28	97.24	97.42	97.22	97.52	97.31	96.96	97.10

Table 4 (ctd.): Amphibole compositions obtained using wavelength dispersive analysis

Sample no.	**ND15-40B**	**ND15-40B**	**ND15-40B**	**ND15-40B**	**ND15-40B**	**ND15-48A**	**ND15-48A**	**ND15-48A**	**ND15-48A**	**ND15-48A**	**ND15-48A**
Lithology	Diabase	Diabase	Diabase	Diabase	Diabase	Meta-peridotite	Meta-peridotite	Meta-peridotite	Meta-peridotite	Meta-peridotite	Meta-peridotite
Unit	NMC	NMC	NMC	NMC	NMC	NMC	NMC	NMC	NMC	NMC	NMC
Analysis no.	156	157	158	159	160	37	38	39	40	52	53
SiO_2	48.81	47.26	48.57	49.50	49.09	56.25	57.53	55.91	55.29	56.71	56.39
TiO_2	0.42	0.62	0.53	0.46	0.49	0.05	0.06	0.09	0.08	0.08	0.07
Al_2O_3	7.29	8.85	7.07	6.51	7.18	1.52	0.42	2.36	2.62	2.06	2.40
Cr_2O_3	0.01	0.01	0.00	0.04	0.05	0.00	0.01	0.23	0.21	0.06	0.13
FeO	13.47	14.10	13.62	13.00	13.50	2.39	1.66	2.27	2.14	2.37	2.25
MnO	0.34	0.28	0.26	0.27	0.30	0.03	0.08	0.10	0.06	0.05	0.07
MgO	14.37	13.48	14.15	15.01	14.50	23.51	24.24	23.15	23.14	23.34	23.11
CaO	11.85	11.89	11.74	11.80	12.00	13.26	13.50	13.22	13.11	12.91	13.13
Na_2O	0.95	1.19	0.75	0.54	0.65	0.14	0.06	0.32	0.33	0.24	0.30
K_2O	0.20	0.46	0.34	0.26	0.28	0.16	0.01	0.07	0.10	0.18	0.23
Total	97.71	98.13	97.02	97.41	98.06	97.31	97.57	97.72	97.07	98.00	98.09

Table 4 (ctd.): Amphibole compositions obtained using wavelength dispersive analysis

Sample no.	**ND15-48A**	**ND15-48A**	**ND15-48A**	**ND15-51E**	**ND15-51E**	**ND15-51E**	**ND15-51E**	**ND15-51E**	**ND15-51F**	**ND15-51F**	**ND15-51F**
Lithology	Meta-peridotite	Meta-peridotite	Meta-peridotite	Chlorite schist	Chlorite schist	Chlorite schist	Chlorite schist	Chlorite schist	Meta-diabase	Meta-diabase	Meta-diabase
Unit	NMC	NMC	NMC	NMC	NMC	NMC	NMC	NMC	NMC	NMC	NMC
Analysis no.	54	55	56	57	58	59	65	66	232	233	234
SiO_2	56.76	55.00	56.41	46.88	45.28	45.26	46.17	46.36	52.65	52.54	52.69
TiO_2	0.08	0.08	0.09	0.04	0.06	0.06	0.08	0.16	0.04	0.16	0.15
Al_2O_3	1.99	3.35	2.19	11.62	13.60	13.50	12.00	12.06	3.34	4.28	4.39
Cr_2O_3	0.07	0.34	0.05	0.02	0.02	0.01	0.13	0.48	0.02	0.00	0.06
FeO	2.40	2.41	2.38	5.57	5.91	5.93	6.00	5.73	9.51	10.26	9.65
MnO	0.12	0.07	0.09	0.07	0.08	0.09	0.06	0.11	0.32	0.31	0.36
MgO	23.30	22.92	23.37	17.84	17.21	17.18	17.47	17.69	17.27	16.71	17.06
CaO	13.00	12.96	12.89	12.75	12.62	12.66	12.62	12.71	12.27	12.24	12.14
Na_2O	0.23	0.36	0.25	1.50	1.83	1.82	1.63	1.65	0.39	0.36	0.44
K_2O	0.18	0.28	0.20	0.16	0.22	0.21	0.18	0.20	0.07	0.07	0.11
Total	98.12	97.78	97.91	96.45	96.84	96.71	96.35	97.15	95.89	96.92	97.04

Table 4 (ctd.): Amphibole compositions obtained using wavelength dispersive analysis

Sample no.	**ND15-51F**	**ND15-51F**	**ND15-51F**	**ND15-51F**	**ND15-51F**	**ND15-51F**	**ND15-51F**	**ND15-51F**	**ND15-51F**	**ND15-51F**	**ND15-51F**
Lithology	Meta-diabase	Meta-diabase	Meta-diabase	Meta-diabase	Meta-diabase	Meta-diabase	Meta-diabase	Meta-diabase	Meta-diabase	Meta-diabase	Meta-diabase
Unit	NMC	NMC	NMC	NMC	NMC	NMC	NMC	NMC	NMC	NMC	NMC
Analysis no.	235	236	237	238	239	240	241	242	244	245	247
SiO_2	52.86	52.66	51.53	52.84	51.57	49.54	51.75	51.55	49.73	51.17	51.95
TiO_2	0.13	0.13	0.11	0.11	0.19	0.40	0.42	0.30	0.39	0.23	0.40
Al_2O_3	4.23	3.95	5.04	4.54	5.11	6.41	5.57	5.17	6.38	5.43	6.21
Cr_2O_3	0.12	0.08	0.03	0.09	0.09	0.05	0.03	0.01	0.21	0.02	0.00
FeO	9.30	8.97	10.06	8.37	10.04	11.54	10.97	11.16	11.18	11.17	11.05
MnO	0.31	0.27	0.32	0.24	0.32	0.27	0.31	0.28	0.25	0.33	0.29
MgO	17.39	17.65	16.27	17.83	16.61	15.03	16.12	16.14	15.04	15.96	14.33
CaO	12.26	12.06	12.26	12.56	11.92	11.82	12.00	11.90	12.22	11.56	11.50
Na_2O	0.45	0.44	0.44	0.45	0.52	0.65	0.56	0.49	0.59	0.57	0.57
K_2O	0.11	0.12	0.13	0.17	0.08	0.13	0.09	0.09	0.13	0.15	0.14
Total	97.15	96.33	96.18	97.21	96.45	95.85	97.83	97.09	96.13	96.59	96.43

Table 4 (ctd.): Amphibole compositions obtained using wavelength dispersive analysis

Sample no.	**ND15-51F**	**ND15-51F**	**ND15-51F**	**ND15-53A**	**ND15-53A**	**ND15-53A**	**ND15-53A**	**ND15-53A**	**ND15-53A**	**ND15-53A**	**ND15-53A**
Lithology	Meta-diabase	Meta-diabase	Meta-diabase	Gabbro	Gabbro	Gabbro	Gabbro	Gabbro	Gabbro	Gabbro	Gabbro
Unit	NMC	NMC	NMC	N. Region	N. Region	N. Region	N. Region	N. Region	N. Region	N. Region	N. Region
Analysis no.	248	249	250	44	45	46	47	48	49	50	51
SiO_2	51.05	49.55	51.36	51.56	42.01	43.30	41.42	45.54	42.94	52.67	43.10
TiO_2	0.39	0.44	0.31	0.21	2.46	2.60	2.41	1.00	1.27	0.07	1.92
Al_2O_3	6.01	6.92	5.67	3.98	12.04	10.93	11.78	10.41	11.12	3.02	11.71
Cr_2O_3	0.15	0.21	0.14	0.00	0.00	0.03	0.04	0.04	0.11	0.01	0.02
FeO	11.27	11.57	11.04	12.15	12.16	11.77	11.90	13.27	13.23	12.17	12.32
MnO	0.35	0.33	0.29	0.32	0.19	0.18	0.20	0.21	0.20	0.29	0.19
MgO	15.51	14.88	15.75	17.88	14.78	15.12	14.49	13.72	13.91	16.40	14.65
CaO	12.01	12.08	12.13	10.24	10.97	10.76	10.79	11.41	10.90	12.23	10.88
Na_2O	0.56	0.60	0.44	0.32	1.41	1.18	2.31	1.03	1.19	0.15	1.37
K_2O	0.18	0.22	0.12	0.09	0.17	0.16	0.19	0.14	0.19	0.05	0.18
Total	97.49	96.80	97.24	96.75	96.20	96.03	95.51	96.76	95.08	97.05	96.34

Table 4 (ctd.): Amphibole compositions obtained using wavelength dispersive analysis

Sample no.	**ND15-53A**	**ND15-53A**	**ND15-53A**	**ND15-53A**	**ND15-53A**	**ND15-53A**	**ND15-53A**	**ND15-53A**	**ND15-53A**	**ND15-53A**	**ND15-53B**
Lithology	Gabbro	Gabbro	Gabbro	Gabbro	Gabbro	Gabbro	Gabbro	Gabbro	Gabbro	Gabbro	Basalt
Unit	N. Region	N. Region	N. Region	N. Region	N. Region	N. Region	N. Region	N. Region	N. Region	N. Region	N.Region
Analysis no.	52	61	62	63	64	65	66	67	68	69	79
SiO_2	51.15	51.23	43.47	44.25	52.41	44.68	53.15	52.15	43.53	53.07	39.63
TiO_2	0.31	0.15	1.53	0.97	0.14	0.81	0.16	0.26	1.19	0.08	1.39
Al_2O_3	5.11	4.83	11.08	9.78	3.10	9.28	2.71	3.07	10.55	2.39	17.36
Cr_2O_3	0.52	0.95	0.06	0.01	0.01	0.04	0.03	0.00	0.07	0.00	0.01
FeO	10.58	8.27	12.89	14.58	13.10	15.29	10.85	12.21	13.71	12.87	14.40
MnO	0.21	0.17	0.16	0.22	0.32	0.27	0.26	0.26	0.14	0.42	0.20
MgO	17.21	18.02	14.96	13.92	18.40	13.74	18.67	18.31	14.22	19.04	10.55
CaO	11.23	12.81	10.86	10.78	9.36	10.66	10.92	9.63	11.02	8.83	11.77
Na_2O	0.42	0.32	1.27	1.25	0.28	1.25	0.21	0.29	1.33	0.21	1.85
K_2O	0.03	0.06	0.23	0.17	0.10	0.18	0.10	0.11	0.18	0.05	0.12
Total	96.75	96.82	96.51	95.92	97.24	96.20	97.06	96.28	95.95	96.96	97.30

Table 4 (ctd.): Amphibole compositions obtained using wavelength dispersive analysis

Sample no.	**ND15-53B**	**ND15-53B**	**ND15-53B**	**ND15-53B**	**ND15-53B**	**ND15-53B**	**ND15-53B**	**ND15-53B**	**ND15-53B**	**ND15-53B**	**ND15-53B**
Lithology	Basalt	Basalt	Basalt	Basalt	Basalt	Basalt	Basalt	Basalt	Basalt	Basalt	Basalt
Unit	N.Region	N.Region	N.Region	N.Region	N.Region	N.Region	N.Region	N.Region	N.Region	N.Region	N.Region
Analysis no.	80	81	82	83	87	88	89	90	91	97	98
SiO_2	38.70	38.17	39.87	52.12	47.39	47.71	51.70	47.18	51.62	51.19	52.55
TiO_2	1.81	1.69	1.08	0.20	1.08	1.07	0.26	1.17	0.18	0.24	0.23
Al_2O_3	17.95	17.08	16.62	3.62	6.90	6.71	4.29	7.58	4.18	4.05	1.42
Cr_2O_3	0.01	0.01	0.04	0.10	0.00	0.02	0.07	0.04	0.06	0.03	0.01
FeO	15.14	18.21	16.33	13.25	16.99	16.81	13.31	16.47	12.98	13.19	18.59
MnO	0.32	0.31	0.25	0.29	0.36	0.44	0.21	0.44	0.26	0.27	0.42
MgO	9.89	7.70	9.45	15.45	13.14	13.54	15.09	12.61	15.47	15.23	12.22
CaO	11.19	11.86	11.68	12.00	10.51	10.30	12.35	10.76	12.26	12.44	11.72
Na_2O	1.93	1.59	1.64	0.34	0.74	0.73	0.37	0.77	0.36	0.32	0.20
K_2O	0.06	0.15	0.08	0.04	0.08	0.06	0.06	0.11	0.06	0.08	0.04
Total	97.00	96.78	97.05	97.43	97.20	97.39	97.70	97.12	97.44	97.05	97.40

Table 4 (ctd.): Amphibole compositions obtained using wavelength dispersive analysis

Sample no.	**ND15-53B**	**ND15-53B**	**ND15-53B**	**ND15-53B**	**ND15-53B**	**ND15-53C**	**ND15-53C**	**ND15-53C**	**ND15-53C**	**ND15-53C**	**ND15-53C**
Lithology	Basalt	Basalt	Basalt	Basalt	Basalt	Gabbro	Gabbro	Gabbro	Gabbro	Gabbro	Gabbro
Unit	N.Region	N.Region	N.Region	N.Region	N.Region	N. Region	N. Region	N. Region	N. Region	N. Region	N. Region
Analysis no.	99	100	101	102	103	36	37	38	39	40	41
SiO_2	52.30	52.78	52.29	52.39	52.31	44.90	46.82	45.58	45.76	49.31	49.67
TiO_2	0.24	0.24	0.35	0.17	0.37	1.85	1.44	1.60	1.62	0.49	0.46
Al_2O_3	1.89	2.12	3.32	1.52	2.79	8.54	7.07	8.39	8.45	5.55	5.54
Cr_2O_3	0.03	0.04	0.00	0.00	0.00	0.00	0.00	0.04	0.01	0.01	0.04
FeO	15.81	14.68	13.40	18.28	14.31	13.29	13.47	12.96	13.62	11.92	11.57
MnO	0.43	0.44	0.33	0.38	0.23	0.24	0.23	0.28	0.28	0.26	0.21
MgO	14.39	14.96	15.19	12.55	14.77	14.26	14.56	14.29	13.90	15.58	15.48
CaO	11.44	11.69	12.10	11.95	12.07	11.34	11.38	11.45	11.57	12.42	12.57
Na_2O	0.21	0.13	0.16	0.17	0.23	1.25	0.89	1.10	0.94	0.98	0.48
K_2O	0.05	0.02	0.05	0.04	0.04	0.11	0.08	0.12	0.14	0.14	0.22
Total	96.78	97.09	97.20	97.45	97.12	95.78	95.95	95.81	96.29	96.66	96.24

Table 4 (ctd.): Amphibole compositions obtained using wavelength dispersive analysis

Sample no.	**ND15-53C**	**ND15-53C**
Lithology	Gabbro	Gabbro
Unit	N. Region	N. Region
Analysis no.	42	43
SiO_2	49.47	50.27
TiO_2	0.41	0.51
Al_2O_3	5.46	4.82
Cr_2O_3	0.00	0.00
FeO	12.10	11.19
MnO	0.26	0.24
MgO	15.13	16.41
CaO	12.42	12.28
Na_2O	0.06	0.91
K_2O	0.16	0.08
Total	95.47	96.71

Table 5: Feldspar compositions obtained using wavelength dispersive analysis

Sample no.	**ND14-02B**	**ND14-02B**	**ND14-02B**	**ND14-02B**	**ND14-02B**	**ND14-02B**	**ND14-02B**	**ND14-02B**	**ND14-02B**	**ND14-02B**	**ND14-02B**
Lithology	Metagabbro	Metagabbro	Metagabbro	Metagabbro	Metagabbro	Metagabbro	Metagabbro	Metagabbro	Metagabbro	Metagabbro	Metagabbro
Unit	NMC	NMC	NMC	NMC	NMC	NMC	NMC	NMC	NMC	NMC	NMC
Analysis no.	63	64	65	66	67	68	69	70	71	72	73
SiO_2	54.56	52.22	51.36	52.69	51.84	51.17	52.43	55.70	55.39	55.96	50.28
TiO_2	0.00	0.03	0.01	0.00	0.03	0.00	0.02	0.02	0.01	0.03	0.01
Al_2O_3	28.88	30.62	31.17	30.46	30.79	31.47	30.84	28.72	28.75	28.23	32.42
Cr_2O_3	0.01	0.03	0.00	0.00	0.04	0.00	0.00	0.03	0.00	0.00	0.00
FeO	0.20	0.09	0.08	0.05	0.13	0.13	0.10	0.19	0.19	0.14	0.18
MnO	0.03	0.02	0.00	0.00	0.00	0.02	0.00	0.01	0.01	0.03	0.02
MgO	0.02	0.00	0.00	0.00	0.01	0.00	0.00	0.00	0.01	0.00	0.00
CaO	11.06	13.01	13.62	12.49	13.20	13.78	13.14	10.36	10.79	10.27	14.82
Na_2O	5.32	4.13	3.92	4.31	4.01	3.60	4.15	5.57	5.51	5.78	3.24
K_2O	0.24	0.15	0.15	0.21	0.18	0.19	0.10	0.21	0.24	0.27	0.16
Total	100.32	100.31	100.31	100.21	100.22	100.36	100.79	100.81	100.90	100.70	101.13
An	53	63	65	61	64	67	63	50	51	49	71
Ab	46	36	34	38	35	32	36	49	47	50	28
Or	1	1	1	1	1	1	1	1	1	2	1

Table 5 (ctd.): Feldspar compositions obtained using wavelength dispersive analysis

Sample no.	**ND14-02B**	**ND14-02B**	**ND14-02B**	**ND14-02B**	**ND14-02B**	**ND14-02B**	**ND14-02B**	**ND14-02B**	**ND14-02B**	**ND14-02B**	**ND14-02B**
Lithology	Metagabbro	Metagabbro	Metagabbro	Metagabbro	Metagabbro	Metagabbro	Metagabbro	Metagabbro	Metagabbro	Metagabbro	Metagabbro
Unit	NMC	NMC	NMC	NMC	NMC	NMC	NMC	NMC	NMC	NMC	NMC
Analysis no.	74	88	89	90	91	92	93	94	95	96	97
SiO_2	50.94	54.78	47.82	47.81	47.42	51.97	52.98	55.34	48.71	50.99	52.18
TiO_2	0.00	0.00	0.00	0.00	0.00	0.01	0.01	0.02	0.00	0.01	0.00
Al_2O_3	31.73	28.89	33.54	33.66	33.50	30.99	29.76	28.24	33.36	31.76	30.86
Cr_2O_3	0.00	0.00	0.01	0.00	0.00	0.02	0.00	0.00	0.00	0.00	0.00
FeO	0.14	0.10	0.11	0.15	0.19	0.17	0.09	0.26	0.06	0.13	0.29
MnO	0.01	0.00	0.00	0.05	0.00	0.00	0.00	0.00	0.00	0.02	0.01
MgO	0.00	0.00	0.00	0.00	0.00	0.00	0.00	0.00	0.00	0.00	0.01
CaO	14.27	11.03	16.69	16.66	16.64	13.32	11.90	10.47	16.08	14.34	13.28
Na_2O	3.49	5.18	2.19	2.21	2.13	4.06	4.68	5.55	2.48	3.63	4.22
K_2O	0.15	0.19	0.07	0.11	0.09	0.06	0.21	0.27	0.06	0.12	0.11
Total	100.73	100.17	100.42	100.64	99.97	100.60	99.62	100.16	100.76	100.99	100.97
An	69	53	80	80	81	64	58	50	78	68	63
Ab	30	45	19	19	19	35	41	48	22	31	36
Or	1	1	0	1	1	0	1	2	0	1	1

Table 5 (ctd.): Feldspar compositions obtained using wavelength dispersive analysis

Sample no.	**ND14-02B**	**ND14-02B**	**ND14-02B**	**ND14-02B**	**ND14-02B**	**ND14-02B**	**ND14-02B**	**ND14-02B**	**ND14-02B**	**ND14-02B**	**ND14-02B**
Lithology	Metagabbro	Metagabbro	Metagabbro	Metagabbro	Metagabbro	Metagabbro	Metagabbro	Metagabbro	Metagabbro	Metagabbro	Metagabbro
Unit	NMC	NMC	NMC	NMC	NMC	NMC	NMC	NMC	NMC	NMC	NMC
Analysis no.	98	99	125	126	127	128	129	130	131	132	133
SiO_2	48.55	52.74	55.47	47.37	46.30	46.87	48.31	52.49	54.19	52.32	55.52
TiO_2	0.00	0.01	0.00	0.02	0.01	0.00	0.00	0.00	0.00	0.01	0.00
Al_2O_3	33.40	30.47	28.47	34.21	34.94	34.86	33.57	30.84	30.04	30.89	28.88
Cr_2O_3	0.00	0.00	0.01	0.00	0.00	0.00	0.00	0.02	0.00	0.00	0.00
FeO	0.13	0.13	0.12	0.09	0.19	0.14	0.09	0.16	0.08	0.27	0.21
MnO	0.01	0.01	0.02	0.03	0.00	0.00	0.00	0.00	0.00	0.00	0.02
MgO	0.00	0.01	0.00	0.00	0.00	0.00	0.00	0.00	0.02	0.00	0.01
CaO	16.18	12.74	10.28	17.09	17.60	17.90	16.44	13.38	11.82	13.16	10.86
Na_2O	2.33	4.20	5.67	2.01	1.60	1.51	2.39	4.05	4.77	4.12	5.40
K_2O	0.07	0.15	0.26	0.03	0.05	0.03	0.05	0.22	0.16	0.19	0.34
Total	100.67	100.48	100.30	100.84	100.71	101.31	100.85	101.16	101.07	100.95	101.25
An	79	62	49	82	86	87	79	64	57	63	52
Ab	21	37	49	18	14	13	21	35	42	36	46
Or	0	1	1	0	0	0	0	1	1	1	2

Table 5 (ctd.): Feldspar compositions obtained using wavelength dispersive analysis

Sample no.	**ND14-02B**	**ND14-02B**	**ND14-07**	**ND14-07**	**ND14-07**	**ND14-07**	**ND14-07**	**ND14-07**	**ND14-07**	**ND15-15**	**ND15-15**
Lithology	Metagabbro	Metagabbro	Gabbro	Gabbro	Gabbro	Gabbro	Gabbro	Gabbro	Gabbro	Metagabbro	Metagabbro
Unit	NMC	NMC	EMC	EMC	EMC	EMC	EMC	EMC	EMC	NMC	NMC
Analysis no.	134	135	302	303	304	305	315	316	317	232	233
SiO_2	46.64	55.50	46.51	46.99	46.63	46.47	46.34	46.54	46.81	46.31	46.79
TiO_2	0.00	0.02	0.01	0.01	0.01	0.00	0.03	0.02	0.01	0.01	0.00
Al_2O_3	34.95	28.55	34.34	34.60	34.49	34.86	34.81	34.35	34.45	35.18	34.65
Cr_2O_3	0.02	0.00	0.00	0.00	0.00	0.00	0.02	0.00	0.03	0.00	0.00
FeO	0.14	0.07	0.38	0.29	0.29	0.31	0.39	0.32	0.56	0.24	0.20
MnO	0.01	0.00	0.00	0.00	0.04	0.00	0.02	0.00	0.00	0.01	0.00
MgO	0.02	0.00	0.03	0.04	0.04	0.04	0.14	0.06	0.30	0.02	0.00
CaO	17.73	10.71	17.27	17.24	17.12	17.68	17.45	17.44	17.39	17.65	17.06
Na_2O	1.55	5.65	1.63	1.74	1.75	1.61	1.61	1.73	1.69	1.53	1.78
K_2O	0.03	0.22	0.01	0.00	0.03	0.01	0.05	0.02	0.02	0.01	0.01
Total	101.09	100.72	100.19	100.93	100.41	100.99	100.85	100.49	101.26	100.95	100.48
An	86	51	85	85	84	86	85	85	85	86	84
Ab	14	48	15	15	16	14	14	15	15	14	16
Or	0	1	0	0	0	0	0	0	0	0	0

Table 5 (ctd.): Feldspar compositions obtained using wavelength dispersive analysis

Sample no.	**ND15-15**	**ND15-15**	**ND15-15**	**ND15-15**	**ND15-15**	**ND15-15**	**ND15-15**	**ND15-15**	**ND15-15**	**ND15-15**	**ND15-15**
Lithology	Metagabbro	Metagabbro	Metagabbro	Metagabbro	Metagabbro	Metagabbro	Metagabbro	Metagabbro	Metagabbro	Metagabbro	Metagabbro
Unit	NMC	NMC	NMC	NMC	NMC	NMC	NMC	NMC	NMC	NMC	NMC
Analysis no.	234	236	259	260	261	262	263	264	265	266	267
SiO_2	47.72	46.28	48.65	48.23	48.04	49.93	48.57	48.67	48.74	48.65	49.11
TiO_2	0.00	0.02	0.03	0.00	0.00	0.01	0.04	0.00	0.00	0.01	0.00
Al_2O_3	33.13	34.69	33.42	33.49	33.36	32.56	33.32	33.61	33.17	34.11	33.03
Cr_2O_3	0.00	0.00	0.00	0.01	0.00	0.00	0.06	0.00	0.00	0.01	0.00
FeO	0.59	0.28	0.20	0.30	0.21	0.17	0.18	0.27	0.17	0.31	0.21
MnO	0.00	0.00	0.00	0.00	0.01	0.01	0.00	0.00	0.00	0.00	0.00
MgO	0.29	0.00	0.03	0.00	0.00	0.00	0.00	0.00	0.00	0.00	0.02
CaO	15.37	17.56	15.13	15.70	15.92	14.74	15.59	15.94	15.51	16.03	15.27
Na_2O	2.27	1.64	2.64	2.44	2.40	3.07	2.57	2.49	2.73	2.43	2.81
K_2O	0.03	0.02	0.34	0.02	0.01	0.01	0.01	0.04	0.02	0.01	0.02
Total	99.40	100.49	100.43	100.19	99.95	100.51	100.35	101.01	100.33	101.56	100.47
An	79	85	74	78	79	73	77	78	76	78	75
Ab	21	14	23	22	21	27	23	22	24	21	25
Or	0	0	2	0	0	0	0	0	0	0	0

Table 5 (ctd.): Feldspar compositions obtained using wavelength dispersive analysis

Sample no.	**ND15-15**	**ND15-15**	**ND15-15**	**ND15-15**	**ND15-15**	**ND15-15**	**ND15-22C**	**ND15-22C**	**ND15-22C**	**ND15-22C**	**ND15-22C**
Lithology	Metagabbro	Metagabbro	Metagabbro	Metagabbro	Metagabbro	Metagabbro	Metagabbro	Metagabbro	Metagabbro	Metagabbro	Metagabbro
Unit	NMC	NMC	NMC	NMC	NMC	NMC	NMC	NMC	NMC	NMC	NMC
Analysis no.	268	269	270	271	272	257	70	71	72	73	74
SiO_2	49.72	46.09	48.48	48.87	49.16	46.81	57.13	58.29	55.43	57.99	57.84
TiO_2	0.00	0.01	0.00	0.01	0.00	0.00	0.01	0.02	0.01	0.00	0.02
Al_2O_3	33.03	35.56	33.80	33.32	33.44	35.34	26.52	25.80	26.96	26.50	26.51
Cr_2O_3	0.00	0.02	0.00	0.00	0.00	0.00	0.00	0.00	0.00	0.03	0.02
FeO	0.19	0.24	0.21	0.25	0.19	0.26	0.24	0.07	0.09	0.19	0.11
MnO	0.03	0.00	0.01	0.00	0.00	0.05	0.02	0.00	0.02	0.02	0.00
MgO	0.01	0.00	0.02	0.00	0.00	0.01	0.00	0.00	0.00	0.02	0.00
CaO	15.07	17.94	15.86	15.52	15.51	17.61	8.14	7.27	9.21	7.79	8.01
Na_2O	2.87	1.41	2.49	2.65	2.71	1.65	6.88	7.44	6.25	7.10	7.17
K_2O	0.02	0.04	0.01	0.02	0.03	0.02	0.04	0.11	0.04	0.01	0.03
Total	100.96	101.31	100.89	100.64	101.04	101.75	98.97	99.01	98.01	99.64	99.72
An	74	87	78	76	76	85	39	35	45	38	38
Ab	26	12	22	24	24	15	60	65	55	62	62
Or	0	0	0	0	0	0	0	1	0	0	0

Table 5 (ctd.): Feldspar compositions obtained using wavelength dispersive analysis

Sample no.	**ND15-22C**	**ND15-22C**	**ND15-34B**	**ND15-34B**	**ND15-34B**	**ND15-34B**	**ND15-34B**	**ND15-34B**	**ND15-34B**	**ND15-34B**	**ND15-34B**
Lithology	Metagabbro	Metagabbro	Gabbro	Gabbro	Gabbro	Gabbro	Gabbro	Gabbro	Gabbro	Gabbro	Gabbro
Unit	NMC	NMC	N. Region	N. Region	N. Region	N. Region	N. Region	N. Region	N. Region	N. Region	N. Region
Analysis no.	75	76	170	171	172	173	174	175	176	191	192
SiO_2	55.14	62.94	45.01	44.98	45.05	45.00	44.82	45.17	45.63	44.70	44.32
TiO_2	0.03	0.03	0.02	0.02	0.02	0.00	0.00	0.02	0.00	0.00	0.00
Al_2O_3	28.61	22.91	35.44	35.73	35.33	35.81	36.09	35.76	35.65	35.79	36.11
Cr_2O_3	0.03	0.00	0.00	0.00	0.01	0.00	0.00	0.00	0.00	0.02	0.00
FeO	0.12	0.29	0.30	0.24	0.38	0.37	0.23	0.28	0.29	0.36	0.12
MnO	0.00	0.01	0.00	0.00	0.02	0.00	0.02	0.00	0.00	0.00	0.03
MgO	0.00	0.00	0.00	0.01	0.00	0.00	0.00	0.00	0.00	0.01	0.00
CaO	10.47	3.84	18.60	18.67	18.70	19.05	19.34	18.82	18.46	19.04	19.23
Na_2O	5.71	9.43	0.99	0.87	0.92	0.77	0.69	0.85	1.08	0.73	0.61
K_2O	0.03	0.03	0.02	0.02	0.00	0.00	0.03	0.01	0.00	0.05	0.00
Total	100.15	99.50	100.39	100.54	100.43	101.00	101.22	100.91	101.11	100.69	100.42
An	50	18	91	92	92	93	94	92	90	93	95
Ab	50	82	9	8	8	7	6	8	10	6	5
Or	0	0	0	0	0	0	0	0	0	0	0

Table 5 (ctd.): Feldspar compositions obtained using wavelength dispersive analysis

Sample no.	**ND15-34B**	**ND15-34B**	**ND15-34B**	**ND15-34B**	**ND15-36A**	**ND15-36A**	**ND15-36A**	**ND15-36A**	**ND15-36A**	**ND15-36A**	**ND15-36A**
Lithology	Gabbro	Gabbro	Gabbro	Gabbro	Metagabbro	Metagabbro	Metagabbro	Metagabbro	Metagabbro	Metagabbro	Metagabbro
Unit	N. Region	N. Region	N. Region	N. Region	NMC	NMC	NMC	NMC	NMC	NMC	NMC
Analysis no.	193	194	218	219	182	183	184	185	191	192	193
SiO_2	44.38	44.05	44.90	44.24	48.37	46.59	48.59	46.76	48.81	47.59	47.02
TiO_2	0.03	0.00	0.01	0.04	0.00	0.00	0.00	0.00	0.01	0.00	0.00
Al_2O_3	35.59	35.71	35.65	35.24	33.19	34.19	33.82	35.29	32.26	34.01	33.82
Cr_2O_3	0.00	0.01	0.00	0.02	0.02	0.00	0.00	0.00	0.00	0.01	0.00
FeO	0.37	0.31	0.34	0.28	0.38	0.30	0.33	0.30	0.45	0.14	0.38
MnO	0.01	0.02	0.03	0.03	0.00	0.00	0.00	0.01	0.01	0.03	0.00
MgO	0.01	0.00	0.01	0.00	0.00	0.02	0.00	0.05	0.08	0.00	0.03
CaO	18.95	19.17	18.79	18.87	15.87	17.27	15.99	17.61	15.47	16.72	17.10
Na_2O	0.76	0.59	0.83	0.75	2.66	1.55	2.93	1.87	2.55	1.80	2.04
K_2O	0.00	0.00	0.01	0.03	0.01	0.00	0.01	0.00	0.04	0.01	0.00
Total	100.11	99.86	100.56	99.49	100.50	99.92	101.67	101.88	99.67	100.31	100.39
An	93	95	93	93	77	86	75	84	77	84	82
Ab	7	5	7	7	23	14	25	16	23	16	18
Or	0	0	0	0	0	0	0	0	0	0	0

Table 5 (ctd.): Feldspar compositions obtained using wavelength dispersive analysis

Sample no.	**ND15-36A**	**ND15-36A**	**ND15-36A**	**ND15-36A**	**ND15-36A**	**ND15-36A**	**ND15-36A**	**ND15-36A**	**ND15-36A**	**ND15-36A**	**ND15-36B**
Lithology	Metagabbro	Metagabbro	Metagabbro	Metagabbro	Metagabbro	Metagabbro	Metagabbro	Metagabbro	Metagabbro	Metagabbro	Metagabbro
Unit	NMC	NMC	NMC	NMC	NMC	NMC	NMC	NMC	NMC	NMC	NMC
Analysis no.	194	195	202	203	204	205	206	218	219	220	227
SiO_2	46.16	49.48	46.79	45.75	46.17	46.44	45.80	45.77	46.19	47.31	47.31
TiO_2	0.00	0.00	0.00	0.01	0.00	0.01	0.05	0.01	0.03	0.00	0.02
Al_2O_3	32.18	32.93	33.48	33.49	35.56	33.17	33.36	34.73	34.23	33.86	32.69
Cr_2O_3	0.03	0.00	0.01	0.00	0.00	0.04	0.00	0.02	0.01	0.01	0.01
FeO	0.66	0.34	0.38	0.34	0.22	0.33	0.30	0.41	0.45	1.18	0.40
MnO	0.03	0.00	0.00	0.01	0.00	0.00	0.01	0.03	0.00	0.02	0.00
MgO	0.38	0.06	0.02	0.00	0.00	0.11	0.00	0.01	0.00	0.75	0.00
CaO	16.63	15.37	17.19	17.70	18.23	17.42	17.47	18.27	17.85	15.72	16.86
Na_2O	1.76	2.68	1.92	1.53	0.84	1.53	1.45	1.02	1.38	1.62	1.74
K_2O	0.00	0.04	0.05	0.02	0.02	0.01	0.04	0.00	0.01	0.05	0.03
Total	97.83	100.90	99.85	98.84	101.03	99.07	98.49	100.27	100.16	100.53	99.06
An	84	76	83	86	92	86	87	91	88	84	84
Ab	16	24	17	14	8	14	13	9	12	16	16
Or	0	0	0	0	0	0	0	0	0	0	0

Table 5 (ctd.): Feldspar compositions obtained using wavelength dispersive analysis

Sample no.	**ND15-36B**	**ND15-36B**	**ND15-36B**	**ND15-36B**	**ND15-36B**	**ND15-36B**	**ND15-36B**	**ND15-36B**	**ND15-36B**	**ND15-36B**	**ND15-36B**
Lithology	Metagabbro	Metagabbro	Metagabbro	Metagabbro	Metagabbro	Metagabbro	Metagabbro	Metagabbro	Metagabbro	Metagabbro	Metagabbro
Unit	NMC	NMC	NMC	NMC	NMC	NMC	NMC	NMC	NMC	NMC	NMC
Analysis no.	228	229	230	231	232	233	234	235	237	251	252
SiO_2	49.14	48.03	48.70	46.75	49.62	47.88	50.68	48.23	47.78	48.39	48.02
TiO_2	0.00	0.00	0.00	0.01	0.00	0.02	0.02	0.00	0.01	0.05	0.00
Al_2O_3	31.46	31.71	31.56	32.40	31.97	33.98	31.63	32.29	32.58	32.63	32.21
Cr_2O_3	0.00	0.00	0.01	0.01	0.01	0.05	0.00	0.00	0.04	0.00	0.05
FeO	0.40	0.44	0.44	0.41	0.41	0.43	0.45	0.38	0.42	0.40	0.38
MnO	0.00	0.00	0.00	0.00	0.00	0.00	0.04	0.00	0.02	0.02	0.00
MgO	0.00	0.00	0.00	0.00	0.00	0.02	0.07	0.01	0.01	0.00	0.01
CaO	15.42	16.05	15.72	16.87	15.57	16.97	14.88	16.48	16.77	16.69	16.66
Na_2O	2.70	2.13	2.73	1.95	2.67	1.73	2.25	2.07	1.89	2.55	2.40
K_2O	0.07	0.05	0.03	0.04	0.05	0.02	0.06	0.03	0.03	0.04	0.04
Total	99.19	98.41	99.20	98.45	100.32	101.10	100.09	99.50	99.55	100.76	99.78
An	76	80	76	83	76	84	78	81	83	78	79
Ab	24	19	24	17	24	16	21	18	17	22	21
Or	0	0	0	0	0	0	0	0	0	0	0

Table 5 (ctd.): Feldspar compositions obtained using wavelength dispersive analysis

Sample no.	**ND15-36B**	**ND15-36B**	**ND15-36B**	**ND15-36B**	**ND15-36B**	**ND15-36B**	**ND15-36B**	**ND15-36B**	**ND15-36B**	**ND15-36B**	**ND15-36B**
Lithology	Metagabbro	Metagabbro	Metagabbro	Metagabbro	Metagabbro	Metagabbro	Metagabbro	Metagabbro	Metagabbro	Metagabbro	Metagabbro
Unit	NMC	NMC	NMC	NMC	NMC	NMC	NMC	NMC	NMC	NMC	NMC
Analysis no.	254	255	276	277	278	279	280	281	282	283	284
SiO_2	56.55	50.17	47.50	48.32	47.46	46.76	46.31	47.94	48.39	47.96	46.32
TiO_2	0.01	0.01	0.02	0.01	0.04	0.01	0.00	0.00	0.02	0.02	0.02
Al_2O_3	27.46	31.48	33.70	33.03	34.12	34.71	34.65	33.59	33.37	33.45	34.44
Cr_2O_3	0.00	0.01	0.02	0.00	0.00	0.02	0.00	0.00	0.01	0.01	0.00
FeO	0.34	0.46	0.42	0.45	0.44	0.24	0.32	0.43	0.33	0.44	0.31
MnO	0.00	0.00	0.03	0.00	0.00	0.02	0.00	0.02	0.01	0.00	0.00
MgO	0.02	0.00	0.00	0.04	0.00	0.00	0.00	0.00	0.06	0.00	0.00
CaO	10.43	15.35	17.27	16.73	17.48	17.84	18.39	17.21	17.12	17.40	18.78
Na_2O	5.81	3.03	1.66	2.15	1.73	1.58	1.25	1.84	1.87	1.87	1.03
K_2O	0.18	0.06	0.02	0.04	0.06	0.03	0.05	0.04	0.03	0.04	0.02
Total	100.81	100.58	100.62	100.76	101.33	101.20	100.97	101.07	101.20	101.18	100.91
An	49	73	85	81	85	86	89	84	83	84	91
Ab	50	26	15	19	15	14	11	16	17	16	9
Or	1	0	0	0	0	0	0	0	0	0	0

Table 5 (ctd.): Feldspar compositions obtained using wavelength dispersive analysis

Sample no.	**ND15-40B**	**ND15-40B**	**ND15-40B**	**ND15-40B**	**ND15-40B**	**ND15-40B**	**ND15-40B**	**ND15-40B**	**ND15-40B**	**ND15-40B**	**ND15-40B**
Lithology	Diabase	Diabase	Diabase	Diabase	Diabase	Diabase	Diabase	Diabase	Diabase	Diabase	Diabase
Unit	NMC	NMC	NMC	NMC	NMC	NMC	NMC	NMC	NMC	NMC	NMC
Analysis no.	118	119	120	121	122	123	124	125	126	127	138
SiO_2	52.93	64.38	44.72	53.51	53.01	45.01	51.53	45.27	53.91	51.51	51.87
TiO_2	0.00	0.02	0.00	0.00	0.00	0.02	0.00	0.02	0.00	0.00	0.02
Al_2O_3	29.04	18.27	33.91	28.66	28.86	34.33	29.84	34.11	28.23	30.01	30.43
Cr_2O_3	0.00	0.02	0.00	0.01	0.00	0.00	0.03	0.01	0.00	0.00	0.00
FeO	0.18	0.22	0.26	0.24	0.30	0.26	0.28	0.21	0.14	0.30	0.29
MnO	0.03	0.03	0.01	0.00	0.00	0.02	0.00	0.02	0.02	0.00	0.03
MgO	0.00	0.00	0.00	0.00	0.01	0.00	0.00	0.00	0.00	0.01	0.00
CaO	11.91	0.06	18.15	11.70	11.92	18.26	13.10	18.28	11.34	13.10	13.20
Na_2O	4.79	0.33	0.93	4.98	4.82	1.24	4.18	1.21	5.01	4.09	4.17
K_2O	0.05	16.77	0.02	0.05	0.07	0.04	0.05	0.01	0.05	0.06	0.04
Total	98.95	100.11	97.99	99.14	98.99	99.18	98.99	99.13	98.70	99.08	100.04
An	58	0	91	56	58	89	63	89	55	64	64
Ab	42	3	8	43	42	11	37	11	44	36	36
Or	0	97	0	0	0	0	0	0	0	0	0

Table 5 (ctd.): Feldspar compositions obtained using wavelength dispersive analysis

Sample no.	**ND15-40B**	**ND15-40B**	**ND15-40B**	**ND15-40B**	**ND15-40B**	**ND15-40B**	**ND15-40B**	**ND15-40B**	**ND15-40B**	**ND15-40B**	**ND15-40B**
Lithology	Diabase	Diabase	Diabase	Diabase	Diabase	Diabase	Diabase	Diabase	Diabase	Diabase	Diabase
Unit	NMC	NMC	NMC	NMC	NMC	NMC	NMC	NMC	NMC	NMC	NMC
Analysis no.	139	140	141	142	143	145	146	147	148	149	152
SiO_2	45.38	52.73	45.85	67.63	49.53	56.57	51.28	46.90	53.27	52.61	54.61
TiO_2	0.02	0.05	0.02	0.00	0.03	0.00	0.01	0.00	0.00	0.00	0.00
Al_2O_3	35.10	30.42	34.79	22.90	32.50	27.64	31.20	33.65	29.69	30.50	28.79
Cr_2O_3	0.00	0.00	0.00	0.00	0.01	0.00	0.00	0.00	0.00	0.00	0.03
FeO	0.28	0.23	0.49	0.26	0.35	0.27	0.28	0.26	0.21	0.16	0.21
MnO	0.00	0.00	0.00	0.00	0.01	0.05	0.02	0.04	0.00	0.00	0.00
MgO	0.00	0.03	0.00	0.03	0.00	0.01	0.00	0.00	0.00	0.00	0.00
CaO	18.19	12.50	17.91	0.50	15.05	9.45	13.56	16.72	11.57	12.55	10.83
Na_2O	1.12	4.39	1.44	10.43	2.92	6.21	3.70	1.86	4.46	4.38	5.36
K_2O	0.01	0.04	0.00	0.46	0.05	0.09	0.02	0.03	0.26	0.01	0.07
Total	100.09	100.41	100.50	102.22	100.45	100.29	100.06	99.46	99.46	100.21	99.89
An	90	61	87	2	74	45	67	83	58	61	0
Ab	10	39	13	95	26	54	33	17	40	39	0
Or	0	0	0	3	0	1	0	0	2	0	100

Table 5 (ctd.): Feldspar compositions obtained using wavelength dispersive analysis

Sample no.	**ND15-40B**	**ND15-40B**	**ND15-48E**	**ND15-48E**	**ND15-48E**	**ND15-48E**	**ND15-48E**	**ND15-48E**	**ND15-48E**	**ND15-48E**	**ND15-48E**
Lithology	Diabase	Diabase	Gabbro	Gabbro	Gabbro	Gabbro	Gabbro	Gabbro	Gabbro	Gabbro	Gabbro
Unit	NMC	NMC	NMC	NMC	NMC	NMC	NMC	NMC	NMC	NMC	NMC
Analysis no.	153	155	118	119	120	121	122	123	134	135	136
SiO_2	54.80	50.10	45.11	45.63	45.61	44.92	45.80	46.03	45.22	45.9	45.5
TiO_2	0.01	0.00	0.00	0.04	0.00	0.01	0.00	0.00	0.00	0.0	0.0
Al_2O_3	28.84	32.03	35.67	34.81	35.03	34.91	35.38	35.13	34.74	34.9	34.6
Cr_2O_3	0.01	0.03	0.00	0.00	0.01	0.00	0.01	0.00	0.00	0.0	0.0
FeO	0.20	0.25	0.08	0.15	0.12	0.12	0.13	0.13	0.13	0.2	0.2
MnO	0.00	0.02	0.00	0.00	0.00	0.00	0.04	0.02	0.00	0.0	0.0
MgO	0.00	0.03	0.00	0.00	0.01	0.00	0.00	0.00	0.00	0.0	0.0
CaO	10.95	14.63	18.48	17.96	18.14	18.23	18.21	17.96	17.83	17.8	17.8
Na_2O	5.30	3.37	1.15	1.39	1.36	1.28	1.28	1.38	1.34	1.5	1.5
K_2O	0.05	0.02	0.00	0.01	0.01	0.01	0.00	0.02	0.00	0.0	0.0
Total	100.16	100.47	100.49	99.99	100.28	99.46	100.86	100.67	99.27	100.2	99.7
An	0	1	90	88	88	89	89	88	88	87	87
Ab	0	0	10	12	12	11	11	12	12	13	13
Or	100	99	0	0	0	0	0	0	0	0	0

Table 5 (ctd.): Feldspar compositions obtained using wavelength dispersive analysis

Sample no.	**ND15-48E**	**ND15-48E**	**ND15-48E**	**ND15-48E**	**ND15-48E**	**ND15-48E**	**ND15-48E**	**ND15-48E**	**ND15-48E**	**ND15-48E**	**ND15-51F**
Lithology	Gabbro	Gabbro	Gabbro	Gabbro	Gabbro	Gabbro	Gabbro	Gabbro	Gabbro	Gabbro	diabase
Unit	NMC	NMC	NMC	NMC	NMC	NMC	NMC	NMC	NMC	NMC	NMC
Analysis no.	137	138	139	140	141	142	143	144	145	146	220
SiO_2	44.8	46.2	45.6	45.1	44.9	45.4	44.8	45.3	45.2	45.08	58.20
TiO_2	0.0	0.0	0.0	0.0	0.0	0.0	0.0	0.0	0.0	0.03	0.00
Al_2O_3	34.5	35.0	34.6	35.1	35.0	35.5	35.1	35.4	35.2	35.04	27.18
Cr_2O_3	0.0	0.0	0.0	0.0	0.0	0.0	0.0	0.0	0.0	0.00	0.00
FeO	0.2	0.1	0.1	0.1	0.2	0.2	0.1	0.2	0.2	0.14	0.09
MnO	0.0	0.0	0.0	0.0	0.0	0.0	0.0	0.0	0.0	0.00	0.00
MgO	0.0	0.0	0.0	0.0	0.0	0.0	0.0	0.0	0.0	0.00	0.00
CaO	18.0	17.8	17.9	18.4	18.4	18.5	18.5	18.5	18.4	17.99	8.73
Na_2O	1.3	1.5	1.5	1.2	1.2	1.1	1.1	1.1	1.1	1.40	6.64
K_2O	0.0	0.0	0.0	0.0	0.0	0.0	0.0	0.0	0.0	0.00	0.07
Total	98.8	100.7	99.7	100.0	99.7	100.7	99.6	100.6	100.1	99.69	100.92
An	88	87	87	90	90	90	90	90	90	88	42
Ab	12	13	13	10	10	10	10	10	10	12	58
Or	0	0	0	0	0	0	0	0	0	0	0

Table 5 (ctd.): Feldspar compositions obtained using wavelength dispersive analysis

Sample no.	**ND15-51F**	**ND15-51F**	**ND15-51F**	**ND15-51F**	**ND15-51F**	**ND15-51F**	**ND15-51F**	**ND15-51F**	**ND15-51F**	**ND15-51F**	**ND15-51F**
Lithology	diabase	diabase	diabase	diabase	diabase	diabase	diabase	diabase	diabase	diabase	diabase
Unit	NMC	NMC	NMC	NMC	NMC	NMC	NMC	NMC	NMC	NMC	NMC
Analysis no.	221	222	223	224	225	226	227	228	229	230	231
SiO_2	58.06	57.99	58.26	58.14	57.50	57.77	57.35	53.36	58.02	56.34	55.95
TiO_2	0.01	0.00	0.02	0.00	0.00	0.00	0.00	0.00	0.01	0.00	0.00
Al_2O_3	27.01	26.71	26.27	26.49	26.54	26.76	27.21	30.13	26.65	27.62	26.89
Cr_2O_3	0.00	0.02	0.01	0.01	0.00	0.01	0.00	0.00	0.00	0.00	0.00
FeO	0.08	0.07	0.07	0.13	0.11	0.15	0.15	0.09	0.16	0.03	0.14
MnO	0.00	0.00	0.00	0.00	0.00	0.01	0.00	0.01	0.00	0.02	0.01
MgO	0.00	0.00	0.00	0.01	0.00	0.00	0.00	0.00	0.00	0.00	0.00
CaO	8.42	8.47	7.99	8.30	8.50	8.40	8.98	12.09	8.33	8.79	8.86
Na_2O	6.57	6.72	6.89	6.66	6.69	6.58	6.30	4.65	6.74	5.94	6.25
K_2O	0.12	0.33	0.27	0.17	0.09	0.20	0.26	0.14	0.12	0.60	0.20
Total	100.27	100.31	99.77	99.91	99.44	99.89	100.24	100.46	100.03	99.34	98.31
An	41	40	38	40	41	41	43	58	40	43	43
Ab	58	58	60	59	58	58	55	41	59	53	55
Or	1	2	2	1	1	1	1	1	1	4	1

Table 5 (ctd.): Feldspar compositions obtained using wavelength dispersive analysis

Sample no.	**ND15-51F**	**ND15-51F**	**ND15-51F**	**ND15-51F**	**ND15-53A**	**ND15-53A**	**ND15-53A**	**ND15-53A**	**ND15-53A**	**ND15-53A**	**ND15-53A**
Lithology	diabase	diabase	diabase	diabase	Gabbro	Gabbro	Gabbro	Gabbro	Gabbro	Gabbro	Gabbro
Unit	NMC	NMC	NMC	NMC	N. Region	N. Region	N. Region	N. Region	N. Region	N. Region	N. Region
Analysis no.	251	252	253	254	38	40	41	53	54	57	59
SiO_2	55.90	54.78	57.70	58.45	43.43	45.83	44.06	45.31	44.90	45.42	44.87
TiO_2	0.03	0.00	0.01	0.00	0.00	0.00	0.00	0.01	0.00	0.00	0.03
Al_2O_3	28.51	29.30	26.67	26.53	35.40	34.32	35.42	35.52	34.68	34.65	35.63
Cr_2O_3	0.02	0.00	0.00	0.02	0.00	0.00	0.00	0.02	0.00	0.02	0.00
FeO	0.27	0.17	0.18	0.16	0.52	0.57	0.62	0.12	0.64	0.55	0.56
MnO	0.00	0.00	0.05	0.01	0.02	0.01	0.03	0.00	0.00	0.00	0.00
MgO	0.01	0.00	0.00	0.00	0.04	0.02	0.05	0.01	0.03	0.05	0.06
CaO	10.43	11.29	8.53	7.23	18.21	17.21	18.35	18.01	17.76	17.66	18.51
Na_2O	5.61	5.13	6.55	6.99	1.00	1.73	1.10	1.31	1.32	1.48	1.00
K_2O	0.17	0.10	0.13	0.28	0.01	0.02	0.01	0.01	0.01	0.03	0.00
Total	100.94	100.78	99.82	99.67	98.64	99.70	99.63	100.32	99.35	99.87	100.66
An	50	55	42	36	91	85	90	88	88	87	91
Ab	49	45	58	63	9	15	10	12	12	13	9
Or	1	1	1	2	0	0	0	0	0	0	0

Table 5 (ctd.): Feldspar compositions obtained using wavelength dispersive analysis

Sample no.	**ND15-53A**	**ND15-53B**	**ND15-53B**	**ND15-53B**	**ND15-53B**	**ND15-53B**	**ND15-53B**	**ND15-53B**	**ND15-53B**	**ND15-53B**	**ND15-53B**
Lithology	Gabbro	Basalt	Basalt	Basalt	Basalt	Basalt	Basalt	Basalt	Basalt	Basalt	Basalt
Unit	N. Region	N. Region	N. Region	N. Region	N. Region	N. Region	N. Region	N. Region	N. Region	N. Region	N. Region
Analysis no.	60	84	85	86	92	93	94	96	104	105	106
SiO_2	46.27	48.67	48.27	46.61	48.33	48.26	57.83	49.36	55.12	59.51	55.15
TiO_2	0.00	0.03	0.01	0.01	0.01	0.02	0.02	0.03	0.01	0.00	0.01
Al_2O_3	35.37	32.93	33.39	34.26	33.71	33.42	27.56	32.62	28.37	25.97	28.83
Cr_2O_3	0.00	0.00	0.00	0.00	0.02	0.00	0.00	0.03	0.00	0.00	0.00
FeO	0.09	1.10	0.98	0.56	0.41	0.47	0.24	0.59	0.27	0.16	0.16
MnO	0.01	0.00	0.00	0.00	0.01	0.03	0.00	0.02	0.00	0.00	0.03
MgO	0.02	0.06	0.07	0.00	0.03	0.09	0.10	0.07	0.01	0.00	0.00
CaO	17.24	15.60	15.79	16.92	15.73	15.62	8.93	15.14	10.17	6.70	10.74
Na_2O	1.55	2.68	2.72	1.88	2.59	2.60	6.95	2.93	5.54	7.69	5.68
K_2O	0.09	0.02	0.02	0.02	0.00	0.00	0.06	0.02	0.03	0.07	0.04
Total	100.63	101.09	101.25	100.27	100.85	100.50	101.70	100.82	99.52	100.10	100.63
An	86	76	76	83	77	77	41	74	50	32	51
Ab	14	24	24	17	23	23	58	26	50	67	49
Or	1	0	0	0	0	0	0	0	0	0	0

Table 5 (ctd.): Feldspar compositions obtained using wavelength dispersive analysis

Sample no.	**ND15-53B**	**ND15-53B**	**ND15-53B**	**ND15-53B**	**ND15-53C**	**ND15-53C**	**ND15-53C**	**ND15-53C**	**ND15-53C**
Lithology	Basalt	Basalt	Basalt	Basalt	Gabbro	Gabbro	Gabbro	Gabbro	Gabbro
Unit	N. Region	N. Region	N. Region	N. Region	N. Region	N. Region	N. Region	N. Region	N. Region
Analysis no.	107	108	109	110	44	45	46	47	48
SiO_2	47.12	47.69	60.61	49.72	53.99	49.94	44.37	52.94	59.35
TiO_2	0.01	0.03	0.02	0.03	0.03	0.00	0.02	0.02	0.00
Al_2O_3	33.22	33.09	24.77	31.98	28.88	31.80	35.21	28.84	25.60
Cr_2O_3	0.01	0.00	0.00	0.05	0.00	0.00	0.00	0.00	0.00
FeO	0.93	0.67	0.21	0.65	0.26	0.21	0.37	0.32	0.07
MnO	0.01	0.00	0.00	0.00	0.00	0.00	0.04	0.05	0.01
MgO	0.06	0.14	0.01	0.07	0.01	0.06	0.00	0.04	0.02
CaO	16.49	15.86	6.04	14.57	10.92	14.10	18.63	11.46	6.70
Na_2O	2.20	2.41	8.24	3.35	5.72	3.66	1.15	5.29	7.89
K_2O	0.02	0.04	0.07	0.02	0.03	0.03	0.00	0.03	0.05
Total	100.08	99.92	99.97	100.44	99.84	99.81	99.79	98.99	99.69
An	80	78	29	71	51	68	90	54	32
Ab	19	22	71	29	49	32	10	45	68
Or	0	0	0	0	0	0	0	0	0

Table 6: Energy dispersive spectroscopy analyses of plagiogranite from the study area.

Sample no.	**31**	**31**	**31**	**31**	**31**	**31**
Lithology	Plagiogranite	Plagiogranite	Plagiogranite	Plagiogranite	Plagiogranite	Plagiogranite
Unit	N. Region	N. Region	N. Region	N. Region	N. Region	N. Region
Analysis no.	**1-1**	**1-2**	**1-3**	**1-4**	**1-5**	**1-6**
SiO_2	55.69	55.95	55.5	29.6	30.7	58.5
TiO_2						
Al_2O_3	0.73	0.74	1.4	24.3	25.3	24.7
Cr_2O_3						
Fe_2O_3	21.12	20.94	19.6	21.5	21.7	
MnO	0.62	0.66	0.6			
MgO	20.82	20.73	21.5	24.2	23.4	
CaO	1.02	0.98	1.5			7.5
Na_2O						9.3
K_2O						
Total	100.0	100.0	100.0	99.6	101.0	100.0
Phase	cummingtonite	cummingtonite	cummingtonite	chlorite	chlorite	plagioclase
Sample no.	**31**	**31**	**31**	**31**	**31**	**31**
Lithology	Plagiogranite	Plagiogranite	Plagiogranite	Plagiogranite	Plagiogranite	Plagiogranite
Unit	N. Region	N. Region	N. Region	N. Region	N. Region	N. Region
Analysis no.	**1-7**	**2-1**	**2-2**	**2-3**	**2-4**	**2-7**
SiO_2	58.6	58.9	59.1	59.3	59.2	34.9
TiO_2						
Al_2O_3	24.3	24.5	24.2	24.3	24.8	27.5
Cr_2O_3						
Fe_2O_3						13.1
MnO						
MgO						24.5
CaO	7.4	6.9	6.7	6.7	7.4	
Na_2O	9.7	9.7	10.0	9.6	9.6	
K_2O	0.1				0.1	
Total	100.0	100.0	100.0	100.0	101.0	100
Phase	plagioclase	plagioclase	plagioclase	plagioclase	plagioclase	chlorite

Table 6 (ctd.): Energy dispersive spectroscopy analyses of plagiogranite from the study area.

Sample no.	**40A**	**40A**	**40A**	**40A**	**40A**	**40A**
Lithology	Plagiogranite	Plagiogranite	Plagiogranite	Plagiogranite	Plagiogranite	Plagiogranite
Unit	NMC	NMC	NMC	NMC	NMC	NMC
Analysis no.	**1-1**	**1-2**	**1-3**	**1-4**	**1-5**	**1-6**
SiO_2	46.2	43.3	46.6	43.3	48.3	50.8
TiO_2	0.7					
Al_2O_3	19.1	12.8	14.8	12.6	20.6	20.3
Cr_2O_3						
Fe_2O_3	10.0	21.3	15.0	21.0	16.6	15.8
MnO		1.2	0.8	1.0		
MgO	13.4	7.8	8.5	7.8	9.3	9.2
CaO		11.4	11.4	11.9		
Na_2O		1.7	2.5	1.9		
K_2O	5.6	0.5	0.5	0.5	5.3	4.0
Total	95.0	99.9	100.0	100.0	100.0	100.0
Phase	biotite	hornblende	hornblende	hornblende	biotite	biotite
Sample no.	**ND15-40A**	**ND15-40A**	**ND15-40A**	**ND15-40A**	**ND15-40A**	**ND15-40A**
Lithology	Plagiogranite	Plagiogranite	Plagiogranite	Plagiogranite	Plagiogranite	Plagiogranite
Unit	NMC	NMC	NMC	NMC	NMC	NMC
Analysis no.	**2-1**	**2-2**	**2-3**	**2-4**	**2-5**	**3-1**
SiO_2	53.51	53.45	53.49	58.88	49.14	58.88
TiO_2			0.22			
Al_2O_3	2.02	1.6	1.92	24.6	19.49	24.19
Cr_2O_3						
Fe_2O_3	27.46	27.19	27.72		14.14	
MnO	2.38	1.93	1.69			
MgO	13.77	14.93	14.09		10.91	
CaO	0.87	0.91	0.87	6.54		7.05
Na_2O				9.98		9.88
K_2O					6.31	
Total	100.01	100.01	100	100	99.99	100
Phase	grunerite	cummingtonite	cummingtonite	plagioclase	biotite	plagioclase

Appendix 3

Whole-Rock Geochemical Data

Table 1: Major, trace and rare-earth element contents for coarse-grained gabbroic rocks of the mafic complexes and Northern Region. ICP-MS data is italicized. Mg# is calculated as 100*Mg/(Mg+Fe) where total Fe_2O_3 is converted to Fe^{2+}. Abbreviations: b.d: below detection, EMC: Ecemiş Mafic Complex, LOI: loss on ignition, n.a.: not analyzed, NMC: Niğde Mafic Complex, ppm: parts per million, REE: rare earth elements.

Table 2: Major, trace and rare earth element contents for fine-grained mafic rocks of the mafic complexes and Northern Region. Formatting and abbreviations are as in Table 1.

Table 3: Major and trace element contents for felsic rocks of the study area. A/CNK: calculated as molar $Al_2O_3/(CaO + Na_2O + K_2O)$. Abbreviations are as in Table 1.

Table 4: Major, trace and rare-earth element contents for amphibolites of the Aşıgediği and Gümüşler formations of the Niğde Massif. Abbreviations and formatting are as in Table 1.

Table 5: Major and trace element contents for gabbroic cobbles of circum-Niğde Massif basins. Abbreviations are as in Table 1.

Table 1: Major, trace and rare earth element contents for gabbroic rocks of the study area

Sample no.	**ND14-06A**	**ND14-07**	**ND15-06**	**ND15-09J**	**ND15-11**	**ND15-15**	**ND15-16**	**ND15-24**
Lithology	Gabbro	Gabbro	Gabbro	Gabbro	Gabbro	Gabbro	Gabbro	Gabbro
Unit	EMC	EMC	EMC	NMC	NMC	NMC	NMC	NMC
SiO_2 (wt. %)	47.91	46.95	48.16	47.08	47.00	48.93	47.34	49.35
TiO_2	0.12	0.13	0.20	1.11	0.42	0.35	0.45	0.17
Al_2O_3	18.05	17.68	16.18	18.70	18.68	14.97	19.77	17.41
Fe_2O_3*	3.34	4.43	4.96	13.51	10.75	8.25	8.94	4.52
MnO	0.07	0.08	0.09	0.22	0.18	0.16	0.15	0.09
MgO	10.96	11.81	12.18	5.72	8.32	10.71	7.60	10.02
CaO	17.06	15.39	16.77	10.65	12.94	15.00	13.81	16.80
Na_2O	1.19	1.17	0.93	2.64	1.11	1.06	1.29	0.97
K_2O	0.01	0.19	0.02	0.07	0.07	0.08	0.09	0.13
P_2O_5	0.00	0.003	0.005	0.133	0.03	0.007	0.015	0.005
LOI	1.35	2.19	0.98	0.46	0.62	0.61	0.72	0.66
Total	100.06	100.03	100.47	100.30	100.11	100.12	100.18	100.14
(ppm)								
Ba	2	142	7	10	6	8	*38*	*41*
Co	31	37	42	36	45	47	*37*	*31*
Cr	837	963	788	10	36	401	*53*	*1033*
Cu	51	47	99	56	74	52	*62*	*104*
Ga	9	9	9	20	15	11	b.d.	b.d.
Hf	b.d.	*b.d.*	*0*	1	b.d.	*0.5*	*0.2*	b.d.
Mn	617	722	845	2041	1690	1468	b.d.	b.d.
Nb	b.d.	*1.3*	*1.4*	1	1	*8.8*	*3*	b.d.
Ni	224	227	197	10	33	122	*31*	*172*
Rb	b.d.	3	1	2	1	3	b.d.	b.d.
Sc	31	35	43	55	58	53	*38*	*46*
Sr	100	174	100	155	116	104	*138*	*96*
Th	1	*b.d.*	*b.d.*	3	2	*0*	*0*	b.d.
V	96	*102.7*	*133.7*	348	343	*188.8*	*282.3*	*125*
Zn	14	17	21	112	67	46	*52*	b.d.
Zr	2	*1.9*	*3.6*	11	9	*11.5*	*9.1*	11

Table 1 (ctd.): Major, trace and rare earth element contents for gabbroic rocks of the study area

Sample no.	**ND14-06A**	**ND14-07**	**ND15-06**	**ND15-09J**	**ND15-11**	**ND15-15**	**ND15-16**	**ND15-24**
Lithology	Gabbro	Gabbro	Gabbro	Gabbro	Gabbro	Gabbro	Gabbro	Gabbro
Unit	EMC	EMC	EMC	NMC	NMC	NMC	NMC	NMC
REE (ppm)								
La	b.d.	*0.23*	*0.36*	b.d.	b.d.	*0.86*	*0.93*	b.d.
Ce	b.d.	*0.48*	*0.91*	15	8	*3.00*	*2.46*	b.d.
Pr	n.a.	*0.09*	*0.16*	n.a.	n.a.	*0.57*	*0.37*	n.a.
Nd	2	*0.49*	*0.97*	13	4	*3.47*	*1.91*	b.d.
Sm	b.d.	*0.26*	*0.45*	b.d.	b.d.	*1.39*	*0.69*	b.d.
Eu	n.a.	*0.20*	*0.27*	n.a.	n.a.	*0.53*	*0.40*	n.a.
Gd	n.a.	*0.53*	*0.75*	n.a.	n.a.	*2.19*	*0.95*	n.a.
Tb	n.a.	*0.10*	*0.15*	n.a.	n.a.	*0.36*	*0.17*	n.a.
Dy	n.a.	*0.57*	*0.98*	n.a.	n.a.	*2.57*	*1.10*	n.a.
Ho	n.a.	*0.14*	*0.21*	n.a.	n.a.	*0.56*	*0.24*	n.a.
Er	n.a.	*0.38*	*0.58*	n.a.	n.a.	*1.63*	*0.72*	n.a.
Tm	n.a.	*0.04*	*0.07*	n.a.	n.a.	*0.24*	*0.10*	n.a.
Yb	7	*0.31*	*0.45*	6	4	*1.56*	*0.75*	b.d.
Lu	n.a.	*0.04*	*0.06*	n.a.	n.a.	*0.20*	*0.10*	n.a.
Y	3	*3.07*	*4.67*	38	7	*13.65*	*5.80*	b.d.
Mg#	87	84	83	46	61	72	63	82
La_N/Yb_N		0.53	0.57			0.40	0.89	

Table 1 (ctd.): Major, trace and rare earth element contents for gabbroic rocks of the study area

Sample no.	**ND15-34B**	**ND15-36B**	**ND15-38A**	**ND15-48E**	**ND15-48G**	**ND15-50C**
Lithology	Gabbro	Gabbro	Horblendite	Gabbro	Gabbro	Gabbro
Unit	N. Region	NMC	NMC	NMC	NMC	NMC
SiO_2 (wt. %)	48.01	49.85	52.37	48.72	47.90	55.55
TiO_2	0.15	0.18	0.48	0.22	0.16	0.38
Al_2O_3	19.31	17.92	10.07	15.78	19.89	14.85
Fe_2O_3*	4.16	8.04	8.48	5.63	5.05	7.10
MnO	0.08	0.18	0.16	0.11	0.10	0.12
MgO	8.87	8.62	13.60	11.60	9.93	8.87
CaO	18.64	13.99	10.48	16.27	16.48	9.54
Na_2O	0.62	1.28	1.58	1.23	0.89	2.51
K_2O	0.02	0.06	0.79	0.04	0.01	0.44
P_2O_5	0.009	0.015	0.040	0.01	0.00	0.04
LOI	0.54	0.43	1.65	0.50	0.15	0.79
Total	100.42	100.56	99.70	100.12	100.54	100.19
(ppm)						
Ba	47	17	91	11	b.d.	69
Co	26	37	42	41	35	34
Cr	750	93	1383	1133	646	405
Cu	38	41	114	84	35	21
Ga	9	14	10	10	11	13
Hf	*0.1*	*0.1*	2	1	*0*	1
Mn	742	1706	1439	957	914	1110
Nb	*3*	*1.9*	4		*2.1*	2
Ni	67	69	241	179	123	95
Rb	1	1	24	1	1	13
Sc	48	48	53	49	35	37
Sr	112	104	61	97	126	150
Th	*0*	*0*	3	2	*0*	2
V	*132.5*	*128.8*	310	153	*108.8*	205
Zn	19	58	65	29	39	49
Zr	*5*	*7.2*	41	8	*2.7*	24

Table 1 (ctd.): Major, trace and rare earth element contents for gabbroic rocks of the study area

Sample no.	**ND15-34B**	**ND15-36B**	**ND15-38A**	**ND15-48E**	**ND15-48G**	**ND15-50C**
Lithology	Gabbro	Gabbro	Horblendite	Gabbro	Gabbro	Gabbro
Unit	N. Region	NMC	NMC	NMC	NMC	NMC
REE (ppm)						
La	*0.41*	*0.65*	b.d.	b.d.	*0.30*	b.d.
Pr	*0.16*	*0.27*	n.a.	n.a.	*0.12*	n.a.
Nd	*0.95*	*1.60*	12	3	*0.83*	9
Sm	*0.37*	*0.70*	b.d.	b.d.	*0.38*	b.d.
Eu	*0.22*	*0.42*	n.a.	n.a.	*0.27*	n.a.
Gd	*0.59*	*1.04*	n.a.	n.a.	*0.60*	n.a.
Tb	*0.12*	*0.23*	n.a.	n.a.	*0.13*	n.a.
Dy	*0.71*	*1.51*	n.a.	n.a.	*0.80*	n.a.
Ho	*0.16*	*0.34*	n.a.	n.a.	*0.17*	n.a.
Er	*0.47*	*0.92*	n.a.	n.a.	*0.46*	n.a.
Tm	*0.06*	*0.14*	n.a.	n.a.	*0.06*	n.a.
Yb	*0.41*	*1.00*	7	9	*0.40*	5
Lu	*0.05*	*0.13*	n.a.	n.a.	*0.05*	n.a.
Y	*3.73*	*7.62*	15	6	*3.87*	15
Mg#	81	68	76	80	80	71
La_N/Yb_N	0.72	0.47			0.54	

Table 2: Major, trace and rare earth element contents for fine grained mafic rocks of the study area.

Sample no.	**ND15-14**	**ND15-28**	**ND15-29**	**ND15-32**	**ND15-40B**	**ND15-53B**
Lithology	Diabase	Diabase	Diabase	Diabase	Diabase	Basalt
Unit	NMC	NMC	NMC	N. Region	NMC	N. Region
SiO_2 (wt. %)	50.61	54.69	60.69	54.38	49.14	50.43
TiO_2	0.40	0.23	0.65	0.32	0.44	0.49
Al_2O_3	17.89	14.92	15.84	13.09	18.31	16.99
Fe_2O_3*	8.22	7.78	8.17	8.20	8.94	9.13
MnO	0.14	0.14	0.16	0.15	0.15	0.16
MgO	7.51	8.35	3.55	10.25	8.04	7.78
CaO	11.30	11.43	7.37	10.14	10.93	12.34
Na_2O	2.01	1.61	3.16	2.81	2.09	1.92
K_2O	0.53	0.17	0.12	0.10	0.59	0.07
P_2O_5	0.03	0.02	0.09	0.03	0.03	0.04
LOI	1.36	0.91	0.46	0.37	1.42	0.58
Total	100.00	100.25	100.25	99.83	100.08	99.93
(ppm)						
Ba	106	24	23	17	96	41
Co	35	37	27	43	34	38
Cr	85	377	29	678	89	160
Cu	54	35	14	2	125	69
Ga	14	11	15	11	14	13
Hf	1	*0.2*	b.d.	2	*0.6*	*0.5*
Mn	1238	1286	1409	1374	1342	1491
Nb	1	*3*	1	1	*3.1*	*1.8*
Ni	43	75	8	177	41	46
Rb	21	6	2	1	26	1
Sc	39	43	28	40	41	40
Sr	163	399	160	75	194	128
Th	3	*0*	2	2	*1.1*	*0.2*
V	236	*214.9*	191	225	*244.7*	*265.6*
Zn	57	41	73	63	65	61
Zr	28	*7.6*	50	30	*21.8*	*19.9*

Table 2 (ctd.): Major, trace and rare earth element contents for fine grained mafic rocks of the study area.

Sample no.	**ND15-14**	**ND15-28**	**ND15-29**	**ND15-32**	**ND15-40B**	**ND15-53B**
Lithology	Diabase	Diabase	Diabase	Diabase	Diabase	Basalt
Unit	NMC	NMC	NMC	N. Region	NMC	N. Region
REE (ppm)						
La	1	*0.61*	b.d.	b.d.	*3.42*	*1.50*
Ce	12	*1.56*	8	b.d.	*7.60*	*4.19*
Pr	n.a.	*0.25*	n.a.	n.a.	*0.98*	*0.58*
Nd	7	*1.33*	8	2	*4.39*	*2.95*
Sm	2	*0.50*	b.d.	1	*1.20*	*0.99*
Eu	n.a.	*0.30*	n.a.	n.a.	*0.46*	*0.43*
Gd	n.a.	*0.79*	n.a.	n.a.	*1.48*	*1.42*
Tb	n.a.	*0.16*	n.a.	n.a.	*0.28*	*0.25*
Dy	n.a.	*1.10*	n.a.	n.a.	*1.78*	*1.65*
Ho	n.a.	*0.25*	n.a.	n.a.	*0.37*	*0.37*
Er	n.a.	*0.79*	n.a.	n.a.	*1.05*	*1.03*
Tm	n.a.	*0.12*	n.a.	n.a.	*0.16*	*0.16*
Yb	4	*0.82*	4	7	*1.12*	*1.12*
Lu	n.a.	*0.10*	n.a.	n.a.	*0.15*	*0.16*
Y	10	*6.27*	17	11	*9.16*	*9.17*
Mg#	64	68	46	71	64	63
La_N/Yb_N		0.53			2.19	0.96

Table 3: Major and trace element contents for felsic rocks of the study area

Sample no.	**ND15-21B**	**ND15-31**	**ND15-40A**	**ND15-48F**	**ND15-50D**
Lithology	Plagiogranite	Plagiogranite	Plagiogranite	Aplite	Plagiogranite
Unit	NMC	N. Region	NMC	Üçkapılı	NMC
(wt%)					
SiO_2	74.82	78.76	76.98	76.57	73.32
TiO_2	0.28	0.26	0.08	0.02	0.22
Al_2O_3	13.23	12.27	13.63	14.36	13.70
Fe_2O_3*	2.71	0.78	0.90	0.34	3.49
MnO	0.04	0.02	0.02	0.06	0.03
MgO	0.57	0.44	0.23	0.10	0.42
CaO	3.54	3.13	3.48	0.80	4.36
Na_2O	4.51	3.93	4.17	7.60	3.71
K_2O	0.16	0.09	0.25	0.13	0.16
P_2O_5	0.06	0.03	0.04	0.05	0.03
LOI	0.14	0.29	0.26	0.31	0.18
Total	100.05	99.99	100.03	100.34	99.61
(ppm)					
Ba	41	24	62	7	39
Ce	11	7	5	6	4
Co	4	3	1	1	6
Cr	4	31	3	3	14
Cu	b.d.	b.d.	b.d.	21	b.d.
Ga	13	10	11	15	14
Hf	4	1	1	b.d.	4
La	1	b.d.	3	1	b.d.
Mn	332	182	201	349	231
Nb	1	b.d.	b.d.	11	1
Nd	11	4	2	2	3
Ni	3	45	4	6	5
Rb	4	1	15	5	2
Sc	14	3	3	3	4
Sm	6	2	b.d.	2	b.d.
Sr	119	170	123	26	151
Ta	1	1	1	4	1
Th	2	1	1	5	2
V	22	11	7	4	38
Y	41	2	8	13	5
Yb	5	2	3	2	2
Zn	13	7	13	2	23
Zr	136	101	57	28	154
A/CNK	0.94	1.00	1.01	1.02	0.96

Table 4: Major, trace and rare earth element contents for amphibolites of the Niğde Massif

Sample no.	**ND01-17A**	**ND01-32B**	**ND15-47B**	**ND15-52**
Lithology	Amphibolite	Amphibolite	Amphibolite	Amphibolite
Unit	Aşıgediği	Gümüşler	Aşıgediği	Aşıgediği
SiO_2 (wt. %)	55.02	48.15	43.62	43.95
TiO_2	0.50	1.19	2.69	2.91
Al_2O_3	15.39	15.90	11.86	11.96
Fe_2O_3*	7.38	9.02	12.01	12.65
MnO	0.11	0.16	0.92	0.18
MgO	3.41	6.64	9.13	7.65
CaO	11.18	11.71	14.54	14.83
Na_2O	3.39	4.08	0.76	2.47
K_2O	1.39	0.92	1.31	1.18
P_2O_5	0.14	0.17	1.02	0.54
LOI	2.05	2.20	1.72	1.57
Total	99.97	100.15	99.57	99.89
(ppm)				
Ba	179	247	155	384
Co	13	36	59	46
Cr	7	176	280	239
Cu	36	38	b.d.	9
Ga	14	15	19	18
Hf	1	2	7	7
Mn	842	1440	9253	1697
Nb	4	*15.2*	*68.0*	86
Ni	3	44	151	85
Rb	28	24	48	30
Sc	23	43	29	33
Sr	369	593	161	385
Th	6	*2*	*6.8*	11
V	111	*205.1*	*191.6*	297
Zn	89	56	170	107
Zr	57	91	295	223

Table 4 (ctd.): Major, trace and rare earth element contents for amphibolites of the Niğde Massif

Sample no.	**ND01-17A**	**ND01-32B**	**ND15-47B**	**ND15-52**
Lithology	Amphibolite	Amphibolite	Amphibolite	Amphibolite
Unit	Aşıgediği	Gümüşler	Aşıgediği	Aşıgediği
REE (ppm)				
La	5	*12.42*	*45.38*	52
Ce	23	*28.67*	*101.63*	110
Pr	n.a.	*3.63*	*12.34*	n.a.
Nd	14	*15.64*	*52.28*	47
Sm	b.d.	*3.49*	*8.28*	b.d.
Eu	n.a.	*1.31*	*2.46*	n.a.
Gd	n.a.	*3.98*	*7.09*	n.a.
Tb	n.a.	*0.64*	*0.98*	n.a.
Dy	n.a.	*4.01*	*5.67*	n.a.
Ho	n.a.	*0.80*	*0.98*	n.a.
Er	n.a.	*2.09*	*2.43*	n.a.
Tm	n.a.	*0.31*	*0.32*	n.a.
Yb	4	*2.04*	*2.06*	7
Lu	n.a.	*0.28*	*0.25*	n.a.
Y	12	*19.20*	*25.62*	25
Mg #	48	59	60	55
La_N/Yb_N		4.37	15.80	

Table 5: Major and trace element contents for gabbroic cobbles of the basins

Sample no.	**PU15-14**	**ND14-04B**	**ND15-08A**	**ND15-19B**	**ND15-41**	**ND15-43**
Lithology	Gabbro	Gabbro	Gabbro	Gabbro	Diabase	Gabbro
Unit	Çukurbağ	Çukurbağ	Çukurbağ	Çukurbağ	M_3pl	M_3pl
(wt%)						
SiO_2	53.03	50.26	48.38	46.94	57.26	47.77
TiO_2	0.98	0.68	0.16	0.10	0.31	0.12
Al_2O_3	17.45	16.04	19.05	15.34	15.00	19.63
Fe_2O_3*	9.10	7.12	5.73	7.80	7.40	4.21
MnO	0.13	0.13	0.11	0.14	0.19	0.08
MgO	5.93	9.29	8.87	12.78	7.23	10.91
CaO	9.00	12.32	14.86	11.44	9.92	15.01
Na_2O	2.76	2.45	1.56	1.08	1.56	0.98
K_2O	0.08	0.16	0.03	0.02	0.17	0.13
P_2O_5	0.10	0.08	0.00	0.00	0.04	0.00
LOI	1.74	1.53	1.54	4.73	1.18	1.15
Total	100.30	100.05	100.29	100.37	100.27	99.99
(ppm)						
Ba	117	24	147	53	27	50
Ce	8	8	2	b.d.	1	b.d.
Co	32	36	38	54	33	33
Cr	118	338	215	459	319	1082
Cu	b.d.	20	51	14	b.d.	33
Ga	16	12	11	9	13	10
Hf	2	1	b.d.	1	1	b.d.
Mn	1174	1181	1043	1320	1894	704
Nb	1	1	1	b.d.	1	b.d.
Nd	7	7	3	5	5	b.d.
Ni	61	102	78	141	63	244
Rb	1	2	1	1	4	1
Sc	38	40	44	41	42	29
Sm	b.d.	7	b.d.	2	b.d.	1
Sr	162	208	145	115	60	111
Th	2	2	3	1	2	2
V	255	196	146	142	238	83
Y	22	16	4	2	12	3
Yb	6	6	5	5	4	9
Zn	73	47	22	36	82	28
Zr	63	55	2	1	23	1
Mg #	56	72	75	77	66	84

Table 5 (ctd.): Major and trace element contents for gabbroic cobbles of the basins

Sample no.	**ND15-44**	**ND15-46**
Lithology	Gabbro	Gabbro
Unit	M_3pl	M_3pl
(wt%)		
SiO_2	46.95	50.04
TiO_2	0.13	0.49
Al_2O_3	17.68	16.09
Fe_2O_3*	5.60	8.40
MnO	0.10	0.15
MgO	11.85	9.27
CaO	15.67	12.43
Na_2O	0.88	1.95
K_2O	0.09	0.34
P_2O_5	0.01	0.03
LOI	0.85	0.84
Total	99.81	100.03
(ppm)		
Ba	25	92
Ce	b.d.	b.d.
Co	43	40
Cr	975	303
Cu	68	83
Ga	10	13
Hf	b.d.	b.d.
Mn	865	1375
Nb		1
Nd	2	3
Ni	186	81
Rb	2	6
Sc	38	46
Sm	3	3
Sr	82	117
Th	2	3
V	114	282
Y	3	13
Yb	5	4
Zn	31	63
Zr	3	20
Mg #	81	69

Appendix 4

Analyses Used for Thermobarometric Calculations

Table 1: Data used for calculation of gabbro igneous crystallization temperatures using the Wells (1977) two-pyroxene thermometer. Values shown are cationic proportions recalculated from WDS data in Appendix 2.

Table 2: Data used for calculation of metamorphic recrystallization temperatures using the Holland and Blundy (1994) edenite-tremolite thermometer. Values shown are cationic proportions recalculated from WDS data in Appendix 2.

Table 1: Data used for the two-pyroxene thermometer of Wells (1977)

Sample no.	**ND15-15**	**ND15-15**	**ND15-15**	**ND15-34B**	**ND15-34B**	**ND15-34B**
Unit	NMC	NMC	NMC	N. Region	N. Region	N. Region
Opx analysis	**228**	**230**	**285**	**208**	**209**	**210**
T site						
Si	1.933	1.936	1.928	1.948	1.952	1.946
Al	0.039	0.039	0.061	0.052	0.048	0.054
M1 site						
Ti	0.001	0.002	0.001	0.005	0.004	0.005
Al	0.000	0.000	0.000	0.026	0.025	0.027
Cr	0.002	0.001	0.001	0.004	0.005	0.005
Fe^{3+}	0.092	0.086	0.08	0.012	0.011	0.014
Fe^{2+}	0.302	0.297	0.242	0.182	0.177	0.174
Mg	0.632	0.639	0.687	0.77	0.778	0.776
M2 site						
Fe^{2+}	0.307	0.301	0.252	0.183	0.167	0.168
Mn	0.025	0.024	0.013	0.008	0.006	0.008
Mg	0.644	0.648	0.714	0.775	0.733	0.746
Ca	0.025	0.026	0.021	0.033	0.095	0.078
Na	0.000	0.001	0.001	0.000	0.000	0.000
a (Opx)	0.4049	0.4136	0.4911	0.603	0.5732	0.5832
Cpx analysis	**242**	**246**	**246**	**211**	**212**	**213**
T site						
Si	1.931	1.912	1.912	1.966	1.929	1.972
Al	0.067	0.086	0.086	0.034	0.071	0.028
M1 site						
Ti	0.006	0.008	0.008	0.005	0.006	0.002
Al	0.000	0.000	0.000	0.035	0.024	0.03
Cr	0.001	0.001	0.001	0.006	0.007	0.005
Fe^{3+}	0.077	0.094	0.094	0.000	0.042	0.000
Fe^{2+}	0.152	0.128	0.128	0.133	0.102	0.125
Mg	0.767	0.772	0.772	0.822	0.819	0.837
M2 site						
Fe^{2+}	0.012	0.009	0.009	0.007	0.006	0.008
Mn	0.008	0.006	0.006	0.005	0.005	0.005
Mg	0.060	0.055	0.055	0.043	0.045	0.053
Ca	0.901	0.910	0.910	0.938	0.932	0.924
Na	0.019	0.020	0.020	0.008	0.013	0.011
a (Cpx)	0.0476	0.0424	0.0424	0.0382	0.0385	0.0474
X^{Opx}_{Fe}	0.32	0.32	0.26	0.19	0.19	0.18
T (°C)	**895**	**873**	**867**	**842**	**855**	**890**

Table 1 (ctd.): Data used for the two-pyroxene thermometer of Wells (1977)

Sample no.	**ND15-34B**	**ND15-48E**	**ND15-48E**	**ND15-36B**	**ND15-36B**
Unit	N. Region	NMC	NMC	NMC	NMC
Opx analysis	**216**	**127**	**128**	**241**	**250**
T site					
Si	1.958	1.917	1.894	1.933	1.95
Al	0.042	0.081	0.076	0.036	0.039
M1 site					
Ti	0.003	0.002	0.004	0.004	0.005
Al	0.029	0.000	0.000	0.000	0
Cr	0.005	0.004	0.003	0.000	0.001
Fe^{3+}	0.002	0.077	0.128	0.12	0.05
Fe^{2+}	0.211	0.191	0.169	0.273	0.311
Mg	0.75	0.728	0.727	0.63	0.644
M2 site					
Fe^{2+}	0.208	0.202	0.181	0.277	0.308
Mn	0.01	0.013	0.011	0.02	0.019
Mg	0.739	0.767	0.779	0.64	0.636
Ca	0.042	0.018	0.027	0.03	0.038
Na	0.001	0.000	0.001	0.033	0.000
a (Opx)	0.5601	0.5650	0.5561	0.3999	0.4124
Cpx analysis	**214**	**124**	**129**	**242**	**249**
T site					
Si	1.943	1.894	1.895	1.914	1.945
Al	0.057	0.103	0.105	0.076	0.055
M1 site					
Ti	0.007	0.007	0.007	0.008	0.005
Al	0.034	0.000	0.015	0.000	0.005
Cr	0.007	0.005	0.008	0.001	0.000
Fe^{3+}	0.01	0.112	0.092	0.149	0.054
Fe^{2+}	0.121	0.073	0.085	0.113	0.179
Mg	0.82	0.806	0.792	0.741	0.758
M2 site					
Fe^{2+}	0.006	0.007	0.005	0.009	0.02
Mn	0.005	0.007	0.005	0.01	0.009
Mg	0.04	0.074	0.050	0.058	0.084
Ca	0.939	0.890	0.915	0.856	0.874
Na	0.009	0.023	0.025	0.068	0.013
a (Cpx)	0.0368	0.0579	0.0470	0.042	0.0661
X^{Opx}_{Fe}	0.22	0.21	0.19	0.30	0.33
T (°C)	**837**	**922**	**895**	**884**	**954**

Table 2: Data used for the edenite-tremolite thermometer of Holland and Blundy (1994).

Sample no.	**ND14-02B**	**ND14-02B**	**ND14-02B**	**ND14-02B**	**ND14-02B**	**ND14-02B**	**ND15-15**	**ND15-15**	**ND15-15**	**ND15-15**
Unit	NMC	NMC	NMC	NMC	NMC	NMC	NMC	NMC	NMC	NMC
Hbl anal. no.	**75**	**76**	**80**	**81**	**82**	**85**	**254**	**252**	**253**	**274**
SiO_2	47.41	46.46	47.55	46.35	46.45	48.37	48.70	48.77	48.50	49.14
TiO_2	0.48	0.78	0.72	0.41	0.71	0.57	0.92	1.09	1.15	1.04
Al_2O_3	7.79	9.10	8.18	8.77	8.84	7.46	6.75	6.81	6.75	6.44
FeO*	14.57	15.33	14.71	15.48	15.18	14.27	12.24	11.95	11.96	12.75
MgO	13.16	12.50	13.12	12.48	12.72	13.24	15.18	15.47	15.49	15.27
MnO	0.30	0.30	0.27	0.26	0.28	0.29	0.25	0.17	0.23	0.24
CaO	12.62	12.34	12.43	12.53	12.19	12.34	12.18	11.95	12.07	11.79
Na_2O	0.73	0.92	0.82	0.89	0.94	0.77	0.86	0.88	0.93	0.83
K_2O	0.51	0.73	0.59	0.63	0.67	0.46	0.09	0.11	0.08	0.09
Total	97.58	98.47	98.39	97.78	97.98	97.78	97.18	97.19	97.16	97.59
Pl anal. no.	**71**	**71**	**71**	**72**	**72**	**63**	**262**	**260**	**259**	**271**
Ab	0.47	0.47	0.47	0.5	0.5	0.46	0.27	0.22	0.23	0.24
An	0.51	0.51	0.51	0.49	0.49	0.53	0.73	0.78	0.74	0.76
T °C (0 kbar)	752	772	747	774	769	709	799	814	840	799
T °C (5 kbar)	**717**	**740**	**714**	**741**	**736**	**681**	**752**	**766**	**786**	**751**
T °C (10 kb)	682	707	681	709	703	652	705	718	732	702

Table 2 (ctd): Data used for the edenite-tremolite thermometer of Holland and Blundy (1994).

Sample no.	**ND15-15**	**ND15-22C**	**ND15-22C**	**ND15-40B**	**ND15-40B**	**ND15-40B**	**ND15-40B**	**ND15-40B**	**ND15-40B**	**ND15-51F**
Unit	NMC	NMC	NMC	NMC	NMC	NMC	NMC	NMC	NMC	NMC
Hbl anal. no.	**273**	**77**	**67**	**114**	**115**	**128**	**130**	**114**	**136**	**239**
SiO_2	48.90	44.71	44.87	47.94	45.19	46.89	46.62	47.94	48.16	51.57
TiO_2	0.97	1.57	1.25	0.45	0.89	0.62	0.72	0.45	0.48	0.19
Al_2O_3	7.19	10.68	9.94	7.39	9.63	8.28	8.91	7.39	7.51	5.11
FeO*	12.47	13.58	14.46	13.75	14.75	14.05	14.29	13.75	13.82	10.04
MgO	14.57	0.17	0.23	14.21	12.56	13.53	13.24	14.21	14.03	16.61
MnO	0.19	12.16	11.99	0.28	0.28	0.31	0.29	0.28	0.23	0.32
CaO	11.88	12.12	12.19	11.95	11.88	11.64	11.96	11.95	11.91	11.92
Na_2O	0.91	1.64	1.41	0.56	1.03	0.80	0.75	0.56	0.62	0.52
K_2O	0.10	0.38	0.35	0.27	0.60	0.43	0.46	0.27	0.20	0.08
Total	97.18	97.00	96.69	96.80	96.81	96.54	97.25	96.80	96.97	96.36
Pl anal. no.	**266**	**73**	**70**	**118**	**122**	**127**	**127**	**124**	**138**	**230**
Ab	0.21	0.62	0.6	0.42	0.42	0.36	0.36	0.37	0.36	0.53
An	0.78	0.38	0.39	0.58	0.58	0.64	0.64	0.63	0.64	0.43
T °C (0 kbar)	770	743	766	714	793	745	744	719	715	616
T °C (5 kbar)	**736**	**728**	**743**	**680**	**762**	**714**	**716**	**685**	**685**	**590**
T °C (10 kb)	703	713	720	647	732	684	688	650	655	564

Table 2 (ctd): Data used for the edenite-tremolite thermometer of Holland and Blundy (1994).

Sample no.	**ND15-51F**	**ND15-51F**	**ND15-51F**	**ND15-51F**	**ND15-51F**	**ND15-51F**
Unit	NMC	NMC	NMC	NMC	NMC	NMC
Hbl anal. no.	**236**	**234**	**248**	**240**	**245**	**245**
SiO_2	52.66	52.69	51.05	49.54	51.17	51.17
TiO_2	0.13	0.15	0.39	0.40	0.23	0.23
Al_2O_3	3.95	4.39	6.01	6.41	5.43	5.43
FeO*	8.97	9.65	11.27	11.54	11.17	11.17
MgO	17.65	17.06	15.51	15.03	15.96	15.96
MnO	0.27	0.36	0.35	0.28	0.34	0.34
CaO	12.06	12.14	12.01	11.82	11.56	11.56
Na_2O	0.44	0.44	0.56	0.65	0.57	0.57
K_2O	0.12	0.11	0.18	0.13	0.15	0.15
Total	96.25	96.98	97.34	95.81	96.57	96.57
Pl anal. no.	**231**	**227**	**253**	**253**	**251**	**252**
Ab	0.55	0.55	0.58	0.58	0.49	0.45
An	0.43	0.43	0.42	0.42	0.5	0.55
T °C (0 kbar)	592	585	609	643	626	628
T °C (5 kbar)	**561**	**559**	**588**	**620**	**602**	**603**
T °C (10 kb)	530	532	568	597	578	579

Appendix 5

Çukurbağ Formation clast count data

Full results of four clast counts in the Çukurbağ Formation of the Ecemiş Basin. Counts were performed by counting 100 or more clasts of >2 cm diameter and by moving in a 10 cm x 10 cm grid. For clast count locations see Fig. 2.4.

Clast count 1: Sample locality 01

Lithology	Size (cm)						
granite	2	granite	6	gabbro	4	gabbro	10
gabbro	15	gabbro	2	granite	8	granite	3
granite	10	rhyolite	2	gabbro	7	granite	10
gabbro	3	gabbro	9	gabbro	14	gabbro	6
gabbro	9	basalt	5	gabbro	4	basalt	6
gabbro	2	gabbro	2	gabbro	17	gabbro	10
gabbro	2	gabbro	6	gabbro	15	gabbro	7
granite	9	gabbro	10	gabbro	1	gabbro	11
granite	1	basalt	11	gabbro	2	marble	10
granite	4	gabbro	7	gabbro	8	basalt	2
marble	6	gabbro	7	basalt	6	rhyolite	15
basalt	6	gabbro	9	gabbro	6	gabbro	3
gabbro	17	granite	15	gabbro	9	gabbro	15
diorite	6	gabbro	20	gabbro	6	gabbro	2
gabbro	5	gabbro	4	gabbro	7		
gabbro	10	gabbro	2	gabbro	4		
granite	5	basalt	7	gabbro	15		
gabbro	13	gabbro	15	marble	10		
rhyolite	3	gabbro	8	basalt	4		
gabbro	9	gabbro	5	gabbro	4		
gabbro	5	gabbro	10	gabbro	10		
gabbro	12	gabbro	6	granite	7		
basalt	4	gabbro	10	gabbro	15		
gabbro	6	gabbro	2	gabbro	5		
gabbro	2	gabbro	10	gabbro	9		
gabbro	13	clastic	3	epidote	2		
gabbro	10	gabbro	9	gabbro	5		
basalt	10	basalt	4	granite	4		
basalt	4	gabbro	6	granite	9		

Clast count 2: Sample locality 08

Lithology	Size (cm)						
gabbro	6	volcanic	4	volcanic	2	volcanic	2
granite	2	gabbro	3	volcanic	6	volcanic	3
volcanic	2	volcanic	8	volcanic	13	volcanic	8
gabbro	10	volcanic	5	limestone	3	gabbro	2
clastics	8	gabbro	4	granite	3	volcanic	1
granite	5	volcanic	6	volcanic	6	volcanic	2
granite	7	volcanic	4	volcanic	5	limestone	5
granite	15	limestone	10	gabbro	4	limestone	1
basalt	9	basalt	10	gabbro	3	limestone	5
basalt	4	volcanic	2	volcanic	3	gabbro	4
rhyolite	7	granite	5	granite	2	volcanic	2
basalt	4	granite	10	volcanic	7	granite	5
limestone	4	granite	5	gabbro	3	volcanic	4
basalt	8	granite	7	gabbro	3		
gabbro	8	volcanic	6	gabbro	2		
volcanic	2	limestone	4	granite	5		
volcanic	5	gabbro	5	granite	15		
granite	8	volcanic	6	gabbro	4		
volcanic	9	rhyolite	7	gabbro	7		
volcanic	6	volcanic	2	volcanic	3		
gabbro	4	gabbro	8	volcanic	6		
volcanic	5	basalt	10	volcanic	2		
basalt	9	granite	9	volcanic	6		
limestone	2	granite	10	limestone	2		
gabbro	3	volcanic	13	volcanic	5		
limestone	10	granite	6	volcanic	4		
granite	11	volcanic	2	limestone	4		
volcanic	4	gabbro	7	granite	2		
gabbro	9	gabbro	7	gabbro	5		

Clast count 3: Sample locality 19

Lithology	Size (cm)						
gabbro	7	gray chert	3	gabbro	9	gabbro	4
gabbro	4	volcanic	2	volcanic	6	gabbro	7
volcanic	8	gabbro	6	marble	3	marble	15
gabbro	3	volcanic	5	gabbro	2	gabbro	10
granite	2	volcanic	4	gabbro	5	marble	9
marble	5	gabbro	11	marble	5	granite	8
gabbro	10	gabbro	8	volcanic	4	granite	9
marble	5	gabbro	2	gabbro	6	marble	12
gabbro	3	granite	4	volcanic	9	gabbro	16
volcanic	7	gabbro	3	marble	5	marble	17
gabbro	9	granite	3	gabbro	5	gabbro	9
gabbro	5	gabbro	9	gabbro	7	volcanic	5
volcanic	8	marble	3	gabbro	5	gray chert	6
gabbro	4	gabbro	10	gabbro	4		
volcanic	3	volcanic	3	gabbro	10		
gabbro	4	gabbro	6	marble	15		
marble	8	granite	6	gabbro	3		
gabbro	2	volcanic	3	volcanic	5		
gabbro	5	volcanic	3	gabbro	5		
gabbro	5	granite	10	volcanic	5		
gabbro	8	gabbro	4	marble	4		
gray chert	10	granite	8	gabbro	7		
gabbro	10	gabbro	2	gabbro	3		
gabbro	2	gabbro	2	gabbro	7		
gabbro	4	volcanic	10	marble	9		
gabbro	2	gabbro	8	volcanic	7		
gabbro	3	marble	12	gabbro	10		
volcanic	5	granite	7	volcanic	4		
granite	5	gabbro	8	volcanic	11		

Clast count 4: Sample locality PU-14

Lithology	Size (cm)						
gabbro	15	gabbro	5	marble	11	marble	7
marble	11	marble	5	limestone	6	limestone	4
gabbro	5	gabbro	8	marble	5	limestone	3
sandstone	7	volcanic	10	gabbro	6	sandstone	7
limestone	5	limestone	8	marble	2	marble	17
gabbro	4	marble	5	marble	3	sandstone	25
gabbro	2	limestone	4	marble	3	limestone	6
gabbro	3	marble	5	red chert	15	marble	10
limestone	4	marble	3	gabbro	9	epidote	2
marble	4	gabbro	9	limestone	6	sandstone	9
red chert	5	gabbro	10	limestone	8	gabbro	12
gabbro	5	marble	7	marble	6	gabbro	10
limestone	3	marble	4	gabbro	5	gabbro	5
marble	6	volcanic	9	marble	6	limestone	10
gabbro	5	gabbro	7	gabbro	7	limestone	20
gabbro	3	gabbro	9	limestone	4	marble	12
marble	3	marble	4	limestone	5	marble	10
marble	4	limestone	5	limestone	6	sandstone	11
gabbro	9	gabbro	4	volcanic	7	limestone	7
gabbro	5	sandstone	15	marble	7	sandstone	6
gray chert	5	sandstone	6	marble	5		
marble	3	limestone *	7	gabbro	5		
gray chert	2.5	limestone	4	limestone	5		
quartzite	6	limestone	16	marble	6		
limestone	3	marble	8	gabbro	4		
gabbro	6	limestone	3	gabbro	3		
quartzite	3	limestone	5	limestone	9		
gabbro	4	limestone	12	gabbro	4		
gabbro	4	sandstone	7	gabbro	4		